Interacting Electrons in Quantum Dots with Strong Rashba Spin-Orbit Coupling

Inaugural Dissertation

zur Erlangung des Doktorgrades der
Mathematisch-Naturwissenschaftlichen Fakultät der
Heinrich-Heine-Universität Düsseldorf

vorgelegt von

Amin Naseri Jorshari

aus Tehran

Düsseldorf, July 2015

Aus dem Institut für Theoretische Physik IV
der Heinrich-Heine Universität Düsseldorf

Gedruckt mit der Genehmigung der
Mathematisch-Naturwissenschaftlichen Fakultät
der Heinrich-Heine Universität Düsseldorf

Referent: Prof. Dr. Reinhold Egger
Koreferent: Prof. Dr. Thomas Heinzel

Tag der mündlichen Prüfung: . .2015

To my family

Abstract

In this thesis, we present a study of interacting electrons confined in a two-dimensional space in the presence of a parabolic trap and strong Rashba spin-orbit coupling. The system is characterized by dimensionless parameters for the Rashba coupling $\alpha \gg 1$ and the interaction strength $\lambda \lesssim 1$. At the single-particle level, the energy spectrum shows Landau-like bands plus a decoupled rotor expressed in terms of the total angular momentum. The low-energy physics take place on a ring in momentum space. The significant consequence is that two classes of interactions are boosted, namely, interaction of Kramers pairs and exchange interaction. The ground states of the system are discussed in two parts. In the first part, we predict that an interplay between Coulomb interaction and strong Rashba coupling leads to a transition to orbital ferromagnetism in few-electron $N \leqslant 10$ quantum dots. In the regime of ultrastrong Rashba coupling $\alpha \to \infty$ for two electrons, an analytical study shows that an arbitrarily weak interaction induces a large magnetization, which reflects that the orbital angular momentum is behind the effect. For $\alpha = 10$ and $\alpha = 15$, the results of exact-diagonalization technique for $N = 2$ and $N = 3$ indicate that a spontaneous magnetization emerges if the interaction strength exceeds a critical value $\lambda > \lambda_c$. Finally, a Hartree-Fock calculation for $\alpha = 30$ and number of electrons up to $N = 10$ shall be given which reproduces the effect qualitatively. In the second part, we present the study of the many-body system containing large but finite number of electrons $N \lesssim \alpha$. For very weak interactions, the Hamiltonian is bosonized and several correlation functions are computed. Remarkably, we show that Kramers pairs are correlated strongly. Moreover, we establish a connection between our system and the well-studied Richardson pairing model and 1D Heisenberg XXZ spin chain.

Zusammenfassung

In dieser Arbeit diskutieren wir ein zweidimensionales, wechselwirkendes Elektronengas unter Einfluss einer parabolischen Falle und starker Rashba Spin-Bahn Kopplung. Das System wird hierbei durch dimensionslose Parameter für Rashba-Kopplung $\alpha \gg 1$ und Wechselwirkungsstärke $\lambda \lesssim 1$ beschrieben. Auf dem Niveau einer Einzel -Teilchen Beschreibung zeigt sich ein Spektrum, das sich aus Landau-artigen Energiebändern, und einem entkoppelten Rotor, ausgedrückt durch den Gesamtdrehimpuls J, zusammensetzt. Die entsprechende Nieder-Energie Physik kann auf einem Ring im Impulsraum beschrieben werden. Dies hat zur Folge, dass zwei Arten von Wechselwirkungen verstärkt werden, namentlich die Wechselwirkung zwischen Kramers-Paaren und die Austauschwechselwirkung. Wir diskutieren die Grundzustände des Systems in zwei Abschnitten: Im ersten Teil finden wir, dass ein Zusammenspiel von Coulomb-Wechselwirkung und starker Rashba-Kopplung in Quantenpunkten mit $N \leq 10$ Elektronen zu orbitalem Ferromagnetismus führt. Im Regime extrem starker Rashba-Kopplung $\alpha \to \infty$ für zwei Elektronen zeigt unser analytischer Ansatz, dass beliebig schwache Wechselwirkung eine Magnetisierung hervorruft. Dies spiegelt wider, dass der Bahndrehimpuls für den Effekt verantwortlich ist. Für Rashba-Kopplungsstärken $\alpha = 10$ und $\alpha = 15$ deuten unsere Ergebnisse einer exakten Diagonalisierung mit $N = 2$ und $N = 3$ Elektronen die Entstehung einer spontanen Magnetisierung an, sobald die Wechselwirkungsstärke einen kritischen Wert $\lambda > \lambda_c$ übersteigt. Zuletzt präsentieren wir Hartee-Fock Rechnungen für Rashba-Kopplung $\alpha = 30$ und bis zu $N = 10$ Elektronen, die diesen Effekt qualitativ reproduzieren. Im zweiten Teil betrachten wir ein System mit großer (aber endlicher) Zahl von Elektronen $N \lesssim \alpha$. Hier bosonisieren wir den Hamiltonian für sehr schwache Wechselwirkungsstärken, und berechnen verschiedene Korrelationsfunktionen. Insbesondere zeigen wir, dass in diesem Fall die Kramers-Paare stark korreliert sind. Abschließend diskutieren wir die Verbindung zwischen unserem System, und anderen wohlbekannten Modellen, wie dem Richardson pairing Modell und der 1D Heisenberg Spin-Kette.

Acknowledgement

I would like to acknowledge my deep gratitude to Prof. Dr. Reinhold Egger for giving the chance to me to explore the exciting physics presented herein. I also wish to appreciate fruitful discussions, debates and collaborations which I had with him and Dr. Alex Zazunov throughout the past years. I am also grateful to my colleagues at Institute für Theoretische Physik IV for their help and support. I wish to express my special thanks to Laura Cohnitz and Stephan Plugge, particularly for translating the abstract of this thesis into German. The last but not the least, I acknowledge my gratitude to Dr. Peter Schmitteckert for his DMRG calculation presented herein.

Contents

List of Figures

Chapter 1

Introduction

The conventional framework of quantum condensed matter physics relies mainly on the Landau's Fermi liquid and symmetry-breaking theory [1, 39]. The discovery of quantum Hall effects [58] in two-dimensional (2D) electron gases were among those triumphs late in twentieth century which challenged the well-established methods in the field. The electrical resistance in quantum Hall systems can be measured with the unprecedented high precision in spite of rough samples and poor control over details of apparatuses. The satisfactory explanation of the phenomena is involved in topological arguments which are beyond the conventional theories. The integer quantum Hall states constitute the first realized topological insulators which are characterized by an insulating gap in the bulk regime and gapless edge modes [53, 37]. The observation of the effect requires high magnetic fields at extremely low temperature which can only be realized in highly specialized laboratories.

The theoretical explanation of quantum Hall effect led to construction of generalized models which give rise to new classes of topological state [118, 119]. In contrast to the quantum Hall effect, the class of topological insulators with time-reversal symmetry was predicted theoretically first and later observed experimentally [48, 83] almost a decade ago. They rely on the strong spin-orbit coupling (SOC) [108, 41] rather than the magnetic field. SOC locks the spin of an electron to its momentum and can be considered as an effective magnetic field. The absence of an external magnetic field retains the time-reversal symmetry of the systems and renders totally a new class of topological state which is called quantum spin Hall insulator in two spatial dimensions [48, 83]. These topological phases are also insulator in the bulk regime but support an odd number of helical edge states. That is counter-propagating pairs of electrons with opposite spin orientation are present at the edges of the materials. These spin currents are dissipationless and supply potential applications in low power electronic devices and spintronic [81].

SOC has also found crucial roles in the research activities with considerable fundamental interest. The proximity effect of s-wave superconductors and spin-orbit coupled materials are the candidates to realize Majorana fermions [2, 34]. This fermion is its own antiparticle which is not observed unambiguously since its original prediction in high-energy physics.

Experimental discovery of Majorana fermions has become one of the main pursuing themes in the recent solid-state physics as it promises fault tolerant quantum computing [57]. There are also recent proposals for realization of Majorana fermions in spin-orbit coupled materials which exhibit superconducting instability within repulsive electronic gases [38, 92]. That is based on the fact that SOC enhances the instability against superconductivity even in repulsive 2D electron gases [103]. This is in the same spirit of the Kohn-Luttinger effect which is an electronic mechanism for superconductivity [60] but appears to be very weak in 2D systems [26, 84].

The fascinating physics realized through engaging SOC have stimulated intensive researches both theoretically and experimentally to tailor new spin-orbit coupled materials and explore their novel physics in the past decade. The scientific curiosity underlying this thesis has been flourished on this ground. We study effects of the strong SOC on a 2D system of interacting electrons in the presence of a parabolic trap theoretically. In fact, such a system models the electronic gas confined at the interface of different semiconductors and commonly is referred as quantum dots [88]. At the few-electron level, the electronic properties of quantum dots in semiconductor nanostructure have been extensively studied over the past decades [77, 88]. In the absence of SOC and interaction, the electrostatic confinement of electrons results in a simple 2D harmonic oscillator. However, the role of Coulomb interactions in such devises cannot be dismissed. Apart from the ubiquitous impact of the Coulomb interactions on transport spectroscopy [77], a transition to a finite-size Wigner crystallization is predicted to be induced by a strong Coulomb potential [116, 7]. The "Wigner molecule" is characterized by the suppression of fluctuations due to the electrostatic repulsion and maximizing the interelectron distances [54, 16, 12]. SOC is present at the semiconductor interfaces due to the inversion-asymmetry [108] which modifies the spectrum of the 2D oscillator. We focus on the Rashba term herein which is often the dominant SOC and can be tuned by gate voltages [108]. Though, we expect that other types of SOC generate similar type of physics presented herein. Study of such a setup has been done in different regime of parameters. For instance, the single-particle spectrum of a dot with weak Rashba coupling is discussed in [105, 82], and the effect of interactions in such a dot is considered with density-functional theory [46], quantum Monte Carlo simulations [35, 106, 4], exact diagonalization [30, 29, 24], and configuration-interaction calculations [22]. The transition to Wigner molecule is found to take place for weaker interactions. Also, the related bulk Wigner crystallization is found to be enhanced with Rashba coupling [13, 97].

In this thesis, we are interested in the strong Rashba coupling which appears to be within close experimental reach [72, 115, 56]. Given the above developments, it is not surprising that several theoretical works have already discussed the physics of noninteracting electrons in strong Rashba dots [67, 66, 87, 42, 32]. In this regime, the low-energy single-particle spectrum shows almost degenerate Landau-like bands, see chapter 3. Time-reversal symmetry of the system leads to the Kramers degeneracy and hence the system behaves as a helical liquid in which the counter-propagating electrons with equal but opposite total angular mo-

mentums are present in the absence of interaction. In fact, by virtue of the bulk-boundary correspondence [48], the authors of Ref. [67] argued that the noninteracting strong Rashba dot has features similar to the finite-size version of a 2D topological insulator. The almost flat single-body dispersion leads to the profound effect of interactions. For instance, lattice models in the regime of weak interactions realize topological insulator while illustrate a transition to Mott-insulator or spin-liquid phases for strong interactions [109]. In the case of interacting bosons with strong Rashba coupling see [111, 95, 51, 114, 121]. Furthermore, the interplay of a single-particle potential and Coulomb interaction can induce umklapp processes which destroy the helical edge states [113, 110]. Moreover, a prediction of magnetization in interacting quantum dots with Rashba SOC has been recently reported [11] which is quite relevant to the results discussed herein.

Motivated by these developments, we study ground state of interacting electrons in a 2D space in the presence of a trap and strong Rashba coupling. The system at single-particle level has two characteristic length scales. The first is the confinement length scale $l_T = \sqrt{\hbar/m_{\rm e}\omega}$ where ω is the trap frequency and $m_{\rm e}$ is the effective mass. The second is the inverse Rashba wavenumber k_0^{-1} which determines the strength of Rashba term. One of the control parameters in the system is the dimensionless Rashba coupling $\alpha = l_T k_0$. We study the strong $\alpha \gg 1$ and ultrastrong $\alpha \to \infty$ Rashba coupling separately. The other control parameter is the dimensionless interaction strength $\lambda = l_T/a_B$ where $a_B = \hbar^2\varepsilon_0/m_{\rm e}e^2$ is the Bohr radius. The dielectric constant ε_0 accounts for the static external screening of the interaction potential. The structure of this thesis is laid out as follows.

In chapter 2, we briefly review the spin-orbit coupling effect in the nonrelativistic quantum mechanic and mention several condensed matter systems in which the strong Rashba coupling can be expected. The single-body Hamiltonian which describes our system is discussed in chapter 3. In the regime of strong Rashba SOC, a low-energy Hamiltonian can be derived which allows writing down the eigenfunction of the system analytically. The eigenenergy includes the spectrum of a 1D oscillator corresponding to the radial degree of freedom with the band indices $n = 0, 1, 2, \cdots$ and a decoupled rotor in terms of the total angular momentum J, which is a half-odd-integer number. Since we are interested later in the regime of weak-to-intermediate interaction strength, a single-band approximation $n = 0$ is introduced which provides possibility of analytical progress. The low-energy excitations are localized around a ring in momentum space which indicates the system is quasi-one dimensional. Furthermore, two different approaches of taking the limit $\alpha \to \infty$ are considered and the associated eigenfunctions are presented. In one of them, the trap is switched off asymptotically $\omega \to 0$ while the other maintains the trap. The significance of these two approaches will be discussed in following chapters.

In chapter 4, interaction matrix elements (IMEs) are presented. First, we discuss the symmetry relations of IMEs represented in the eigenbasis. It will be shown that the interplay between the time reversal symmetry of a interaction potential and the eigenbasis induces phase constraints on the matrix elements i.e how the sign of IMEs alters. Next, the nu-

merical values of matrix elements, for Coulomb and contact potentials, are presented. The matrix elements are nonuniform in the sense that their magnitudes depend to the momentums of interacting particles and the exchanged momentum. We will discuss that the maximum absolute magnitude of matrix elements take place for two types of interactions: either while the net angular momentum of interacting particles is zero, which is called BCS-like interaction, or when two interacting particles exchange their momentum, which is called exchange-type interaction. The reason of boosted IMEs is based on the peculiarity of scattering processes on the momentum-space ring, which is caused by strong Rashba coupling. We investigate this fact by considering the limit $\alpha \to \infty$ through switching off the trap asymptotically $\omega \to 0$. It is worth mentioning that a toy model is proposed and studied, presented in appendix A, in order to clarify the intricate but physically rich features of the IMEs. In fact, one of the rewards is that having known how electrons are correlated in the interaction term gives rise to the insight into the competing phases intuitively, which is turned out to be non-trivial. Moreover, we discuss the Coulomb-matrix elements for $\alpha \to \infty$ through maintaining the trap. Although the matrix elements admit the symmetry relations mentioned before, an odd-even-parity effect arises in this regime where interactions with an odd exchanged momentum vanish identically. Weak interactions in the resulting model for $\alpha \to \infty$ induce already strongly correlated phases.

We present the ground states of Coulomb-interacting few-electron dots $N \leqslant 10$ in chapter 5. In the regime of $\alpha \to \infty$, an arbitrary weak interaction gives rise to a large magnetization $M \approx (\lambda\alpha)^{1/4}\hbar$ for $N = 2$. Such a large magnetization reflects that the orbital angular momentum is behind the phenomenon. The ground-state results derived by means of the exact-diagonalization technique, for $N = 2$ and $N = 3$ with Rashba coupling $\alpha = 10$ and $\alpha = 15$, demonstrate a transition to the orbital ferromagnetism for interaction strength exceeding a critical value $\lambda > \lambda_c$. The parameter λ_c becomes smaller with increase in α which is consistent with the results of $\alpha \to \infty$. We also present a few results obtained by density matrix renormalization group (DMRG) [107, 25, 93]. The DMRG technique is found to be able to reproduced the exact-diagonalization outcomes with a high accuracy. Study of our system by means of the DMRG technique is still in progress. In the end of this chapter, we discuss the results of Hartree-Fock calculations for the system containing up to $N \leqslant 10$ electrons and $\alpha = 30$, where the exact diagonalization becomes computationally too expensive. The Hartree-Fock calculations show qualitatively the same effect, reflecting that orbital ferromagnetism represents the generic behavior of weakly Coulomb-interacting electrons in quantum dots with strong Rashba coupling.

In chapter 6, we study the many-body system with a well-defined $J_F \sim \alpha$ where J_F is the Fermi momentum in the absence of interactions. α is assumed to be an arbitrary large number but finite. Therefore, we deal with a canonical ensemble. In the regime of very weak interactions, we estimate the matrix elements corresponding to the states close to the Fermi momentums $\pm J_F$ with a uniform coupling constant if the variations of the IMEs are small in comparison with the level spacing. The resulting effective model can be diagonalized readily and is amenable to bosonization, and hence, exact calculation of

correlation functions. Many intermediate calculations of bosonization and part of the results are relegated to appendix D in order to enhance the readability of the chapter. The remarkable outcome of the bosonization study is the strong correlation of Kramers pairs either for a repulsive or attractive coupling constant, which is a sign of superconductivity in grand canonical systems. Furthermore, the ground state is shown to be unmagnetized which is expected in the considered regime of weak interactions. Relying on the strong correlation, a uniform pairing Hamiltonian is constructed though for a repulsive pairing force. The model is shown to be equivalent to the Richardson pairing model which bears an exact solution. Although, without solving the model, we show that a transition is possible with increase in interaction strength even by means of such a truncated model. Having realized the important interaction channels in the considered regime, we construct an extended Hartree-Fock Hamiltonian. The model shall be shown to be equivalent to a 1D Heisenberg XXZ model. In principle, we are interested to engage the model and explore the chance of a transition to orbital ferromagnetism for electrons interacting with different type of potentials, e.g. Coulomb or contact potential. Although an analytical solution of the model is not found, it inspires us the application of numerical resolutions like the DMRG technique.

Part of the materials in chapters 3 and 4 and almost all the results presented in chapter 5 are published in [76]. Also the Hamiltonian in different regime of parameters is being solved by means of DMRG technique and the results are expected to be published in the near future.

Chapter 2

Spin-Orbit Coupling in Condensed-Matter Systems

In this chapter, we give a brief review of spin-orbit coupling in condensed-matter systems. The effect intuitively can be understood as follows. Consider an electron moving in the electric field $\mathbf{E}$ with velocity $\mathbf{v}$. A magnetic field $\mathbf{B}_{\text{eff}} = \mathbf{v} \times \mathbf{E}$ then appears in the rest frame of the electron according to the law of Lorentz transformation. The magnetic field is coupled to the spin angular momentum of the electron $\mathbf{s}$ which contributes to the Hamiltonian as a Zeeman term $\propto \mathbf{B}_{\text{eff}} \cdot \mathbf{s} = (\mathbf{v} \times \mathbf{E}) \cdot \mathbf{s}$. This intuitive picture describes the emergence of the Rashba spin splitting where the momentum of the electron is coupled with its spin. In the following, we consider formally the relativistic corrections to the Schrödinger equation [21, 108, 98, 94] which gives rise to the Rashba term. In principle, the spin-orbit coupling (SOC) appears as weak as the second order relativistic correction in $1/c$ .The relativistic corrections often in condensed-matter physics can be neglected since the electronic velocities v encountered in solid-state materials are smaller than the velocity of light c in several orders of magnitude $v/c \ll 1$. Though, there are situations where this effect can be magnified and should be taken into account.

Consider an electron which is described by the Dirac equation. If we expand it in the powers of $1/c$, the Schrödinger equation in the presence of electromagnetic fields can be obtained in the first-order

$$H^{(1)} = \frac{1}{2m_{\text{e}}} \left[\mathbf{p} + e\mathbf{A}(\mathbf{r})\right]^2 + U(\mathbf{r}) - g_{\text{e}}\mu_{\text{B}}\mathbf{B} \cdot \mathbf{s}, \tag{2.1}$$

where m_{e} is the mass of the electron, $\mathbf{p}$ is the canonical momentum, $\mathbf{A}(\mathbf{r})$ and $U(\mathbf{r})$ are vector and scaler potential, $\mu_{\text{B}} = e\hbar/2m_{\text{e}}$, and g_{e} is the electron g-factor. The Pauli matrices $\boldsymbol{\sigma}$ are related to the spin operator as $\mathbf{s} = \frac{1}{2}\boldsymbol{\sigma}$. The terms second order in the powers of $1/c$ take the form

$$H^{(2)} = -\frac{1}{8m_{\text{e}}^3c^2} \left[\boldsymbol{\sigma} \cdot (\mathbf{p} + e\mathbf{A})\right]^4 + \frac{\hbar^2}{8m_{\text{e}}^2c^2}\nabla^2 U(\mathbf{r}) + \frac{\hbar}{4m_{\text{e}}^2c^2}\boldsymbol{\sigma} \cdot \left[\nabla U(\mathbf{r}) \times (\mathbf{p} + e\mathbf{A})\right]. \tag{2.2}$$

The first term contains correction to the kinetic and Zeeman energy which is negligible in solid-state physics. The second term is called Darwin term which in the atomic Coulomb potential is important only for s-electrons [98]. The last term is spin-orbit interaction. It can be written as a coupling of spin and orbital angular momentum term if the potential $U(\mathbf{r})$ is central, that is

$$\nabla U(\mathbf{r}) = \frac{dU(\mathbf{r})}{dr}\frac{\mathbf{r}}{r}. \tag{2.3}$$

Neglecting the vector potential, we obtain

$$H_{\mathrm{SO}}^{(\mathrm{I})} = \frac{\hbar^2}{2m_{\mathrm{e}}^2c^2}\frac{1}{r}\frac{dU(\mathbf{r})}{dr}\mathbf{L}\cdot\mathbf{s}, \tag{2.4}$$

where $\hbar\mathbf{L} = \mathbf{r}\times\mathbf{p}$ is the orbital angular momentum. It can be shown that this term gives a contribution $\propto Z^2$ for an atom with atomic number Z and therefore can be important for heavy elements while it is negligible for light elements. The spin-orbit-coupling term has the following form if $U(\mathbf{r})$ is the scaler potential of a uniform external electric field $\mathbf{E}$ along z direction perpendicular to the 2D plane

$$H_{\mathrm{SO}}^{(\mathrm{II})} = \gamma\left(\sigma_x p_y - \sigma_y p_x\right), \tag{2.5}$$

where the electric field is absorbed into γ. This term is called Rashba spin-orbit interaction which its effect in quantum dots is under focus in this thesis. Rashba coupling is often the dominant spin-orbit interaction in semiconductors. In addition, it can be tuned by gate voltages [108], in contrast to the other type spin-orbit interaction like the Dresselhaus coupling which is expected to have the similar physics as described herein. SOC is normally weak enough in semiconductors to be treated in perturbation theory [108]. Although, we consider strong Rashba coupling. This regime seems to be within close experimental reach [59, 72, 8, 9, 43, 115, 56, 74]. In principle, the electronic systems at interfaces of different semiconductors exhibit inversion-asymmetry which gives rise to SOC. Another possibility to realize the SOC in 2D systems is the electronic gases at oxide interferences [78, 55, 120, 50] which is discovered almost a decade ago and present correlated states unprecedented in conventional semiconductors interfaces. There is a growing research activity on the emergent properties at these new quantum wells [52]. Electron gases at oxide heterostructures manifest ferromagnetism and superconductivity which illustrate the promising potential of the oxide interfaces and stimulated intensive research to discover novel physics of the 2D electron gases. Also, it is worth noting that there is an active research in the field of ultracold quantum gases to engineer variety of SOCs [41, 117]. Internal degrees of freedom of cold atoms can be coupled with laser fields that render synthesis SOC. Cold gases are highly tunable and can be prepared on demand. Particularly, the inter-particle interactions of the cold atoms can be designed which makes them one of the suitable candidates to testify the predictions made in this thesis. In the following chapters, we present first the model Hamiltonian which describes a single electron confined in a 2D space in the presence of a parabolic trap and strong Rashba coupling. Next, we discuss the interaction-driven physics of the system in different regimes of control parameters.

Chapter 3

Single-Particle Hamiltonian

A Model Hamiltonian is introduced which describes a single electron in a two-dimensional (2D) space in the presence of a parabolic trap and Rashba spin-orbit coupling (SOC). In the regime of strong Rashba coupling, the low-energy physics is characterized by almost flat Landau-like bands. Effective eigenfunctions of the single-particle Hamiltonian is written in this regime. Two different limits of ultrastrong Rashba coupling and their corresponding eigenfunctions are presented, one corresponds to the localization of electrons on a ring in momentum space which does not admit the trap while the other one maintains the trap.

3.1 Model Hamiltonian

The following Hamiltonian describes a single electron with mass m confined in a 2D space in the presence of a parabolic trap and Rashba SOC

$$\mathrm{H}_0 = \frac{\mathbf{p}^2}{2m} + \frac{1}{2}m\omega^2\mathbf{r}^2 - \frac{\hbar k_0}{m}\boldsymbol{\sigma}\cdot(\mathbf{p}\times\hat{z}) + \frac{\hbar^2 k_0^2}{2m} \tag{3.1}$$

where $\mathbf{p} = (p_x, p_y)$ and $\mathbf{r} = (x, y)$, the trap frequency is ω, the strength of Rashba coupling is determined by k_0, and the Pauli matrices are $\boldsymbol{\sigma} = (\sigma_x, \sigma_y, \sigma_z)$. The constant term $\hbar^2 k_0^2/2m$ has been introduced for later convenience. The system enjoys time reversal symmetry $\mathcal{T}\mathrm{H}_0\mathcal{T}^{-1} = \mathrm{H}_0$ where the explicit form of the time reversal operator $\mathcal{T}$ is given below. Furthermore, the total angular momentum $J_z = L_z + \hbar\sigma_z/2$, with L_z the generator of rotation about $\hat{z}$, is conserved $[\mathrm{H}_0, J_z] = 0$. The trap breaks the translational symmetry $[\mathrm{H}_0, \mathbf{p}] \neq 0$ and the Rashba term breaks the parity symmetry of the system $[\mathrm{H}_0, \mathcal{P}] \neq 0$.

The Hamiltonian H_0 does not bear an exact solution. We attempt to expose the solutions of H_0 in different regimes. In the absence of the Rashba term $k_0 = 0$, the Hamiltonian reduces to a 2D harmonic oscillator which is exactly solvable. The eigenenergies are labeled by two band indices. If the trap is switched off $\omega = 0$, the helicity operator $\mathcal{P}_h = (k_y\sigma_x - k_x\sigma_y)/k$

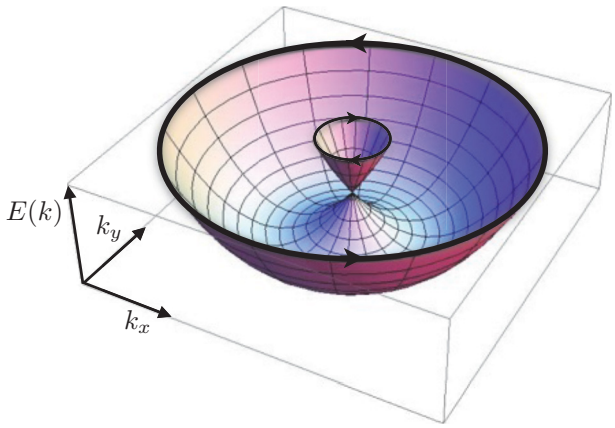

Figure 3.1: Dispersion of an electron with strength of Rashba SOC k_0 when the trap is switched off $\omega = 0$. The low-energy sector lies on a ring $k = k_0$ due to Rashba term. The polarization of spin is shown by the oriented black circles on top of the two bands.

is a conserved operator with eigenspinors

$$|\Phi_\pm(\phi)\rangle = \frac{1}{\sqrt{2}} \begin{pmatrix} \pm 1 \\ \\ -ie^{i\phi} \end{pmatrix} \tag{3.2}$$

where ϕ is the azimuthal angle in momentum space. The eigenvalues of the helicity operator read $\mathcal{P}_h|\Phi_\pm\rangle = \mp|\Phi_\pm\rangle$. The Hamiltonian for $\omega = 0$ is also exactly solvable with the dispersion $E(k) = \hbar^2(k \mp k_0)^2/2m$ which is illustrated in Fig. 3.1. The lowest-energy physics takes place over a ring in momentum space with the radius k_0 corresponding to the positive-helicity sector.

In the presence of both Rashba SOC and trap, the system has two characteristic length scale, the confinement scale $l_T = \sqrt{\hbar/m\omega}$ and the spin-orbit length k_0^{-1}. The ratio of these length scales defines the dimensionless Rashba coupling $\alpha = k_0 l_T$. In the regime of large Rashba coupling $\alpha \gg 1$, the slow and fast degrees of freedom can be separated with the aid of Born-Oppenheimer approximation [17].

3.2 Born-Oppenheimer Approximation

We are interested in the strong Rashba SOC $\alpha \gg 1$ where the negative helicity is separated by a gap $E_{\rm so} = \alpha^2\hbar\omega$ from the positive helicity and can be safely projected out. In principle, spin is the fast degree of freedom in the regime of $\alpha \gg 1$ and we can proceed with Born-Oppenheimer approximation. The projected low-energy Hamiltonian can be

derived through

$$H_0^+ = \langle\Phi_+|\mathrm{H}_0|\Phi_+\rangle \;\; = \;\; \frac{\hbar^2}{2m}\left(k - k_0^2\right) + \frac{m\omega^2}{2}\Big\{\langle\Phi_+|\mathbf{r}^2|\Phi_+\rangle + 2\langle\Phi_+|\mathbf{r}|\Phi_+\rangle + \mathbf{r}^2\Big\}. \quad (3.3)$$

We use the normalized spinor $\langle\Phi_+|\Phi_+\rangle = 1$ to simplify the relations in Eq. 3.3. Acting by $\mathbf{r}$ on the relation yields

$$\langle\Phi_+|\mathbf{r}\,\Phi_+\rangle + \langle\mathbf{r}\,\Phi_+|\Phi_+\rangle = 0, \quad (3.4)$$
$$\langle\Phi_+|\mathbf{r}^2\,\Phi_+\rangle + 2\langle\mathbf{r}\,\Phi_+|\mathbf{r}\,\Phi_+\rangle + \langle\mathbf{r}^2\,\Phi_+|\Phi_+\rangle = 0, \quad (3.5)$$

where for the sake of consistency, we put $\langle\Phi_+|\mathbf{r}\,\Phi_+\rangle \equiv \langle\Phi_+|\mathbf{r}|\Phi_+\rangle$. In the momentum space, we have $\mathbf{r} = i\nabla_{\mathbf{k}}$ where in the cylindrical coordinate takes the form $\nabla_{\mathbf{k}} = \partial_k\hat{e}_k + \frac{1}{k}\partial_\phi\hat{e}_\phi$. With the aid of the the Berry connection [112]

$$\mathcal{A}_{\mathbf{k}} = -i\langle\Phi_+|\nabla_{\mathbf{k}}|\Phi_+\rangle = \frac{1}{2k}\hat{e}_\phi, \quad (3.6)$$

the projected Hamiltonian reads

$$H_0^+ = \frac{\hbar^2}{2m}\left(k - k_0^2\right) + \frac{m\omega^2}{2}\left(i\nabla_{\mathbf{k}} - \mathcal{A}_{\mathbf{k}}\right)^2 + V_{\mathrm{BO}}\left(\mathbf{k}\right), \quad (3.7)$$

where Born-Oppenheimer potential is defined by

$$V_{\mathrm{BO}}\left(\mathbf{k}\right) = \frac{m\omega^2}{2}\Big\{\langle\nabla_{\mathbf{k}}\,\Phi_+|\nabla_{\mathbf{k}}\,\Phi_+\rangle - \langle\nabla_{\mathbf{k}}\,\Phi_+|\Phi_+\rangle\langle\Phi_+|\nabla_{\mathbf{k}}\,\Phi_+\rangle\Big\} = \frac{m\omega^2}{8k^2}. \quad (3.8)$$

From here on, the unit of length is set to l_T and we measure energy in the unit of $\hbar\omega$, therefore, we drop $\hbar\omega$ and define dimensionless variables $\kappa = kl_T$ and $\varrho = r/l_T$. Collecting the terms in the projected Hamiltonian H_0^+ gives

$$H_0^+ \;\; = \;\; \frac{1}{2}\left(\kappa - \alpha^2\right) - \frac{1}{2}\frac{\partial^2}{\partial\kappa^2} - \frac{1}{2\kappa}\frac{\partial}{\partial\kappa} + \frac{1}{2\kappa^2}\left(L_z + \frac{1}{2}\right)^2 + \frac{1}{8\kappa^2}, \quad (3.9)$$

where $L_z = -i\partial_\phi$ with integral eigenvalues $m \in \mathbb{Z}$. The gauge field Eq. 3.6 induces a half flux-quantum magnetic field threading the system through z-axis in momentum space [42]. Engaging the ansatz $u(\kappa)\,e^{im\phi}/\sqrt{\kappa}$ and the following relation

$$\left(\frac{\partial^2}{\partial\kappa^2} + \frac{1}{\kappa}\frac{\partial}{\partial\kappa} - \frac{1}{4\kappa^2}\right)\frac{u}{\sqrt{\kappa}} = \frac{1}{\sqrt{\kappa}}\frac{\partial^2 u}{\partial\kappa^2}, \quad (3.10)$$

we require then to solve the radial 1D eigenvalue problem for given $J = m + \frac{1}{2}$

$$\left(-\frac{\partial^2}{\partial\kappa^2} + \frac{1}{2}\left(\kappa - \alpha\right)^2 + \frac{J^2}{2\kappa^2} - E_{n,J}\right)u_{n,J}(\kappa) = 0, \quad (3.11)$$

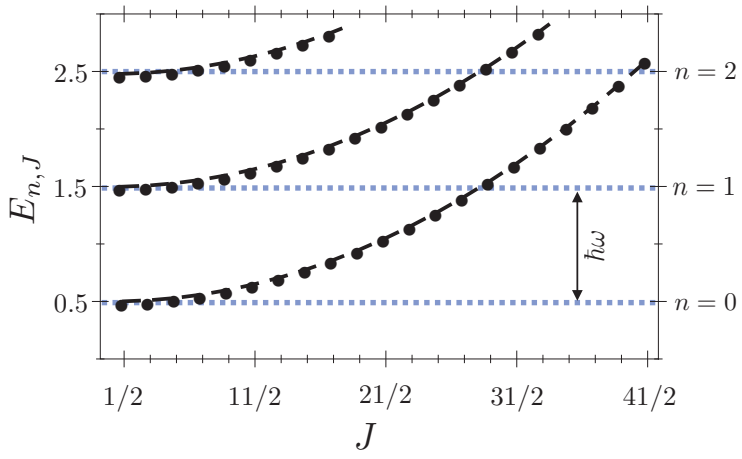

Figure 3.2: Dispersion of the low-energy projected Hamiltonian in Eq. 3.13 illustrated versus positive total angular momentum $J > 0$ for several band indices. The dimensionless Rashba coupling is set to $\alpha = 10$. The energies of eigenstates in a given band are connected by a thick dashed line as a guide to the eye. The thin dashed blue lines show the bottom of each band which are gapped by an energy $\hbar\omega$.

to find out the low-energy eigenstate

$$\psi_{n,J}(\kappa, \phi) = \frac{e^{i(J-1/2)\phi}}{\sqrt{2\pi\kappa}} u_{n,J}(\kappa)\Phi_+(\phi), \tag{3.12}$$

where n is the radial number. In the regime of $\alpha \gg 1$, we approximate $J^2/2\kappa^2 \to J^2/2\alpha^2$ since the low-energy states are expected to be localized around the deep valley defined by the 1D harmonic trap in Eq. 3.11. Thus, we neglect the correction in the order of $1/\alpha^3$. Consequently, the angular degree of freedom is decoupled from the radial one. The eigenvalue problem in Eq. 3.11 then becomes a shifted 1D harmonic oscillator plus a rigid rotor problem with the moment of inertia $1/\alpha^2$. The energy takes the form

$$E_{n,J} = n + \frac{1}{2} + \frac{J^2}{2\alpha^2}, \tag{3.13}$$

where $n = 0, 1, 2, \cdots$ labels the band index. A plot of $E_{n,J}$ is given in Fig. 3.2 which resembles Landau-like bands. The eigenvalue is turned out to be highly accurate for $\alpha \gtrsim 4$ according to the numerical calculation which is performed on the Hamiltonian in Eq. 3.1.

3.3 Single-Band Approximation

In the regime of weak-to-intermediate Coulomb-interaction strength, discussed in the following chapters, we consider only the zeroth band $n = 0$ given the Fermi momentum is

set within the band $J_F \lesssim \alpha$. Accordingly, the excitations within the zeroth band are considered and from here on we drop the index n. This scheme will be called the single-band approximation. The low-energy Hilbert space is spanned by the basis constructed from orthonormal eigenfunctions

$$\psi_J(\kappa,\phi) = \frac{\pi^{1/4} l_T}{\sqrt{\kappa}} e^{-(\kappa-\alpha)^2/2} \begin{pmatrix} e^{i(J-1/2)\phi} \\ \\ -ie^{i(J+1/2)\phi} \end{pmatrix}. \tag{3.14}$$

The corresponding energy is $E_J = J^2/2\alpha^2$ regardless of the c-number contribution. The momentum-space density of probability is independent of J and concentrated around a ring $k = k_0$ with a Gaussian distribution

$$\rho(k) = \frac{2\sqrt{\pi} l_T}{k} e^{-(k-k_0)^2 l_T^2}. \tag{3.15}$$

We study the time-reversal (TR) symmetry of the eigenfunctions. TR operator can be constructed as $\Theta = \sigma_y U K$ in which σ_y is the Pauli matrix, U is a unitary operator and K is the conjugation operator [91]. The TR operator acts merely on the angular part of the eigenfunction in Eq. 3.14. The time-reversed partner of $\psi_J(\kappa,\phi)$ is

$$\begin{aligned} \Theta\,\psi_J(\kappa,\phi) &= \sigma_y U K \frac{\pi^{1/4} l_T}{\sqrt{\kappa}} e^{-(\kappa-\alpha)^2/2} \begin{pmatrix} e^{i(J-1/2)\phi} \\ \\ -ie^{i(J+1/2)\phi} \end{pmatrix} \\ &= \begin{pmatrix} 0 & -i \\ i & 0 \end{pmatrix} \frac{\pi^{1/4} l_T}{\sqrt{\kappa}} e^{-(\kappa-\alpha)^2/2} \begin{pmatrix} e^{-i(J-\frac{1}{2})(\phi+\pi)} \\ \\ ie^{-i(J+\frac{1}{2})(\phi+\pi)} \end{pmatrix} \\ &= (-1)^{J+\frac{1}{2}}\,\psi_{-J}(\kappa,\phi), \end{aligned} \tag{3.16}$$

and obviously $\Theta^2 = -1$ which is the characteristic of spin-1/2, or more specifically, J half-integer states. Therefore, in the Dirac bracket notation, the relation takes the following from

$$\Theta|\psi_J\rangle = (-1)^{J+1/2}|\psi_{-J}\rangle. \tag{3.17}$$

With the help of the identity in Eq. 3.16, a symmetry relation for the matrix elements of a one-body potential V, even or odd under TR $\Theta V \Theta^{-1} = \pm V$, can be derived

$$\langle\psi_J|V|\psi_{J'}\rangle = \pm(-1)^{J+J'+1}\langle\psi_{-J'}|V|\psi_{-J}\rangle. \tag{3.18}$$

It can be readily seen that V cannot mix time-reversed partners $\langle\psi_J|V|\psi_{-J}\rangle = 0$ if $\Theta V \Theta^{-1} = V$, and the diagonal elements also vanish $\langle\psi_J|V|\psi_J\rangle = 0$ if $\Theta V \Theta^{-1} = -V$. In the next chapter, we will discuss the peculiar symmetry relations for matrix elements

of a two-body potential as the consequence of the TR symmetry. The coordinate-space representation of $\psi_J(\kappa,\phi)$ can be derived by a Fourier transform

$$\tilde{\psi}_J(\varrho,\theta)=\frac{i^{J-1/2}}{l_T}e^{i(J-1/2)\theta}\begin{pmatrix}F_{J-1/2}(\varrho)\\ \\ e^{i\theta}F_{J+1/2}(\varrho)\end{pmatrix}, \tag{3.19}$$

and the auxiliary function is

$$F_m(\varrho)=\int_0^\infty \frac{d\kappa\sqrt{\kappa}}{2\pi^{3/4}}e^{-(\kappa-\alpha)^2/2}\,J_m(\kappa\varrho), \tag{3.20}$$

and $J_m(x)$ is the Bessel function for $m\in\mathbb{Z}$. We will use the coordinate representation to compute interaction matrix elements since it is more convenient for numerical calculation.

We study asymptotic forms of $\psi_J(\mathbf{k})$ and $\tilde{\psi}_J(\mathbf{r})$ as they will be used in the regime of ultra strong Rashba coupling $\alpha\to\infty$. The limit $\alpha=k_0l_T\to\infty$ can be taken formally in two ways. The first one, by holding k_0 finite and taking $l_T\to\infty$. In fact, this approach leads to a homogeneous system by switching off the trap $\omega\to 0$ and makes the single band approximation ill-defined i.e. the band gap $\hbar\omega$ shrinks to zero. Although, the representation of interaction matrix elements by means of this asymptotic form provides valuable insight in clarifying the features of finite α system, see the next chapter.

The density of probability in Eq. 3.15 becomes $\rho(k)=(2\pi/k_0)\delta(k-k_0)$ which describes localization on a ring in momentum space $k=k_0$. Therefore, $\psi_J(\kappa,\phi)$ behaves as

$$\lim_{\alpha\to\infty}\psi_J(\mathbf{k})=\sqrt{\frac{2\pi^{3/2}}{k_0l_T}}\delta(k-k_0)\begin{pmatrix}e^{i(J-1/2)\phi}\\ \\ -ie^{i(J+1/2)\phi}\end{pmatrix}. \tag{3.21}$$

Since the radial degree of freedom is not affected by TR operator, the asymptotic wavefunction behaves in the same way as $|\psi_J\rangle$ under the operation of Θ

$$\Theta\lim_{\alpha\to\infty}\psi_J(\mathbf{k})=(-1)^{J+\frac{1}{2}}\lim_{\alpha\to\infty}\psi_{-J}(\mathbf{k}). \tag{3.22}$$

The Second approach is to take the limit by holding l_T finite versus $k_0\to\infty$. The integral representation of the auxiliary function can be evaluated in this regime

$$F_m(\varrho)=\int_{-\alpha}^\infty \frac{d\bar{\kappa}\sqrt{\kappa}}{2\pi^{3/4}}e^{-\bar{\kappa}^2/2}\,J_m(\alpha\varrho+\bar{\kappa}\varrho), \tag{3.23}$$

by asymptotic expansion of Bessel function

$$J_m(z)\approx\sqrt{\frac{2}{\pi z}}\cos(z-\frac{m\pi}{2}-\frac{\pi}{2})+\mathcal{O}(1/z). \tag{3.24}$$

We replace the square root of κ in Eq. 3.23 by $\sqrt{\alpha}$ in the regime of large α and with the aid of the asymptotic expansion of the Bessel function, we obtain

$$\lim_{\alpha\to\infty}\tilde{\psi}_J(\varrho,\theta)=\frac{i^{J-1/2}e^{i(J-1/2)\theta}e^{-\varrho^2/2}}{\pi^{3/4}l_T\sqrt{\varrho}}\begin{pmatrix}\cos\left(\alpha\varrho-\pi J/2\right)\\ \\ e^{i\theta}\sin\left(\alpha\varrho-\pi J/2\right)\end{pmatrix}. \tag{3.25}$$

On the contrary to the asymptotic form of $\psi_J(\mathbf{k})$ in Eq. 3.21, the Gaussian factor $e^{-\varrho}$ in Eq. 3.25 reflects the trap. Different forms of the eigenfunctions in $\alpha\gg 1$ will be engaged to describe the interacting system in different regimes.

3.4 Second Quantized Representation

We proceed to represent the single-particle Hamiltonian in a second quantized representation

$$H_0=\hbar\omega\sum_J\frac{J^2}{2\alpha^2}c_J^\dagger c_J, \tag{3.26}$$

where we have restored the energy unit $\hbar\omega$. The fermion creation and annihilation operators $c_J^\dagger$ and c_J, respectively, obey anticommutation relation $\{c_J^\dagger,c_{J'}\}=\delta_{JJ'}$. The TR of the operators can be constructed from the relation in Eq. 3.16

$$\Theta c_J^\dagger=(-1)^{J+1/2}c_{-J}^\dagger. \tag{3.27}$$

The field operators in the momentum- and coordinate-space are given by

$$\Psi(\mathbf{k}) = \sum_J\psi_J(\mathbf{k})c_J, \tag{3.28}$$

$$\tilde{\Psi}(\mathbf{r}) = \sum_J\tilde{\psi}_J(\mathbf{r})c_J, \tag{3.29}$$

where the eigenfunctions in Eqs. 3.14 and 3.19 are used. The ground state in the non-interacting system constructs a Fermi sea with all the states occupied up to Fermi points $|J|\leq J_F\lesssim\alpha$. The ground state for an even number of particles $N=2J_F+1$ is unique and has the energy

$$E_0=\hbar\omega N(N^2-1)/24\alpha^2. \tag{3.30}$$

Although, the ground state is twofold degenerate for odd N. One of the crucial quantity herein is the net total angular momentum, which we call it magnetization from here on, and is defined as the sum of the total angular momentum of all the electrons. The corresponding operator in the first quantization reads

$$\sum_{i=1}^N J_{z_i}=\hbar\sum_{i=1}^N(-i\partial_{\phi_i}+\sigma_{z_i}/2), \tag{3.31}$$

and in the second quantization

$$\hat{M} = \hbar \sum_J J c_J^\dagger c_J. \tag{3.32}$$

The conservation of $\hat{M}$ follows from the conservation of total angular momentum $[J_z, H_0] = 0$. The ground state expectation value of magnetization $\langle \hat{M} \rangle_0$ in the non-interacting regime is zero in the case of even number of particles and, otherwise, has a value equal to $\pm\hbar J_F$. We discuss later how the interaction can magnetize the system spontaneously.

3.5 Summary

The system is time-reversal invariant and also conserves the total angular momentum. Although, the parity is broken and the system is not translationally invariant. A single-body Hamiltonian is introduced which describes an electron confined in a 2D space in the presence of a parabolic trap and Rashba SOC. In the regime of strong Rashba Coupling, the effective eigenfunctions indicate that electrons are localized around a ring in momentum space. In the single-band approximation, the only dynamical degree of freedom is the total angular momentum. The ultrastrong limit of dimensionless Rashba coupling $\alpha \to \infty$ leads to two different asymptotic forms. One corresponds to the localization of electrons on the momentum-space ring by holding k_0 finite while switching off the trap $\omega \to 0$. The second asymptotic form is achieved by maintaining the trap and taking the limit $k_0 \to \infty$. It will be shown in chapters 4 that both the asymptotic forms give rise to an odd-even parity for Coulomb-matrix elements. Although, in the resulting model of $\alpha \to \infty$, a very weak interaction induces correlated states.

Chapter 4

Interaction Matrix Elements

In this chapter, we discuss the representation of interaction potentials in the eigenbasis of the system. The matrix elements of Coulomb and contact potentials are presented. We introduce the partial time-reversal symmetry of interaction potentials to study the symmetry relation of interaction matrix elements (IMEs). In fact, using the time-reversal symmetry of eigenbasis and partial time-reversal symmetry of interaction potentials, we derive the phase constraints on IMEs. The IMEs in the regime of ultrastrong Rashba coupling $\alpha \to \infty$ are also discussed. In this limit, the kinetic term vanishes. Therefore, the ultrastrong Rashba-coupling limits are called flat-band model. The limit by $l_T \to \infty$ and holding k_0 finite realizes a ring in momentum space and makes it possible to explain the boosted elements of BCS-like and exchange-type interactions in the case of finite α. We call the resulting model in this limit "flat-band model in momentum space". Moreover, the Coulomb-matrix elements in the regime of $\alpha \to \infty$, through keeping l_T finite versus $k_0 \to \infty$, are presented which show an odd-even-parity effect. That is interactions with an odd exchanged momentum vanishes identically. The model in the latter limit is distinct by the name "flat-band model in coordinate space".

4.1 Symmetry Relations of Interaction Matrix Elements

Switching on the inter-particle interaction, the full Hamiltonian $H = H_0 + H_I$ incorporates kinetic term H_0 and the interaction term H_I. The second quantized representation of H is written formally as

$$H = \hbar\omega \sum_J \frac{J^2}{2\alpha^2} c_J^\dagger c_J + \frac{1}{2} \sum_{\substack{J_1,J_2 \\ J_1',J_2'}} \langle \psi_{J_1'}, \psi_{J_2'} | V | \psi_{J_2}, \psi_{J_1} \rangle c_{J_1'}^\dagger c_{J_2'}^\dagger c_{J_2} c_{J_1}, \tag{4.1}$$

where $c_J^\dagger$ (c_J) creates (annihilates) an electron with angular momentum $J \in \mathbb{Z} + 1/2$. The fermion operators satisfy the anticommutation relation $\{c_J^\dagger, c_{J'}\} = \delta_{J,J'}$. We study the symmetry relations of IMEs $\langle \psi_{J_1'}, \psi_{J_2'} | V | \psi_{J_2}, \psi_{J_1} \rangle$ in this bracket representation. In the

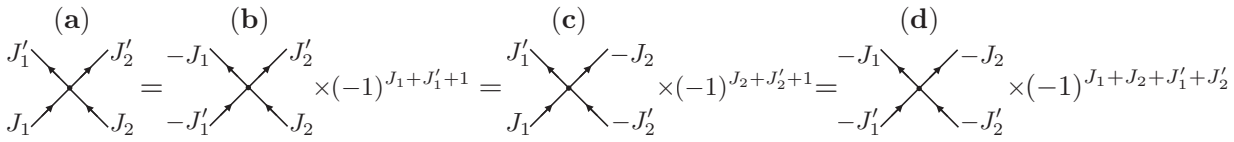

Figure 4.1: The corresponding scattering processes of matrix elements which are equivalent under partial time reversal up to a phase factor. The TR in each single-particle Hilbert space reverses the motion of particles and exchanges outgoing particle with the incoming one. For instance, in the process **(a)**, $J_{1,2}$ and $J'_{1,2}$ can be taken to be incoming and outgoing particles, respectively. Under partial TR on J_1 and J'_1, the angular momentums of the incoming and outgoing particles are reversed and exchanged to become $-J'_1$ and $-J_1$, respectively, depicted in the process **(b)**, in spite of the intact incoming and outgoing momentums of the other pair J_2 and J'_2. Furthermore, a phase factor $(-1)^{J_1+J'_1+1}$ is generated under the partial TR. In the process **(c)**, the partial TR is carried out on the pair J_2 and J'_2 while J_1 and J'_1 are left intact in comparison with the process in **(a)**. Finally, the whole scattering process is reversed in **(d)** and is multiplied with the appropriate phase factor.

following sections, we write them in concrete eigenbases of the system which are derived in the preceding chapter. We begin by considering the hermicity $V^\dagger = V$, which gives rise to the following relation between IMEs

$$\langle \psi_{J'_1}, \psi_{J'_2} | V | \psi_{J_2}, \psi_{J_1} \rangle = \langle \psi_{J_1}, \psi_{J_2} | V | \psi_{J'_2}, \psi_{J'_1} \rangle, \tag{4.2}$$

independent of the representation obviously. Indistinguishability of particles yields

$$\langle \psi_{J'_1}, \psi_{J'_2} | V | \psi_{J_2}, \psi_{J_1} \rangle = \langle \psi_{J'_2}, \psi_{J'_1} | V | \psi_{J_1}, \psi_{J_2} \rangle. \tag{4.3}$$

Next, we investigate the consequences of time reversal (TR) symmetry on the IMEs. In fact, a two-body potential connects two Hilbert spaces, i.e.V connects the two-body state $|\psi_J,\, \psi_{J'}\rangle$ to $\langle \psi_{J'_1}, \psi_{J'_2}|$. Although, we are going to analysis the representation of V in the basis by means of the single-particle TR operator Θ. Suppose $\Theta V \Theta^{-1} = V$ that means V is even under TR invariant in each of the Hilbert spaces which we call it partial TR. Note that V is a two-body potential but Θ is a single-body operator. TR symmetry of the basis, Eq. 3.17, induces phase restrictions on the matrix elements of V

$$\begin{aligned}
\langle \psi_{J'_1}, \psi_{J'_2} | V | \psi_{J_2}, \psi_{J_1} \rangle &= \langle \psi_{-J_1}, \psi_{J'_2} | V | \psi_{J_2}, \psi_{-J'_1} \rangle (-1)^{J_1+J'_1+1} \\
&= \langle \psi_{J'_1}, \psi_{-J_2} | V | \psi_{-J'_2}, \psi_{J_1} \rangle (-1)^{J_2+J'_2+1} \\
&= \langle \psi_{-J'_1}, \psi_{-J'_2} | V | \psi_{-J'_2}, \psi_{-J'_1} \rangle (-1)^{J_1+J_2+J'_1+J'_2},
\end{aligned} \tag{4.4}$$

The relations are illustrated in Fig. 4.1. The operation of Θ reverses the motion of the particles which are in the same Hilbert space, and therefore, the incoming particle

becomes outgoing and vice versa. In Eq. 4.4, in the first line, the equality relation is induced by $\Theta|\psi_{J_1}\rangle = (-1)^{J_1+1/2}|\psi_{-J_1}\rangle$ and $\Theta|\psi_{J_1'}\rangle = (-1)^{J_1'+1/2}|\psi_{-J_1'}\rangle$, and in the second line by operation on $|\psi_{J_2}\rangle$ and $|\psi_{J_2'}\rangle$. Since the phase constraints on IMEs are stemmed from TR symmetry of $|\psi_J\rangle$, they are independent of the analytical form of V as far as $\Theta V \Theta^{-1} = V$. That is the case for Coulomb and contact potential. As we are interested in the rotational invariant potentials, the total angular momentum of interacting particles is conserved $J_1 + J_2 = J_1' + J_2'$. Introducing the exchanged angular momentum m, we write $J_{1,2}' = J_{1,2} \pm m$. The relations in Eq. 4.4 then take the form

$$\begin{aligned}\langle\psi_{J_1+m}, \psi_{J_2-m}|V|\psi_{J_2}, \psi_{J_1}\rangle &= (-1)^m\langle\psi_{-J_1}, \psi_{J_2-m}|V|\psi_{J_2}, \psi_{-J_1-m}\rangle \\ &= (-1)^m\langle\psi_{J_1+m}, \psi_{-J_2}|V|\psi_{-J_2+m}, \psi_{J_1}\rangle \\ &= \langle\psi_{-J_1}, \psi_{-J_2+m}|V|\psi_{-J_1-m}, \psi_{-J_2}\rangle, \end{aligned} \tag{4.5}$$

The immediate implication of the phase constraints is that direct scattering into the time-reversed partner $J \to -J$ is forbidden

$$\langle\psi_{-J}, \psi_{J'-2J}|V|\psi_{J'}, \psi_J\rangle = 0, \tag{4.6}$$

for arbitrary J' but the exchanged momentum $m = 2J$ which is an odd number. It is interesting to note that the phenomenon which is observed at the single-particle level, compare with the discussion after Eq. 3.18, persists in the two-body potential. Incidentally, we have shown in appendix B the similar symmetry relations discussed here persist in 2D and 3D isotropic systems.

4.2 Coulomb-Matrix Elements

In this section, the numerical value of matrix elements of Coulomb potential $V = e^2/\varepsilon_0 r$ in the eigenbasis of the system are presented in two regimes of strong $\alpha = k_0 l_T \gg 1$ and ultrastrong $\alpha \to \infty$ Rashba coupling. The limit $\alpha \to \infty$ vanishes the kinetic term $J^2/2\alpha^2 \to 0$, therefore, the model in this regime is called flat-band model. In the ultrastrong Rashba coupling, IMEs are studied separately for two different asymptotic wave-functions, namely, in momentum and coordinate representation which are introduced in Eqs. 3.21 and 3.25, respectively.

4.2.1 Finite Rashba Coupling

For finite α, it is more convenient to work in the coordinate-space representation. First, we define

$$\begin{aligned} V^{J_1,J_2}_{J_1',J_2'} &= \frac{1}{2}\langle\psi_{J_1'}, \psi_{J_2'}|V|\psi_{J_2}, \psi_{J_1}\rangle \\ &= \frac{1}{2}\int d\mathbf{r}_1 d\mathbf{r}_2\, \tilde{\psi}^\dagger_{J_1'}(\mathbf{r}_1)\tilde{\psi}^\dagger_{J_2'}(\mathbf{r}_2)\, V(\mathbf{r}_1 - \mathbf{r}_2)\, \tilde{\psi}_{J_2}(\mathbf{r}_2)\tilde{\psi}_{J_1}(\mathbf{r}_1) \end{aligned} \tag{4.7}$$

where the factor 1/2 is introduced to absorb all the numerical prefactor in the numerical definition of the matrix elements. Substituting the coordinate representation of $|\psi_J\rangle$

$$\tilde{\psi}_J(\varrho,\theta) = \frac{i^{J-1/2}}{l_T} e^{i(J-1/2)\theta} \begin{pmatrix} F_{J-1/2}(\varrho) \\ e^{i\theta} F_{J+1/2}(\varrho) \end{pmatrix}, \tag{4.8}$$

leads to the integral form of the Coulomb-matrix elements

$$V^{J_1,J_2}_{J_1',J_2'} = \frac{\lambda}{2l_T^3} \int_0^{2\pi} d\theta_1 d\theta_2 \, e^{i(J_1-J_1')(\theta_1+\frac{\pi}{2})} e^{i(J_2-J_2')(\theta_2+\frac{\pi}{2})} \int_0^\infty \frac{dr_1 dr_2}{|\mathbf{r}_1-\mathbf{r}_2|} \mathcal{F}_{J_1J_1'}(r_1)\mathcal{F}_{J_2J_2'}(r_2), \tag{4.9}$$

where

$$\mathcal{F}_{JJ'}(r) = r \sum_{\sigma=\pm1} F_{J+\sigma/2}(r) F_{J'+\sigma/2}(r) \tag{4.10}$$

is defined in terms of the auxiliary function

$$F_m(\varrho) = \int_0^\infty \frac{d\kappa\sqrt{\kappa}}{2\pi^{3/4}} e^{-(\kappa-\alpha)^2/2} \, J_m(\kappa\varrho), \tag{4.11}$$

The new variables $\theta_{1,2} = \theta_s \pm \theta/2$ make it possible to perform the integral over θ_s which gives the conservation of the angular momentum constraint

$$V^{J_1,J_2}_{J_1',J_2'} = \lambda\hbar\omega \, \delta_{J_1+J_2,J_1'+J_2'} \, V^{(m)}_{J_1J_2}, \tag{4.12}$$

and the exchanged momentum m is defined as $J'_{1,2} = J_{1,2} \pm m$. The product of the auxiliary functions satisfies

$$\mathcal{F}_{-J,-J'}(r) = (-1)^m \mathcal{F}_{JJ'}(r) \tag{4.13}$$

which relies on

$$J_{-n}(r) = (-1)^n J_n(r), \tag{4.14}$$

for $n \in \mathbb{Z}$. The full Hamiltonian for finite α takes the form

$$H = \hbar\omega \sum_J \frac{J^2}{2\alpha^2} c_J^\dagger c_J + \lambda\hbar\omega \sum_{\substack{J_1,J_2 \\ m}} V^{(m)}_{J_1J_2} \, c^\dagger_{J_1+m} c^\dagger_{J_2-m} c_{J_2} c_{J_1}. \tag{4.15}$$

The dimensionless strength of Coulomb interaction is

$$\lambda = \frac{e^2}{\varepsilon_0 l_T \hbar\omega}, \tag{4.16}$$

where dielectric constant ε_0 accounts for static external screening. The integral representation of dimensionless IMEs reads

$$V_{J_1J_2}^{(m)} = 2\pi \int_0^{\pi} d\theta \cos(m\theta) \int_0^{\infty} d\varrho d\varrho' \frac{\mathcal{F}_{J_1,J_1+m}(\varrho)\mathcal{F}_{J_2,J_2-m}(\varrho')}{\sqrt{\varrho^2+\varrho'^2-2\varrho\varrho'\cos\theta}}. \tag{4.17}$$

The Coulomb term can be expanded by Legendre functions $P_l \cos(\theta)$

$$\left.\frac{1}{\sqrt{r_1^2+r_2^2-2r_1r_2\cos\theta}}\right|_{r_2>r_1} = \sum_{l=0}^{\infty} \frac{r_1^l}{r_2^{l+1}} P_l(\cos\theta). \tag{4.18}$$

The expansion makes it possible to perform the angular part of the integral. First, we introduce

$$\mathcal{R}_l^{(m)} = \frac{1}{\pi} \int_0^{\pi} d\theta \cos(m\theta) P_l(\cos\theta), \tag{4.19}$$

which has nonzero value for even $l+m$ and $l \geqslant m$ [33]

$$\mathcal{R}_l^{(m)} = \frac{(2l-1)!!}{2^l l!} \prod_{n=1}^{(l+|m|)/2} \frac{(n-1/2)(l-n+1)}{n(l-n+1/2)}, \tag{4.20}$$

with $\mathcal{R}_0^{(0)} = 1$. The ultimate integral form of IMEs takes the form

$$V_{J_1J_2}^{(m)} = \sum_{l=|m|,|m|+2,\cdots} 2\pi^2 \mathcal{R}_l^{(m)} \int_0^{\infty} \frac{d\varrho}{\varrho^{l+1}} \int_0^{\varrho} d\varrho' \varrho'^l \left[\mathcal{F}_{J_1,J_1+m}(\varrho)\mathcal{F}_{J_2,J_2-m}(\varrho') + (\varrho \leftrightarrow \varrho')\right]. \tag{4.21}$$

In fact, the Legendre expansion transforms one of the integrals in Eq. 4.17 to a sum which can be evaluated with more control over the numerical error.

Before proceeding further, we examine the symmetry relations of IMEs derived in the preceding section by means of the coordinate representation in Eq. 4.21. It can be readily shown

$$V_{J_1J_2}^{(m)} = V_{J_2-m,J_1+m}^{(m)} = V_{J_2J_1}^{(-m)}, \tag{4.22}$$

which follow from the hermicity in Eq. 4.2 and indistinguishability of particles in Eq. 4.3, respectively. With the aid of the relation in Eq. 4.13, we find

$$V_{J_1J_2}^{(m)} = (-1)^m V_{-J_1-m,J_2}^{(m)} = (-1)^m V_{J_1,-J_2+m}^{(m)} = V_{-J_1-m,-J_2+m}^{(m)}, \tag{4.23}$$

which are the phase constraints on IMEs revealed by TR symmetry in Eq. 4.5. Using the relation in Eq. 4.22, the phase constraints also can be represented like

$$V_{J_1J_2}^{(m)} = V_{J_2-m,J_1+m}^{(m)} = (-1)^m V_{-J_2,J_1+m}^{(m)} = (-1)^m V_{J_2-m,-J_1}^{(m)} = V_{-J_2,-J_1}^{(m)}, \tag{4.24}$$

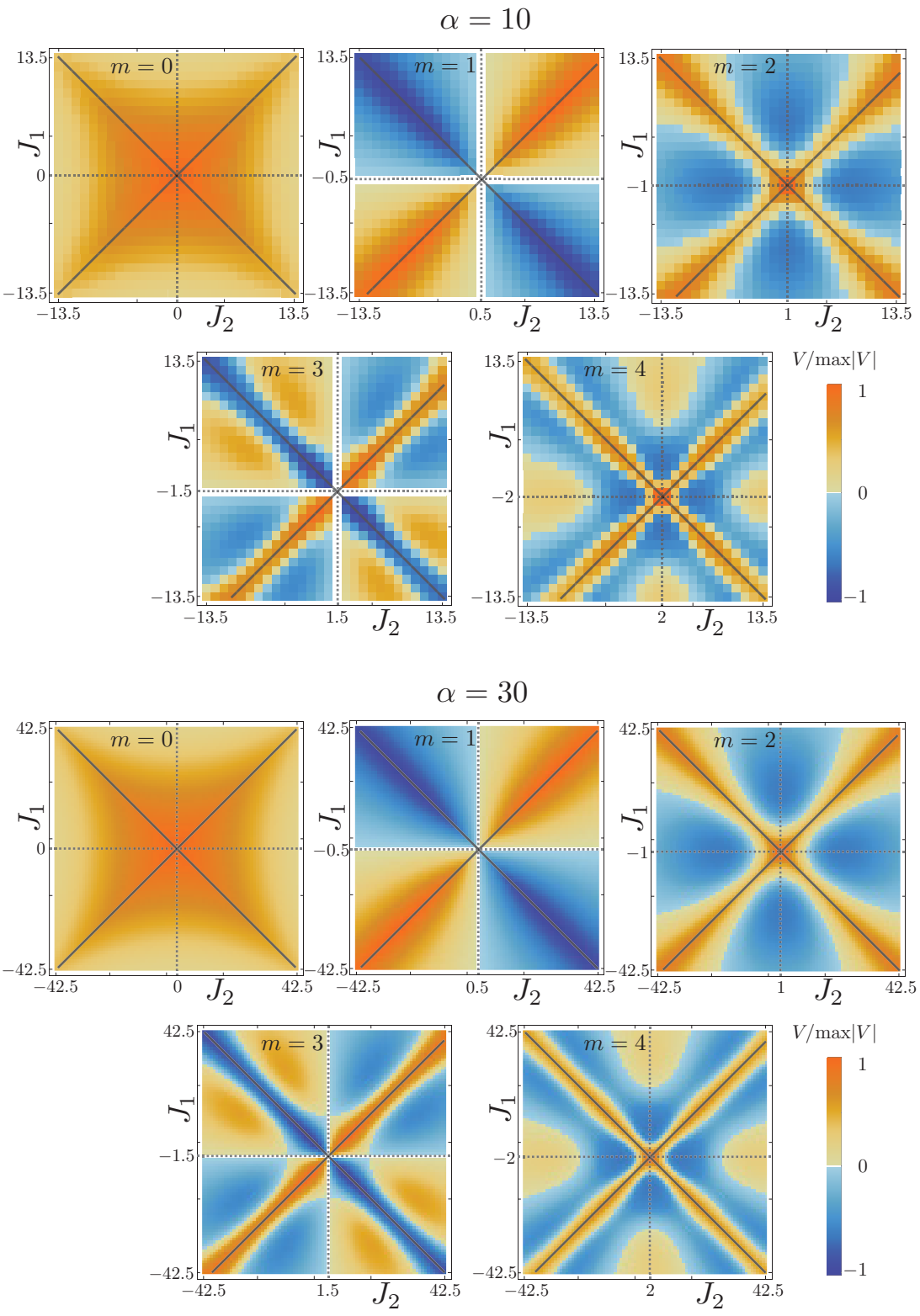

Figure 4.2: Color-scale plot of the Coulomb-matrix elements $V^{(m)}_{J_1,J_2}$ in (J_2, J_1) plane, normalized to their maximum in the shown region, for $\alpha = 10$ in the upper panels and $\alpha = 30$ in the lower panels. The exchanged momentum m is fixed in each panel. The maximal absolute magnitude values of elements take place along two solid lines in each panel, corresponding to BCS-like $J_1 = -J_2$ and exchange-type $J_2 = J_1 + m$ interactions. The symmetry centers $(m/2, -m/2)$ are the points where two dotted lines intersect. For even m, the symmetry center does not refer to a matrix element.

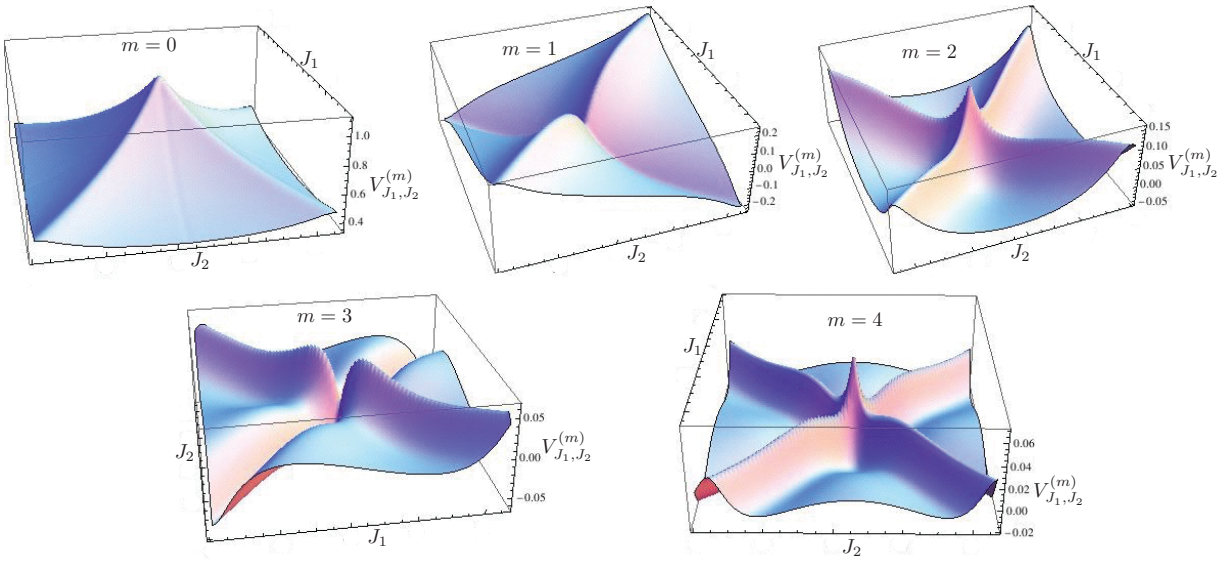

Figure 4.3: 3D representation of the matrix elements shown in Fig. 4.2 for $\alpha = 30$.

The forbidden backward scattering condition Eq. 4.6 reads

$$V^{(m)}_{m/2,J'} = V^{(m)}_{J',m/2} = 0, \tag{4.25}$$

which can be satisfied for $m = 2J$, which is an odd number, and arbitrary J'. $V^{(m)}_{J_1J_2}$ is nonuniform and depends significantly on the angular momentums of incoming particles $J_{1,2}$ besides their exchanged momentum m. The numerical values of $V^{(m)}_{J_1J_2}$ are shown in figures 4.2, 4.3 and 4.4. The salient features of IMEs are summarized in the following.

1. For a given m, IMEs show a point group symmetry in the (J_2, J_1) plane with the symmetry center at $(m/2, -m/2)$. The point group relies on the TR symmetry of two-body potential i.e. $\sim \mathbb{Z}_2 \times \mathbb{Z}_2$. The symmetry center is a matrix element only for odd m. $|V^{(m)}_{J_1J_2}|$ has four reflection axes, $J_1 = -J_2$, $J_2 = J_1 + m$ and $J_{1,2} = \mp m/2$ which intersect at the symmetry center.

2. The maximal absolute values of $V^{(m)}_{J_1J_2}$ take place along two lines, BCS-like $J_1 = -J_2$ and exchange-type $J_2 = J_1 + m$ interaction. In the presence of the Rashba coupling, low-lying eigenstates are localized on a ring in momentum space. The scattering processes on a ring are restricted topologically to BCS-like and exchange-type interaction, see section 4.2.2, which boost the same type of processes in the angular momentum space i.e. $J_1 = -J_2$ and $J_2 = J_1 + m$.

3. The partial TR connects elements of BCS-like and exchange-type interactions $V^{(m)}_{J_1,-J_1} = (-1)^m V^{(m)}_{J_1,J_1+m}$.

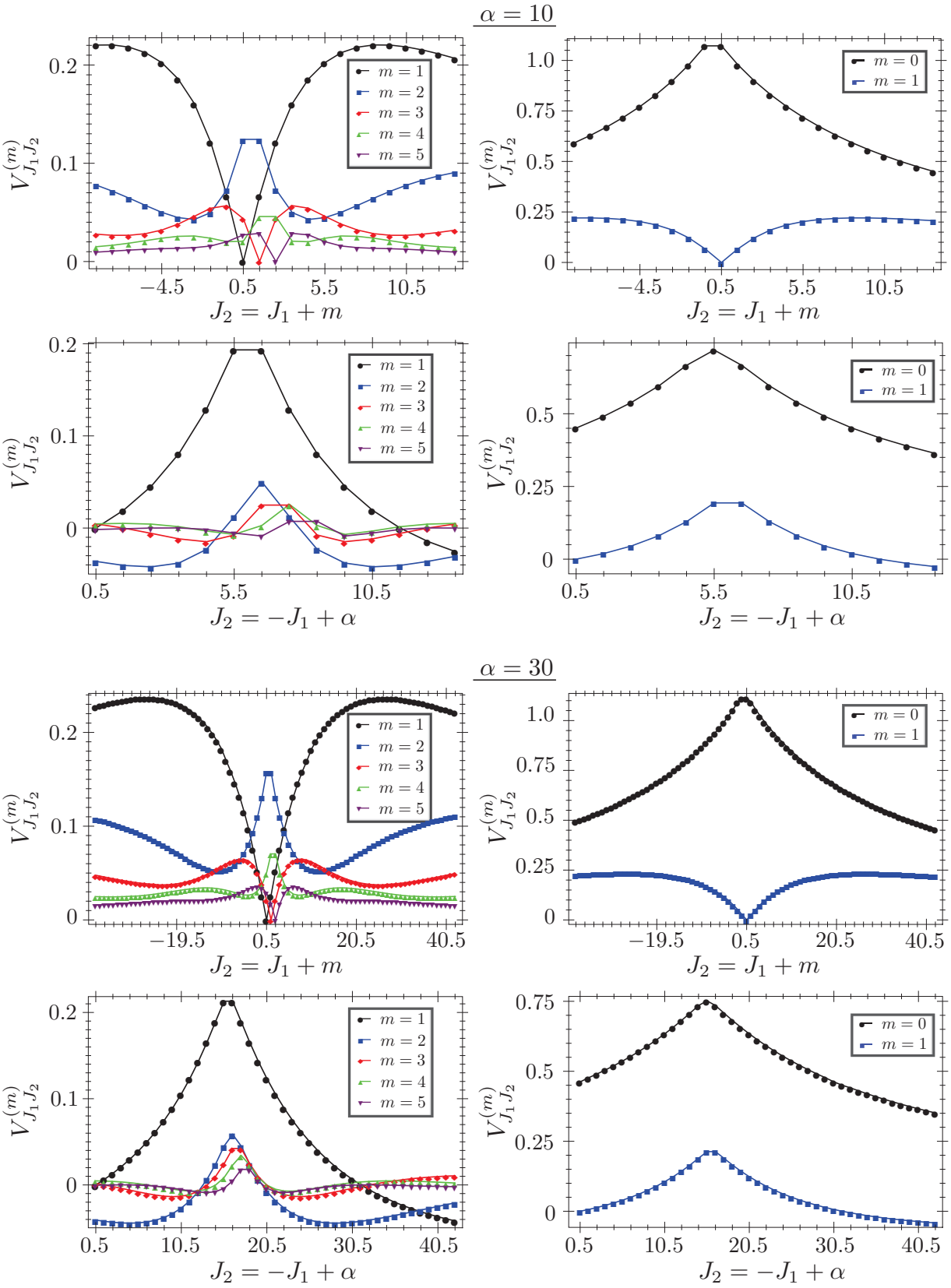

Figure 4.4: Coulomb-matrix elements for $\alpha_{42} = 10$ in the upper panels and $\alpha = 30$ in the lower panels and several m. The matrix elements are shown along one of the maximal absolute magnitude lines, namely, the exchange-type interactions $J_2 = J_1 + m$ and the line $J_2 = -J_1 + \alpha$ crossing the line $J_2 = J_1 + m$ transversely. The elements for $m = 0$ are shown together with elements of $m = 1$ in separate panels.

4. The absolute magnitude of $V^{(m)}_{J_1J_2}$ decreases with increase in m. Particularly, for (J_2, J_1) far from the symmetry center, there is a hierarchy along the maximal absolute-magnitude lines $|V^{(0)}_{J_1,-J_1}| > |V^{(1)}_{J_1,-J_1}| > |V^{(2)}_{J_1,-J_1}| > \cdots$, and also the same hierarchy along $J_2 = J_1 + m$. The rate of decay versus increase in m is determined by the concrete analytical form of V. Although, the rate is higher for a long-range potential, e.g. Coulomb potential, rather than a short-range one like contact interaction potential, see the next section.

4.2.2 Flat-Band Model in Momentum Space

In this subsection, Coulomb potential is represented in the asymptotic state which is derived by holding k_0 finite while taking the limit $l_T \to \infty$. Despite the fact that this limit violates the single-band approximation as $\omega \to 0$ to obtain $l_T \to \infty$, it is worth to study IMEs in this limit since some deep physics of the interacting system can be revealed which are veiled by the coordinate-space representations. The asymptotic wave-function realizes a ring in momentum space $k = k_0$. The wave-function is quasi-one dimensional due to absence of the radial degree of freedom in the wave-function

$$\Psi_J(\mathbf{k}) = \lim_{\alpha\to\infty} \psi_J(\mathbf{k}) = \sqrt{\frac{2\pi^{3/2}}{k_0 l_T}}\delta(k-k_0) \begin{pmatrix} e^{i(J-1/2)\phi} \\ \\ -ie^{i(J+1/2)\phi} \end{pmatrix}. \tag{4.26}$$

The advantage of $\Psi_J(\mathbf{k})$ is that it allows to proceed the derivation of IMEs in momentum representation. The Coulomb-matrix elements read

$$\mathcal{V}^{J_1,J_2}_{J_1',J_2'} = \frac{1}{2}\int \frac{d\mathbf{k}_1\mathbf{k}_2 d\mathbf{q}}{(2\pi)^6}\, \Psi^\dagger_{J_1'}(\mathbf{k}_1+\mathbf{q})\, \Psi^\dagger_{J_2'}(\mathbf{k}_2-\mathbf{q})\, V_q\, \Psi_{J_2}(\mathbf{k}_2)\, \Psi_{J_1}(\mathbf{k}_1), \tag{4.27}$$

where $V_q = 2\pi e^2/q$ is the momentum representation of Coulomb potential in two dimensional (2D) space. We refer to $\mathbf{k}_{1,2}$ as momenta of incoming particles and $\mathbf{k}'_{1,2}$ the momenta of outgoing ones. The translational invariance of V enforces conservation of translational momentum $\mathbf{k}'_{1,2} = \mathbf{k}_{1,2} \pm \mathbf{q}$ which the exchanged (translational) momentum $\mathbf{q}$ is introduced. The Dirac delta function in $\Psi_J(\mathbf{k})$ constrains the magnitude of momenta to stay on the ring

$$\mathbf{k}_{1,2} = k_0 e^{i\phi_{1,2}}, \tag{4.28}$$

$$\mathbf{k}'_{1,2} = \mathbf{k}_{1,2} \pm \mathbf{q} = k_0 e^{i\phi'_{1,2}}, \tag{4.29}$$

where 2D vectors are written in the complex plane $\mathbf{k} = ke^{i\phi}$. The constraints for $\mathbf{k}'_{1,2}$ indicate

$$e^{i2\phi'_{1,2}} = \frac{k_0 e^{i2\phi_{1,2}} \pm q e^{i2\phi}}{k_0 e^{-i2\phi_{1,2}} \pm q e^{-i2\phi}}, \tag{4.30}$$

$$k_0^2 = \left(k_0 e^{i2\phi_{1,2}} \pm q e^{i2\phi}\right)\left(k_0 e^{-i2\phi_{1,2}} \pm q e^{-i2\phi}\right). \tag{4.31}$$

Performing the integrals of $k_{1,2}$ in Eq. 4.29 and implementing the constraints, we arrive at

$$\mathcal{V}^{J_1,J_2}_{J_1',J_2'} = \frac{\lambda\hbar\omega}{(2l_T)^2}\int_0^q \frac{dq}{(2\pi)^2}\int_0^{2\pi} d\phi_1 d\phi_2 d\phi\, \delta(k_1'-k_0)\delta(k_2'-k_0)\, e^{i(J_1+J_2-J_1'-J_2')\phi}$$
$$\times e^{i(J_1-J_1')\phi_1} e^{i(J_2-J_2')\phi_2} \sum_{\substack{\sigma_1=\pm1\\ \sigma_2=\pm1}} \left(1+\frac{q}{k_0}e^{i\phi_1}\right)^{J_1'+\sigma_1/2} \left(1-\frac{q}{k_0}e^{i\phi_2}\right)^{J_2'+\sigma_2/2}, \quad (4.32)$$

where the integration variables are shifted $\phi_{1,2} \to \phi_{1,2}+\phi$. Therefore, $k'_{1,2}$ in the argument of delta functions take the form

$$k'_{1,2} = \sqrt{k_0^2+q^2 \pm 2k_0 q\cos\phi_{1,2}}. \quad (4.33)$$

Note that the measure of $\mathbf{q}$ integral cancels the $1/q$ of Coulomb potential. The magnitude of the exchanged momentum is limited by ring-constraint $0 \leqslant q \leqslant 2k_0$. Evaluating the integral of ϕ gives the conservation of angular momentum. The dimensionless IMEs can be defined by

$$\mathcal{V}^{J_1,J_2}_{J_1',J_2'} = \lambda\hbar\omega\, \delta_{J_1+J_2,J_1'+J_2'}\, \mathcal{V}^{(m)}_{J_1J_2}. \quad (4.34)$$

For a given q, the delta functions in Eq. 4.32 can be satisfied by

$$\cos\phi_1 = -\cos\phi_2 = -\frac{q}{2k_0}, \quad (4.35)$$

which restricts the relative orientation of the incoming particles $\phi_2 = \pi \pm \phi_1$. Note that $\phi_{1,2}$ are associated with $\mathbf{k}_{1,2}$ which are the momenta of incoming particles according to the convention. The latter constraint restricts the interaction on the ring to two different types of scattering processes: BCS-like $\phi_2 = \pi + \phi_1$ and exchange-type $\phi_2 = \pi - \phi_1$ which are shown in Fig. 4.5. Parametrizing $q = 2k_0\cos\vartheta$ by $\vartheta \in [0, \pi/2]$ yields, with the aid of Eq. 4.35, to $\phi_1 = \pi \pm \vartheta$ and $\phi_2 = \pm\vartheta$. By means of this parametrization, the delta functions can be written as

$$\delta(k_1'-k_0)\delta(k_2'-k_0) = \frac{1}{q^2\sin^2\vartheta}\sum_{\substack{\sigma_1=\pm1\\ \sigma_2=\pm1}} \delta(\phi_1-\pi-\sigma_1\vartheta)\,\delta(\phi_2-\sigma_2\vartheta). \quad (4.36)$$

Performing the integral over $\phi_{1,2}$ and using the following identities

$$1-\frac{q}{k_0}e^{i\phi} = 1-2\cos\phi\, e^{i\phi} = -e^{i2\phi}, \quad (4.37)$$

$$\sum_{\substack{\sigma_1=\pm1\\ \sigma_2=\pm1}} i^{\sigma_1+\sigma_2} e^{i\phi(\sigma_1+\sigma_2)} = 4\sin^2\phi, \quad (4.38)$$

$$\sum_{\substack{\sigma_1=\pm1\\ \sigma_2=\pm1}} i^{\sigma_1+\sigma_2} e^{i\phi(\sigma_1-\sigma_2)} = -4\sin^2\phi, \quad (4.39)$$

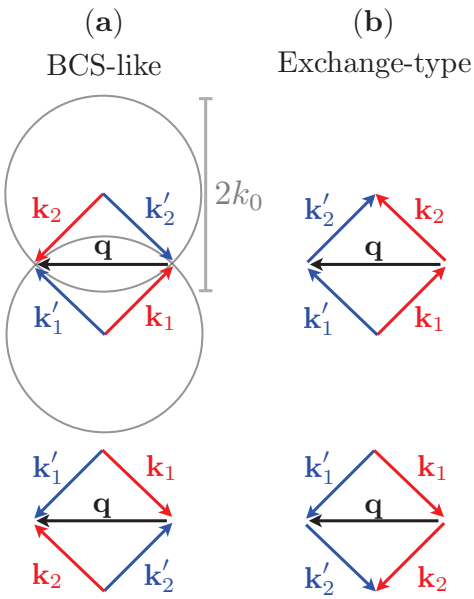

Figure 4.5: Two-particle scattering processes $\mathbf{k}_{1,2} \to \mathbf{k}'_{1,2} = \mathbf{k}_{1,2} \pm \mathbf{q}$ for a given exchanged momentum $\mathbf{q}$, in the $\alpha \to \infty$ limit where particle momenta are constrained to a ring of radius k_0. For a non-zero exchanged momentum $|\mathbf{q}| \neq 0$, there exist four processes which can be classified into (**a**) BCS-like interactions where $\mathbf{k}_1 = -\mathbf{k}_2$ are scattered to $\mathbf{k}'_1 = -\mathbf{k}'_2$, and (**b**) exchange-type interactions by which $\mathbf{k}_2 = \mathbf{k}_1 + \mathbf{q}$, or equivalently $\mathbf{k}_1 = \mathbf{k}'_2$ and $\mathbf{k}_2 = \mathbf{k}'_1$.

the integral representation of dimensionless IMEs $\mathcal{V}^{(m)}_{J_1 J_2}$ reads

$$\mathcal{V}^{(m)}_{J_1 J_2} = (-1)^{J_1+J_2+m} \frac{1}{2\pi\alpha} \int_0^{\pi/2} \frac{\sin\vartheta}{\cos^2\vartheta} \Big\{ \cos\left[2(J_1+J_2)\vartheta\right] - \cos\left[2(J_1-J_2+m)\vartheta\right] \Big\}. \quad (4.40)$$

The integral is divergent for even m since $\cos^{-2}\vartheta$ at the upper limit of the integral $\pi/2$ vanishes versus non-zero numerator. Although, the integral renders finite value for $m =$ odd as the numerator becomes also zero at $\pi/2$

$$\cos\left[(J_1+J_2)\pi\right] - \cos\left[(J_1-J_2+m)\pi\right] = (-1)^{J_1+J_2} + (-1)^{J_1-J_2} = 0, \quad (4.41)$$

which is due to half-odd-integer J. It is worth pointing that the singularity stems from the radial degree of freedom, i.e. delta functions, which is not a degree of freedom for particles on a ring. The singularity can be regularized by introducing a long-distance cutoff so that $q \sim 1/l_T \ll k_0$. Practically, the replacement $\cos^2\vartheta \to \cos^2\vartheta + \alpha^{-2}$ in the denominator removes the singularity for $m = 2n$ and one obtains

$$(-1)^{J_1+J_2} \int_0^{\pi/2} \frac{\sin\vartheta}{\cos^2\vartheta + \alpha^{-2}} \Big\{ \cos\left[2(J_1+J_2)\vartheta\right] - \cos\left[2(J_1-J_2+2n)\vartheta\right] \Big\} \approx \alpha, \quad (4.42)$$

and ultimately the dimensionless IMEs read

$$\mathcal{V}^{(m)}_{J_1J_2} \approx \delta_{m,\text{even}}, \tag{4.43}$$

since $\mathcal{V}^{(m)}_{J_1J_2}$, for odd m, is suppressed by a factor of α^{-1} in Eq. 4.40.
We analyze the representation of $\mathcal{V}^{(m)}_{J_1J_2}$ in Eq. 4.40 to explain the observed properties of IMEs in the regime of finite Rashba coupling $V^{(m)}_{J_1J_2}$, derived in the preceding section. It is possible to do so although the numerical values of $\mathcal{V}^{(m)}_{J_1J_2}$ show odd-even-parity effect despite those of $V^{(m)}_{J_1J_2}$: The single-particle states are localized strictly or effectively on a ring in momentum space in both ultrastrong Rashba coupling by $l_T \to \infty$ and finite α regime, respectively. This restriction of phase space reduces the scattering processes to those given in Fig. 4.5, namely, BCS-like and exchange-type processes. Furthermore, $\Psi_J(\mathbf{k})$ and $\psi_J(\mathbf{k})$ satisfy the same set of symmetries and induces the same phase constraint on IMEs which are derived in section 4.1.

We discuss why IMEs have maximal absolute magnitudes along BCS-like and exchange-type interactions. Note that $\cos[2(J_1+J_2)\vartheta]$ in Eq. 4.40 comes out from the BCS-like scattering processes which constrain the orientation of interacting particles $\phi_2 = \pi + \phi_1$, see the discussion after Eq.4.35. If $J_1 + J_2 = 0$, then $\cos[2(J_1+J_2)\vartheta]$ takes on its maximum and the contribution of the BCS-like processes is maximized to the integral. Also $\cos[2(J_1 - J_2 + m)\vartheta]$ stems from the exchange-type scattering processes $\phi_2 = \pi - \phi_1$. If $J_2 = J_1 + m$, the contribution of exchange-type scattering processes becomes maximum[1]. Furthermore, the absolute magnitude of IMEs along $J_2 = -J_1$ and $J_2 = J_1 + m$ are equal for given J_1 and m

$$\mathcal{V}^{(m)}_{J_1,-J_1} = (-1)^m \frac{1}{2\pi\alpha} \int_0^{\pi/2} \frac{\sin\vartheta}{\cos^2\vartheta} \Big\{1 - \cos[2(2J_1+m)\vartheta]\Big\} = (-1)^m \mathcal{V}^{(m)}_{J_1,J_1+m}. \tag{4.44}$$

And if both $J_2 = -J_1$ and $J_2 = J_1 + m$ are met simultaneously, the contribution of BCS-like and exchange-type processes cancel each other precisely out. This implies

$$(J_2, J_1) = \left(\frac{m}{2}, -\frac{m}{2}\right), \tag{4.45}$$

which is the center of symmetry of IMEs in the (J_2, J_1)-plane for a given m, see Fig. 4.2, i.e. the intersection of two maximal absolute lines. In fact, the symmetry relations of IMEs can be derived readily from the representation in Eq. 4.40 without a prior knowledge of relations in Eq. 4.4, and hence, the TR symmetry of eigenstates

$$\mathcal{V}^{(m)}_{J_1J_2} = (-1)^m \mathcal{V}^{(m)}_{-J_1-m,J_2} = (-1)^m \mathcal{V}^{(m)}_{J_1,-J_2+m} = \mathcal{V}^{(m)}_{-J_1-m,-J_2+m}. \tag{4.46}$$

[1]The lines $J_2 = -J_1$ and $J_2 = J_1 + m$ for given m define the maximal absolute of $\mathcal{V}^{(m)}_{J_1J_2}$ only for odd m. For even m the integral in Eq. 4.40 is singular and independent of $J_{1,2}$. In appendix A, we study a strictly 1D ring in momentum space which IMEs have the similar form to the integral in Eq. 4.40 but nonsingular.

To summarize, the momentum conserving interaction of two particles on a ring in translational momentum space are restricted topologically to merely BCS-like and exchange-type scattering processes. These processes boost the same type of interactions in the angular momentum space, i.e. the maximal absolute lines of IMEs along BCS-like $J_2 = -J_1$ and exchange-type $J_2 = J_1 + m$ interactions. Also, it is possible to derive the symmetry relations of IMEs

Finally, we observed that electrons are allowed to interact either by exchanging momenta or being time-reversed partners. The strong correlation of time-reversed partners takes place in superconducting phase [3]. And exchange interaction favors magnetic phase [10]. It is then plausible to look for counterparts of these phases in our system in different regime of parameters. In fact, we shall see in chapter 5 that Coulomb interacting few-electron dots realizes orbital ferromagnetism even for weak interactions. And Kramers pairs are strongly correlated for weak short-range interactions, see chapter 6.

4.2.3 Flat-Band Model in Coordinate Space

In this section, Coulomb-matrix elements are evaluated by means of the coordinate wavefunction in Eq. 3.25 in the limit of $\alpha \to \infty$, while l_T is held finite and $k_0 \to \infty$

$$\bar{\psi}_J(\varrho,\theta) = \lim_{\alpha\to\infty} \tilde{\psi}_J(\varrho,\theta) = \frac{i^{J-1/2} e^{i(J-1/2)\theta} e^{-\varrho^2/2}}{\pi^{3/4} l_T \sqrt{\varrho}} \begin{pmatrix} \cos(\alpha\varrho - \pi J/2) \\ e^{i\theta}\sin(\alpha\varrho - \pi J/2) \end{pmatrix}. \tag{4.47}$$

The auxiliary function takes the following form

$$\tilde{\mathcal{F}}_m(\varrho) = \lim_{\alpha\to\infty} \mathcal{F}_{J,J+m}(\varrho) = \pi^{-3/2}\cos(m\pi/2) e^{-\varrho^2}. \tag{4.48}$$

Substituting the wavefunction in the integral form of Coulomb-matrix elements in Eq.4.9, IMEs obtain a compact form

$$\lim_{\alpha\to\infty} V^{(m)}_{J_1 J_2} = S_m, \tag{4.49}$$

which does depend solely on the exchanged momentum m. Moreover,

$$S_m|_{m=\text{odd}} = 0, \tag{4.50}$$

which gives rise to the odd-even-parity effect. S_m satisfies the symmetry relations discussed before. Namely, $S_m = S_{-m}$, and also since S_m is identically zero for odd m, the phase constraint in Eq. 4.6 is fulfilled trivially. In terms of $\mathcal{R}^{(m)}_l$, see Eq.4.20, S_m takes the form

$$S_m = \delta_{m,\text{even}} \sum_{l=|m|+|m|+2,\cdots} e^{-\eta l} \mathcal{R}^{(m)}_l C_l, \tag{4.51}$$

m	S_m
0	1.117 57
2	0.172 844
4	0.086 297 1
6	0.055 603 5
8	0.040 137 6
10	0.030 900 1
12	0.024 796 4
14	0.020 483 8
16	0.017 287 7

Table 4.1: Non-zero values of S_m in Eq. 4.49 for $m \leqslant 16$.

where

$$C_l = \frac{2}{\sqrt{\pi}} \int_0^{\pi/4} d\phi \frac{\tan^l \phi}{\cos \phi}. \tag{4.52}$$

The small parameter $\eta \ll 1$ in Eq.4.51 is introduced to regularize the logarithmic singularity of l summation. This weak divergence arises out of the $1/r$ Coulomb potential at $r \to 0$, which practically is cut off by the transverse confinement. The non-zero values of S_m are shown in Table 4.1. S_m has a maximum at $m = 0$ and decreases monotonically versus increase in $|m|$. The full Hamiltonian is written

$$H_\infty = \hbar\omega \sum_J E_J c_J^\dagger c_J + \lambda\hbar\omega \sum_{\substack{J_1, J_1 \\ m \neq 0}} S_m c_{J_1+m}^\dagger c_{J_2-m}^\dagger c_{J_2} c_{J_1} + E_s, \tag{4.53}$$

where $E_J = J^2/2\alpha^2$ and the contribution of zero-exchange interaction is $E_s = \lambda\hbar\omega S_0 N(N-1)$ for system of N electrons. In principle, in the ultrastrong Rashba coupling, the kinetic term vanishes although it is incorporated perturbatively. In chapter 5, we exploit the Hamiltonian derived here to study the ground state of a system containing two electrons. It will be shown that even a weak interaction induces a very large magnetization.

4.3 Matrix Elements of Contact Interaction Potential

In this section, IMEs of a contact potential $\lambda\hbar\omega\delta(\mathbf{r})$ are evaluated in the eigenbasis of finite Rashba coupling. It allows then to compare the IMEs of a short-range potential with the long-range Coulomb potential which discussed before. Briefly, a short-range potential in coordinate space appears as a long-range in the representation exploited here. That is the IMEs decay quite slowly with increase in the exchanged momentum m, particularly, in comparison with the Coulomb-matrix elements.

We start with the coordinate representation

$$\begin{aligned}\bar{V}^{J_1,J_2}_{J_1',J_2'} &= \hbar\omega\frac{\lambda}{2}\int d\mathbf{r}_1 d\mathbf{r}_2\, \tilde{\psi}^\dagger_{J_1'}(\mathbf{r}_1)\tilde{\psi}^\dagger_{J_2'}(\mathbf{r}_2)\,\delta(\mathbf{r}_1-\mathbf{r}_2)\tilde{\psi}_{J_2}(\mathbf{r}_2)\tilde{\psi}_{J_1}(\mathbf{r}_1)\\ &= \hbar\omega\frac{\lambda}{2l_T^{-2}}\int d\mathbf{r}\,\tilde{\psi}^\dagger_{J_1'}(\mathbf{r})\tilde{\psi}^\dagger_{J_2'}(\mathbf{r})\,\tilde{\psi}_{J_2}(\mathbf{r})\tilde{\psi}_{J_1}(\mathbf{r}).\end{aligned} \tag{4.54}$$

Substituting the eigenfunction in Eq. 4.8, we obtain the dimensionless IMEs

$$\bar{V}^{(m)}_{J_1J_2} = \pi\int_0^\infty \varrho d\varrho \bar{\mathcal{F}}_{J_1J_1'}(\varrho)\bar{\mathcal{F}}_{J_2J_2'}(\varrho), \tag{4.55}$$

where the dimensionless IMEs are defined by

$$\bar{V}^{J_1,J_2}_{J_1',J_2'} = \lambda\hbar\omega\delta_{J_1+J_2,J_1'+J_2'}\bar{V}^{(m)}_{J_1J_2}. \tag{4.56}$$

The function $\bar{\mathcal{F}}_{JJ'}(r)$ is defined in terms of the auxiliary functions (given in Eq. 4.11)

$$\bar{\mathcal{F}}_{JJ'}(r) = \sum_{\sigma=\pm1} F_{J+\sigma/2}(r)F_{J'+\sigma/2}(r). \tag{4.57}$$

Clearly $\bar{V}^{(m)}_{J_1J_2}$ satisfy the same symmetry relations discussed in sections 4.1 and 4.2. The numerical values of $\bar{V}^{(m)}_{J_1J_2}$ are depicted in figures 4.6 and 4.7.

4.4 Summary

In this chapter, interaction matrix elements in the eigenbasis of the system are discussed, either for finite $\alpha \gg 1$ or $\alpha \to \infty$. In the case of finite α, the time-reversal symmetry of the eigenbasis and interaction potentials induce phase constraints on the interaction matrix elements $V^{(m)}_{J_1J_2}$ which are independent of the analytical form of interaction potentials. $V^{(m)}_{J_1J_2}$ depends significantly on the angular momenta of interacting particles (J_2, J_1) and the odd-even parity of m. In fact, $V^{(m)}_{J_1J_2}$ has maximal absolute magnitude alongs BCS-like $J_1 = -J_2$ and exchange-type $J_2 = J_1 + m$ interactions for a given m. Those boosted interactions rely on the topological restriction of the scattering processes on the ring in momentum space generated by the strong Rashba coupling. The sign of IMEs along BCS-like interaction is switched by the phase factor $(-1)^m$, whereas, the sign of exchange-type interaction is determined by the sign of the interaction potential V itself. Two different interaction potentials are represented in the eigenbasis, namely, Coulomb and contact potential. It was discussed that the short-range potential becomes a long-range one in the representation as a function of exchanged momentum m; in the sense that the matrix elements decay quite slowly with increase in m, particularly, in comparison with the long-range Coulomb potential which its matrix elements decay quickly with increase in m. For the ultrastrong

Rashba coupling $\alpha \to \infty$, by maintaining the trap while taking the limit $k_0 \to \infty$, the matrix elements show an odd-even-parity effect by which the interactions with an odd exchanged momentum vanish identically.

Intuitively speaking, the peculiar form of the IMEs implies that the ground state of the system in different regimes of interaction strength λ will be determined by a competition between BCS-like and exchange-type interactions, that is to say, strong correlation of Kramers pairs and magnetic phases. Indeed, it will be shown that a transition from the state with the maximum number of occupied Kramers pairs occurs to the orbital ferromagnetism in the few-particle Coulomb interacting system, see chapter 5. In addition, the strong correlation of Kramers pairs is shown in chapter 6 by means of the bosonization machinery in the regime of very weak interactions.

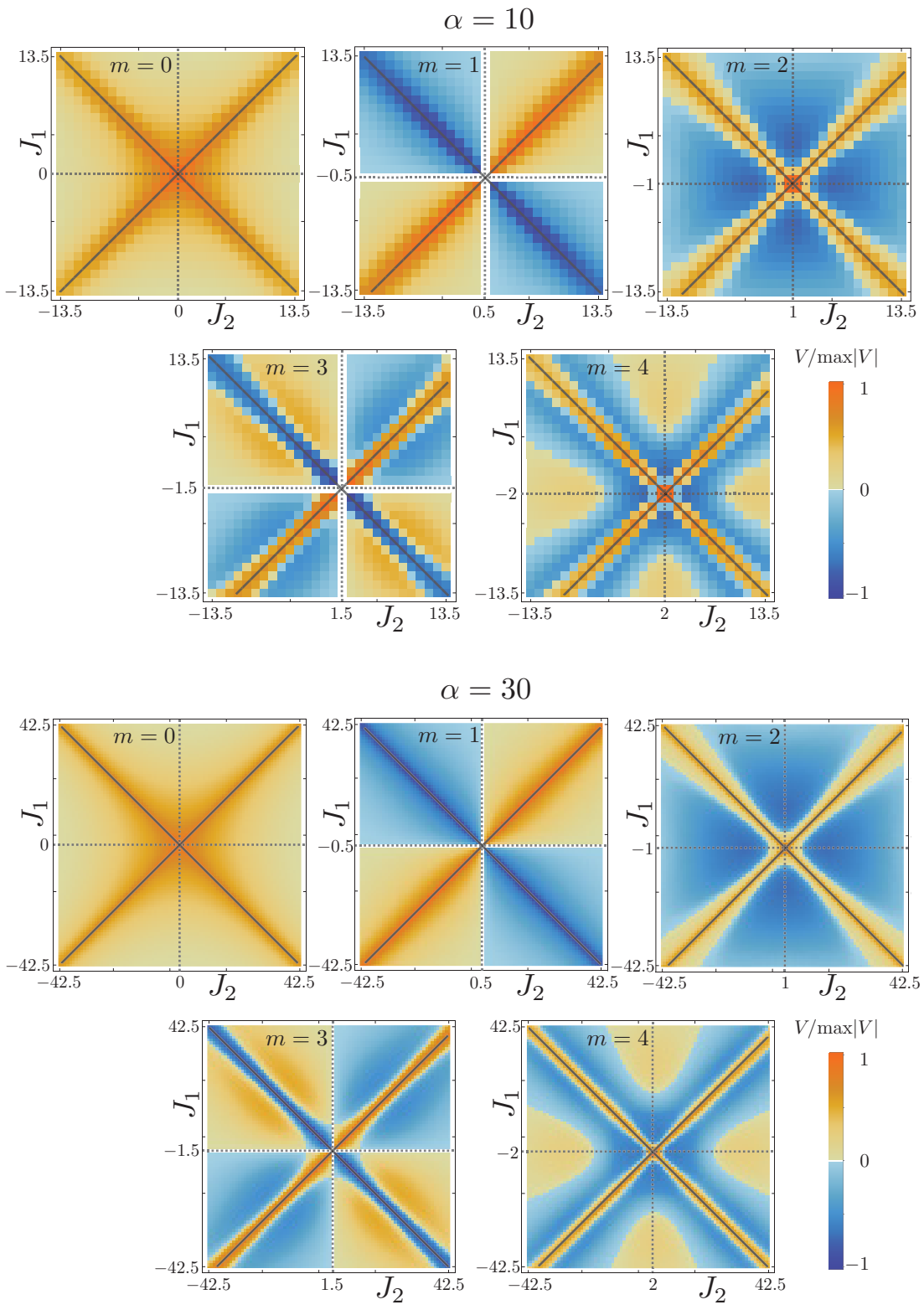

Figure 4.6: Color-scale plot of the contact potential matrix elements $\bar{V}^{(m)}_{J_1,J_2}$ in (J_2, J_1) plane, normalized to their maximum in the shown region, for $\alpha = 10$ in the upper panels and $\alpha = 30$ in the lower panels. The exchanged momentum m is fixed in each panel. The maximal absolute magnitude values of elements take place along two solid lines in each panel, corresponding to BCS-like $J_1 = -J_2$ and exchange-type $J_2 = J_1 + m$ interactions. The symmetry centers $(m/2, -m/2)$ are the points where two dotted lines intersect. For even m, the symmetry center does not refer to a matrix element.

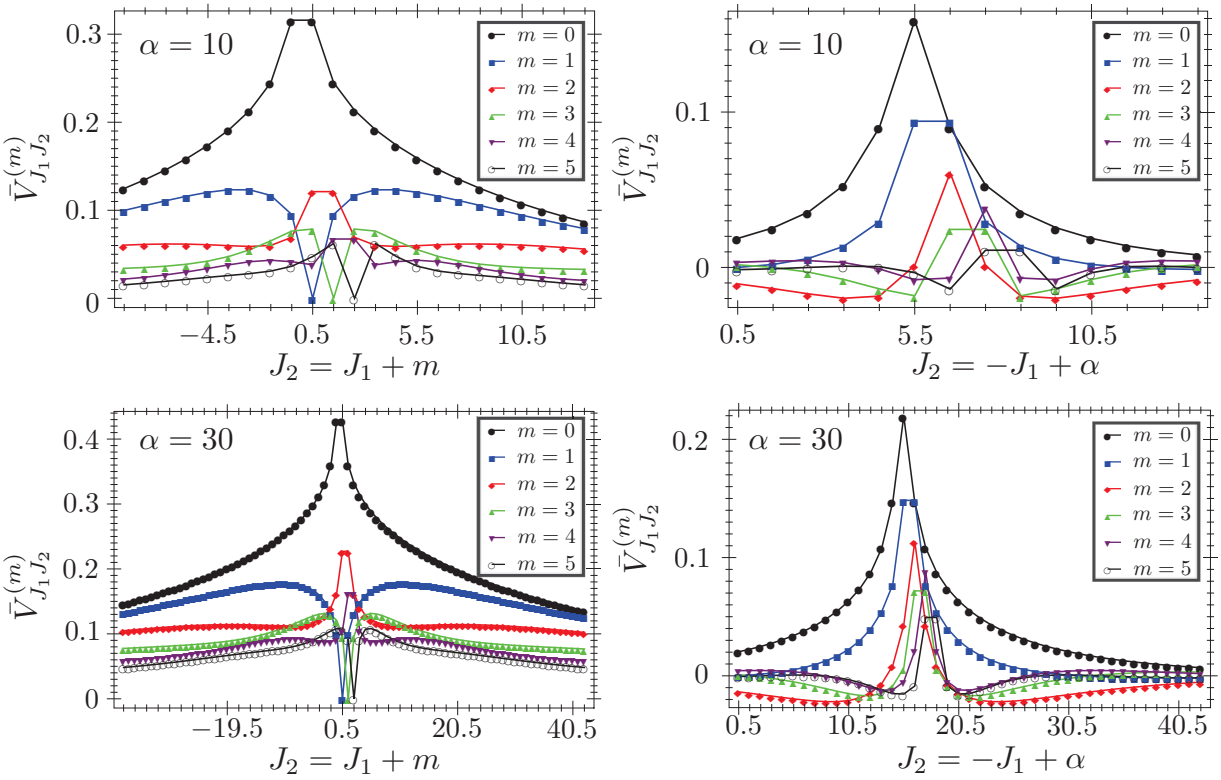

Figure 4.7: Contact potential matrix elements for $\alpha = 10$ in the upper panels and $\alpha = 30$ in the lower panels and several m. The matrix elements are shown along one of the maximal absolute magnitude lines, namely, the exchange-type interactions $J_2 = J_1 + m$ and the line $J_2 = -J_1 + \alpha$ crossing the line $J_2 = J_1 + m$ transversely.

Chapter 5

Few-Body System

We begin in this chapter to investigate Coulomb-interacting few-electron dots in the presence of strong Rashba spin-orbit coupling (SOC) $\alpha \gg 1$. We are mainly interested in the interaction-driven features of the system. We need to deal with a discrete finite system. The interactions must be weak enough in order to admit the single-band approximation $|J| \lesssim \alpha$ which formally we take it into account through restricting the interaction strength as $\lambda \lesssim 1$. Practically, one must check that the highest occupied states stay far from the bottom of the next band.

We start to study the system of two electrons $N = 2$ in the ultrastrong Rashba coupling $\alpha \to \infty$. The limit is taken by holding the trap length scale l_T finite while $k_0 \to \infty$ (dimensionless Rashba coupling is defined by $\alpha = k_0 l_T$). The kinetic term vanishes in this limit although it is treated in the perturbation theory. The peculiarity of the ultrastrong Rashba coupling is the odd-even-parity effect in the interaction term. That is matrix elements with an odd exchanged momentum vanish. It shall be shown that the ground state is highly degenerate although a spontaneous large ground-state magnetization emerges if the Coulomb corrections is contributed in a perturbation-theory manner. Consequently, a very weak interaction leads to a large magnetization in the system. Since the system is effectively spinless, the orbital angular momentum merely contribute to the magnetization, and hence, the phase is called orbital ferromagnetism. In principle, the magnetization is the sum of angular momentums of occupied states, in a mean-field sense, and gives rise to a nonzero value if one of the two time-reversed partners is occupied. That is the magnetization requires broken Kramers pairs. Although the ground state has the Kramers degeneracy in the orbital ferromagnetic state, the energy barrier between two minima breaks time-reversal symmetry practically.

Next, we engage the standard exact diagonalization to find out the features of the few-electron systems $N = 2$ and $N = 3$ with a finite but large Rashba coupling as a function of interaction strength λ. The ground-state energy as a function of λ shows non-analytical features at different values of critical interaction strength λ_c which mark transitions to magnetized states. The derivative of the ground-state energy with respect to the λ shows

discontinuity at the transition points. The analysis of the system at two different values of Rashba coupling $\alpha = 10, 15$ suggests that the transition from unmagnetized state to the spontaneous ferromagnetism takes place at a weaker interaction strength if α is increased.

We present also a few results for $N = 4$ and $\alpha = 15$ calculated by means of the density matrix renormalization group (DMRG) [107, 25, 93]. DMRG is one of the most powerful technique for discrete 1D systems. In fact, after reproducing the results of the exact diagonalization for $N = 2, 3$ with DMRG, the study of the system is extended for larger N with the technique which is computationally much more efficient in comparison with the exact diagonalization.

Finally, a Hartree-Fock (HF) calculation is carried out on the system with $N \leqslant 10$ and $\alpha = 30$. The results of HF admit the spontaneous magnetization qualitatively. Though, since the standard HF Hamiltonian dose not contain BCS-like interactions, the Kramers pairs are broken quickly even for a very weak interaction, particularly, with increase in N. In the next chapter, we consider an extended Hartree-Fock Hamiltonian which is expected to remedy this insufficiency.

5.1 Ultrastrong Rashba Coupling

In this section, we consider the ultrastrong Rashba coupling $\alpha = l_T k_0 \to \infty$ by holding the trap length l_T finite while taking the limit $k_0 \to \infty$ which is consistent with the single-band approximation. The Hamiltonian, derived in the preceding chapter, has the form

$$H_\infty = \hbar\omega \sum_J E_J c_J^\dagger c_J + \lambda\hbar\omega \sum_{\substack{J_1, J_1 \\ m\neq 0}} S_m c_{J_1+m}^\dagger c_{J_2-m}^\dagger c_{J_2} c_{J_1} + E_s, \tag{5.1}$$

where the kinetic term with $E_J = J^2/2\alpha^2$ is kept as a perturbation in the limit $\alpha \to \infty$. The numerical values of S_m is discussed in section 4.2.3 and $E_s = S_0 N(N-1)\lambda\hbar\omega$. In the following, we consider the ground-state of H_∞ for $N = 2$.

5.1.1 Ground State

Two particle Hilbert space can be spanned by $c_{J_1}^\dagger c_{J_2}^\dagger |0\rangle$ where $J_1 > J_2$ to avoid double counting. $|0\rangle$ is the vacuum state with no particle. The two-particle eigenstates of H_∞ comprise of three families. The corresponding states are presented by $|M, \gamma\rangle$ in which M is integer. $\gamma = 1, 2, 3$ is the family index, see figure 5.1. Expanding the eigenstates in the two-particle basis yields

$$|M, \gamma\rangle = \sum_{J>0} \beta_J c_{J+M+i_\gamma}^\dagger c_{-J+M}^\dagger |0\rangle, \tag{5.2}$$

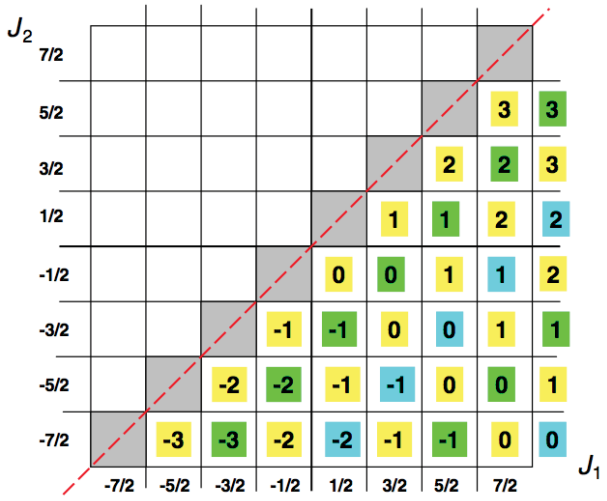

Figure 5.1: Schematic illustration of the invariant two-particle states $|M, \gamma\rangle$ (with integer M and family index $\gamma = 1, 2, 3$) [see Eq. 5.2] in the $J_1 - J_2$ plane. These states span the complete two-particle Hilbert space. Our ordering convention $J_1 > J_2$ implies that only states below the main diagonal (dashed red line) appear. Yellow cells correspond to $\gamma = 1$, where the respective numbers indicate M. Green (blue) cells refer to $\gamma = 2$ ($\gamma = 3$). The interacting ground state has $\gamma = 1$.

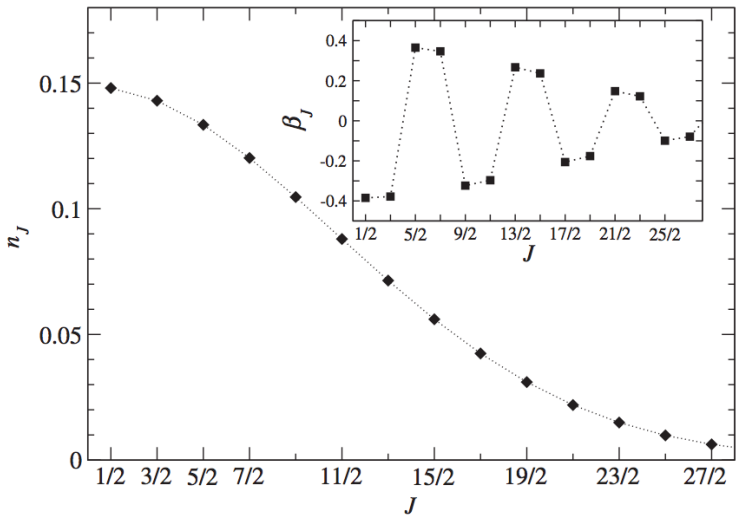

Figure 5.2: Distribution function $n_J = |\beta_J|^2$ versus J for ground state of two-particle system. As a matter of illustration, we have put $\lambda\alpha^2 = 10^4$ which gives $\mathcal{E}_{\rm min} = -0.0992725$. Inset panel, shows the pairwise oscillatory behavior of β_J versus J.

where normalization of the eigenstates require $\sum_{J>0}|\beta_J|^2 = 1$. The auxiliary index i_γ is defined with respect to the family index as $i_1 = 0$ and $i_{2,3} = 1$. The summation in Eq. 5.2 for $\gamma = 2$ ($\gamma = 3$) consists of solely even (odd) $J + 1/2$. Operating with H_∞ on the states, we obtain

$$H_\infty|M,\gamma\rangle = \sum_{J,J'>0} \beta_{J'} \left[\left(E_{J+M+i_\gamma} + E_{-J+M}\right)\delta_{J,J'} + 2\lambda\hbar\omega\left(S_{J-J'} - \delta_{i_\gamma,1}S_{J+J'}\right)\right] c^\dagger_{J+M+i_\gamma} c^\dagger_{-J+M}|0\rangle. \quad (5.3)$$

The M dependence only appears from $E_J \propto \alpha^{-2}$ which indicates states in the same family are degenerate for $\alpha \to \infty$. The ground state must be in the family of $\gamma = 1$ since the exchange energy $S_{J+J'}$ is absent for $\gamma \neq 1$. Therefore, the magnetization of the ground state is even $\langle \hat{M}\rangle = 2M\hbar$. From here on, we drop the family index and proceed with the ground-state family

$$|M\rangle = \sum_{J>0} \beta_J c^\dagger_{J+M} c^\dagger_{-J+M}|0\rangle. \quad (5.4)$$

Matrix elements of H_∞ has the following form

$$\langle M'|H_\infty|M\rangle = \hbar\omega\left(\frac{M^2}{\alpha^2} + 2\lambda\mathcal{E}\right)\delta_{MM'}, \quad (5.5)$$

which is diagonal since H_∞ is rotational invariant and cannot mix states with different magnetization. The dimensionless parameter has the form

$$\mathcal{E} = \sum_{J,J'>0}\left(\frac{J^2}{2\lambda\alpha^2}\delta_{JJ'} + S_{J-J'} - S_{J+J'}\right)\beta_J\beta_{J'}. \quad (5.6)$$

β_J is independent of M and can be chosen real valued. The energy of the ground state depends on Rashba coupling and interaction strength through $\lambda\alpha^2$ in Eq. 5.6. The ground state can be found by minimizing $\mathcal{E}_{\min}$ as a function of β_J numerically. Subsequently, the distribution function $n_J = |\beta_J|^2$ can be obtained readily. β_J and n_J are shown in Fig. 5.2 for typical values of Rashba coupling and interaction strength. The numerical values of n_J can be fitted to a Gaussian factor $e^{-(J/J^*)}$, with $J^* \sim \sqrt{\alpha}$ which fulfilled the single-bad approximation self-consistently. β_J in Fig. 5.2 exhibits a pairwise oscillatory behavior as a function of J. It will be shown in subsection 5.1.4 that the oscillatory behavior of β_J is enforced by the antisymmetry of fermions.

5.1.2 Ground-State Magnetization

The analysis of the preceding section yield to the ground state energy

$$E^0_M = \left(\frac{M^2}{\alpha^2} + 2\lambda\mathcal{E}_{\min}\right)\hbar\omega, \quad (5.7)$$

where $\mathcal{E}_{\min}$ needs to be evaluated numerically. The second order perturbative term M^2/α^2 suggests the ground state has a zero magnetization $M = 0$. Although, the corrections to Coulomb-matrix elements scale as α^{-1} approximately, see Eq. 4.43 and the discussion beyond. The correction then should be taken into account as they are subleading to the contribution of kinetic term M^2/α^2.

A comment is here in order. In the ultrastrong Rashba coupling $\alpha \to \infty$, the eigenfunction is obtained by keeping the lowest order term in the asymptotic expansion of the Bessel function, see Eq. 3.24. In principle, one should keep the higher order terms of the expansion and incorporate them in the computation of Coulomb-matrix elements to estimate the Coulomb correction beyond H_∞. Although, in the following, we take the interaction term H_I of finite in Eq. 5.25 as the corrections to H_∞ in a perturbation theory heuristically in order to determine the ground state.

The expectation value of H_I takes the form

$$\langle M'|H_I|M\rangle = 2\lambda\hbar\omega\delta_{MM'}\sum_{J,J'>0}\beta_J\beta_{J'}\left(V^{(J-J')}_{-J+M,J+M} - V^{(J+J')}_{-J+M,J+M}\right), \tag{5.8}$$

where we have used the symmetry relations discussed in section 4.1. The Coulomb correction treated in perturbation theory is

$$E_M = E_{-M} = E^0_M + \langle M|H_I|M\rangle - 2\lambda\hbar\omega\mathcal{E}_{\min}. \tag{5.9}$$

We measure E_M with respect to the energy of the unmagnetized state $\delta E_M = E_M - E_{M=0}$. The numerical value of δE_M is shown in Fig. 5.3 for concrete values $\alpha = 30$ and $\lambda = 1$ as an illustration. It is interesting to note that $M = 0$ state represents a local energy maximum. The main contribution to δE_m is dominated by terms $J = J'$ as $V^{m=0}_{JJ'}$ is the strongest channel of interaction, see chapter 4. We estimate

$$\delta E_m \approx 2\lambda\hbar\omega\sum_{J>0} n_J\left(V^{(0)}_{-J+M,J+M} - V^{(0)}_{-J,J}\right) < 0, \tag{5.10}$$

where $n_J = |\beta_J|^2$. The inequality holds since $V^{(0)}_{J,J'} > 0$ has maximum values along $J = \pm J'$. Since, we have found herein $M \gg 1$, the effect must stem from the orbital angular momentum rather than the spin one, particularly, here for $N = 2$.

The value of $M = M(\alpha, \lambda)$ can be estimated analytically as follows. We compute $\langle M|H_I|M\rangle$ exploiting matrix elements given in Eq. 4.40 to find

$$\frac{\delta E_M}{\hbar\omega} \approx \frac{M^2}{\alpha^2} - \frac{2\lambda}{\pi\alpha}\int_0^{\pi/2} d\vartheta \frac{\sin\vartheta}{\cos^2\vartheta}\sin^2(2M\vartheta). \tag{5.11}$$

We minimize δE_M with respect to M and find the ground-state magnetization $M = M_0$

$$M_0 = \frac{2\lambda\alpha}{\pi}\int_0^{\pi/2} d\vartheta \frac{\vartheta\sin\vartheta}{\cos^2\vartheta}\sin(4M_0\vartheta). \tag{5.12}$$

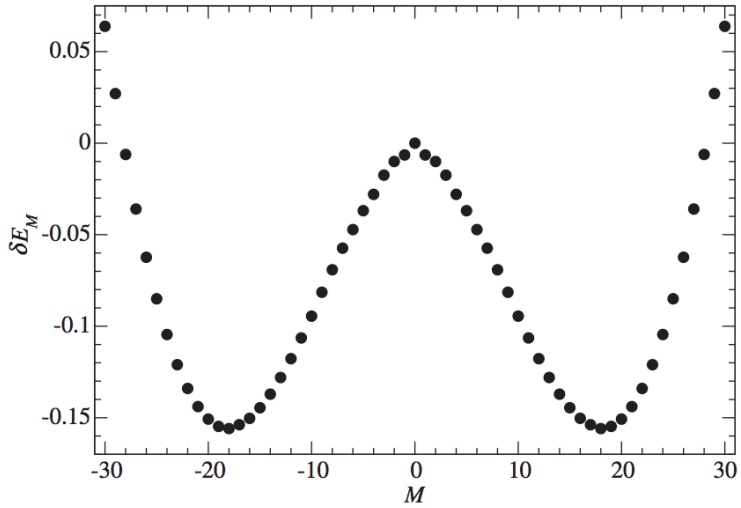

Figure 5.3: Energy of two-particle state in ultrastrong Rashba coupling relative to the energy of unmagnetized state $M = 0$. δE_m is measured in units of $\hbar\omega$. For illustration, we have chosen $\alpha = 30$ and $\lambda = 1$.

The main contribution to the integral comes from $\vartheta \lesssim M_0^{-1}$ for $M_0 \gg 1$. Performing the integral, we obtain $M_0 = (\lambda\alpha)^{1/4}$ which suggest M_0 can be very large even for very weak interaction.

The ground state is degenerate due to the time-reversal symmetry $|\pm M_0\rangle$ with magnetization $\pm 2M_0$. Therefore, a superposition of $|\pm M_0\rangle$ is a ground state also

$$|\Phi\rangle = \sum_{\eta=\pm} c_\eta |\eta M_0\rangle, \qquad \sum_{\eta=\pm} |c_\eta|^2 = 1. \tag{5.13}$$

$|\Phi\rangle$ is not an eigenstate of total magnetization operator $\hat{M}$. The magnetization expectation value $\langle\Phi|\hat{M}|\Phi\rangle = 2M_0\hbar(|c_+|^2 - |c_-|^2)$ is finite except if $|c_+| = |c_-|$. It implies that applying a weak magnetic fields the magnetization takes on one of the minimums $\pm M_0$. Switching off the magnetic field adiabatically, we then obtain $|\Phi\rangle \to |M_0\rangle$. Since the barrier between two minima is finite, the tunneling effect can unmagnetized the state with $|c_+| = |c_-|$. Nonetheless, $\hat{M}^2$ always has non-zero eigenvalue.

We discuss the eccentricity of the quantum dot by which quantum-tunneling processes between energy minima with opposite magnetization $\pm M_0$ becomes relevant. First, we note that the energy barrier between two minima is $B\hbar\omega$ with $B \propto 0.1$, see Fig. 5.3. We employ an effective low-energy Hamiltonian to estimate tunneling rate between minima

$$H_{\text{eff}} = \left[\epsilon\frac{\phi^2}{2} + B\frac{(M^2 - M_0^2)^2}{M_0^4}\right]\hbar\omega, \tag{5.14}$$

where ϕ is the field conjugate to magnetization M, the small parameter ϵ describes the dot eccentricity. The solution of the effective Hamiltonian is known exactly [3]. The parity

symmetry of the Hamiltonian splits the ground state to symmetric and antisymmetric eigenstates. The level splitting of two states

$$\delta E = \hbar\omega B\sqrt{\frac{2}{\pi}}64\exp\left(-\frac{4\sqrt{2B}}{3\sqrt{\epsilon}}M_0\right), \tag{5.15}$$

allows estimation for time scale of tunneling rate

$$\omega\tau = \frac{\hbar\omega}{\delta E} \approx 0.2e^{5.96M_0}, \tag{5.16}$$

where we have put $B = 0.1$ and $\epsilon = 0.01$ for illustration. For $M_0 = 18$ observe in Fig. 5.3, we estimate the time scale for tunneling between minima as $\omega\tau = 10^{45}$. This astronomically long time indicates that on the laboratory-time scale, the tunneling process can be disregarded.

It is useful to compare the phenomenon observed here with the well-known persistent current in the normal-metal quantum ring [20, 45, 23, 49, 100, 15], where a circulating equilibrium electric current flows and can be experimentally observed, see [15] and references therein. The persistent current requires a non-zero flux threading the ring and emerges even in the absence of interactions. Though, the orbital ferromagnetism in a 2D dot is generated by the interplay of Coulomb interactions and strong Rashba SOC. The spontaneous magnetization which is discussed here can be very large. The persistent current analogy suggests how the magnetization predicted here can be observed experimentally in spite of their differences. In addition, the response of the system to a weak magnetic field applied perpendicular to the 2D plane is expected to reveal information about the magnetization. The susceptibility is then should be singular similar to the ordinary ferromagnet. At temperature higher than the energy barrier discussed above, the orbital ferromagnetism in the system will be suppressed and ultimately disappear. An estimation for the relevant temperature is $T_c \approx B\hbar\omega/k_B$. For typical quantum dots [61], $T_c \approx 1$ to 10 K.

5.1.3 Spin and Charge Density

We assume the system of two particles is in a definite state $|M_0\rangle$. The total spin density at position (r, θ) has the form

$$\mathbf{S}(r,\theta) = \sum_{J>0} n_J \left[\mathbf{s}_{J+M_0}(r,\theta) + \mathbf{s}_{-J+M_0}(r,\theta)\right], \tag{5.17}$$

where $\mathbf{s}_J(\mathbf{r}) = \frac{\hbar}{2}\bar{\psi}^*_J(\mathbf{r})\,\boldsymbol{\sigma}\,\bar{\psi}^*_J(\mathbf{r})$ and $\boldsymbol{\sigma} = (\sigma_x, \sigma_y, \sigma_z)$ are Pauli matrices. The x component, for instance, has the form

$$\mathbf{s}_J(r,\theta) \approx \frac{\hbar}{2}\frac{e^{-r^2/l_T^2}}{\pi^{3/2}l_T r}\cos\theta\sin\left(2k_0 r - \pi J\right). \tag{5.18}$$

Substituting the explicit form of $\mathbf{s}_J(r,\theta)$ in Eq. 5.17, two terms cancel each other and vanish the density $S_x(r,\theta) = 0$. The same argument applies to the other component and leads to $\mathbf{S} = 0$.

Charge density for N particles can be derived in the ground state

$$\rho_{\mathrm{C}}(r) = \frac{eN}{\pi^{3/2} l_T r} e^{-r^2/l_T^2}, \tag{5.19}$$

which is radially symmetric and independent of Coulomb interaction in the considered regime $\lambda \lesssim 1$. The λ independence of ρ_{C} is in marked contrast to the case of weak spin-orbit coupling where ρ_{C} has information about interactions and can be exploited to detect Wigner-molecule formation [7, 106]. Such a featureless charge density implies absence of Wigner crystallization which emerges in the regime of weak spin-orbit coupling and strong Coulomb interaction [22]. Furthermore, we compute the pair distribution function in the following subsection which also does not show any sign of crystallization. Although, it contains informations about the oscillatory feature of β_J observed before.

5.1.4 Pair Distribution Function

We see in the following that the pair distribution function in the regime of ultrastrong Rashba coupling reveals a noteworthy constraint on β_J which attributes the pairwise oscillatory behavior observed in Fig. 5.2 to Pauli exclusion principle. The pair distribution function is defined as

$$\mathcal{P}(\mathbf{r},\mathbf{r}') = \langle M|\Psi^\dagger(\mathbf{r})\,\Psi^\dagger(\mathbf{r}')\,\Psi(\mathbf{r}')\,\Psi(\mathbf{r})|M\rangle, \tag{5.20}$$

where $\Psi^\dagger(\mathbf{r})$ and $\Psi(\mathbf{r})$ are fermion field operators which are defined as

$$\Psi^\dagger(\mathbf{r}) = \sum_J \bar{\psi}_J^*(\mathbf{r}) c_J^\dagger, \tag{5.21}$$

and $\bar{\psi}_J(\mathbf{r})$ is the eigenfunction of the free system defined Eq. 4.47. Using the relation in Eq. 5.21 and the eigenstate $|M\rangle$, given in Eq. 5.4, after some algebra, we obtain

$$\mathcal{P}(\mathbf{r},\mathbf{r}') = \frac{2\,e^{-r^2-r'^2}}{\pi^3 l_T^4 r r'} \sum_{\substack{J,J'>0 \\ \eta=\pm 1}} \eta\beta_J\beta_{J'}\,\cos\left[(J-\eta J')(\theta-\theta')\right]\cos^2\left[\pi(J-\eta J')/2\right], \tag{5.22}$$

where in polar coordinate $\mathbf{r} = (r,\theta)$. The pair distribution must vanish for $\mathbf{r} = \mathbf{r}'$ due to Pauli exclusion principle. It implies a constraint on β_J

$$\mathcal{P}(\mathbf{r},\mathbf{r}) = 0 \quad \Rightarrow \quad \sum_{J>0} \beta_J\,\sin(J\pi) = 0. \tag{5.23}$$

The following ansatz for the pair of consecutive β_J satisfies the constraint

$$\begin{aligned} \beta_{1/2} &= \beta_{3/2}, \\ \beta_{5/2} &= \beta_{7/2}, \\ &\vdots \\ \beta_{(4n+1)/2} &= \beta_{(4n+3)/2}, \qquad \text{for } n \in \mathbb{Z}^+, \end{aligned} \tag{5.24}$$

where β_J is suppose to be real. The ansatz mimics the pairwise oscillatory behavior of β_J in Fig. 5.2. It is worth pointing that $\mathcal{P}(\mathbf{r}, \mathbf{r}') = 0$ for $\theta = \theta'$ even if $r \neq r'$. Moreover, the pair correlation function vanishes even for $\theta - \theta' = \pm\pi$. Also, no sign of Wigner crystallization shows up in the considered regime $\alpha \to \infty$ and $\lambda \lesssim 1$.

5.2 Exact Diagonalization

The system of few Coulomb-interacting electrons in the presence of a strong Rashba spin-orbit coupling $\alpha \gg 1$ and parabolic trap is studied numerically. Using the standard exact diagonalization technique, ground-state energy and magnetization of few electrons $N \leqslant 3$ versus variation of interaction strength $\lambda \lesssim 1$ are derived for $\alpha = 10$ and 15. A transition takes place from unmagnetized ground state to an orbital ferromagnet if the interaction strength exceeds a critical value $\lambda > \lambda_c$.

We begin with the full Hamiltonian

$$\begin{aligned} H &= H_0 + H_I \\ &= \hbar\omega \sum_J E_J c_J^\dagger c_J + \lambda\hbar\omega \sum_{\substack{J_1, J_2 \\ m}} V_{J_1 J_2}^{(m)}\, c_{J_1+m}^\dagger c_{J_2-m}^\dagger c_{J_2} c_{J_1}, \end{aligned} \tag{5.25}$$

where $E_J = J^2/2\alpha^2$ and the Coulomb-matrix elements $V_{J_1 J_2}^{(m)}$ are discussed in chapter 4. In principle, the numerical values of $V_{J_1 J_2}^{(m)}$ is a function of Rashba coupling α, which is taken into account implicitly. In this section, we derive the ground-state quantities of H for $\alpha = 10$ and $\alpha = 15$ while varying the interaction strength in the range of $0 \leqslant \lambda \lesssim 1$. We expand H in the basis of N particles, see appendix C, and diagonalize the matrix representation numerically. Having the ground states of the system as a function of α and λ, the physical quantities of the ground state can be evaluated readily.

5.2.1 Ground State

The ground-state results obtained by exact diagonalization for $N = 2$ and $N = 3$ and Rashba coupling $\alpha = 10$ and $\alpha = 15$ versus discrete values of interaction strength λ are

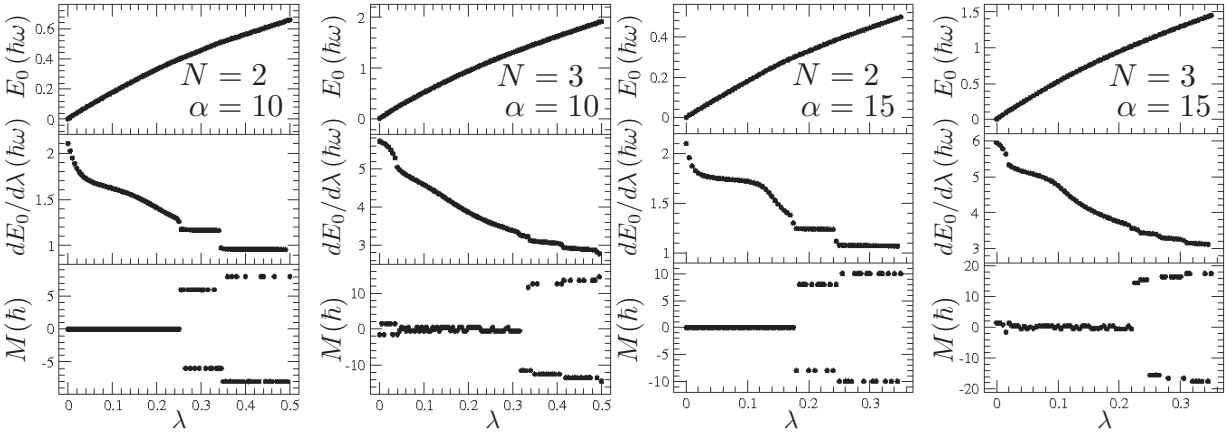

Figure 5.4: Exact-diagonalization results for the ground-state energy E_0 and magnetization M of $N = 2$ and $N = 3$ versus interaction strength λ for $\alpha = 10$ and $\alpha = 15$. The energy $E_0(\lambda)$ is shown in the top panels. The singularities of $dE_0/d\lambda$ at the critical values of λ are visible in the middle panels. The bottom panels show magnetization $M(\lambda)$ where for $\lambda > \lambda_c$ a big jump is visible. For $N = 3$, magnetization is always non-zero even for $\lambda < \lambda_c$. Although, for $N = 2$, the magnetization is zero for $\lambda < \lambda_c$.

shown in Fig. 5.4. We review the observed physics revealed by exact diagonalization. In the non-interacting limit $\lambda = 0$, the ground-state magnetization is equal to zero for an even number of particles, but otherwise, non-zero

$$\begin{cases} \langle \mathrm{GS}|\hat{M}|\mathrm{GS}\rangle\Big|_{\lambda=0} = 0 & \text{if } N = \text{even}, \\ \\ \langle \mathrm{GS}|\hat{M}|\mathrm{GS}\rangle\Big|_{\lambda=0} = \pm\hbar N/2 & \text{if } N = \text{odd}. \end{cases} \tag{5.26}$$

Therefor, the ground-state of non-interacting system with an odd number of particles is degenerate due to time reversal symmetry. If the magnetization of a state is close to the magnetization of the non-interacting states, we call it unmagnetized states for convenience. Increasing the interaction strength, when λ reaches the first critical value λ_c, the ground state shows a sharp transition to a ferromagnetic state with a large magnetization. The large magnetization $|M| \gg 1$, in fact, rules out any spin-based origin for the phenomena. We call the state orbital ferromagnet since it relies on the orbital angular momentum.

Due to time reversal symmetry, the ground state is degenerate in the orbital ferromagnetic state with $\langle \mathrm{GS}|\hat{M}|\mathrm{GS}\rangle = \pm M$. In fact, numerical rounding errors in the exact-diagonalization method corresponds to the initial condition in choosing the realized ground state. Increasing λ further, more jumps in the magnetization take place at larger distinct values of interaction strength. The ground-state magnetization for $N = 2$ in the orbital

ferromagnetic state is always even, while, for $N = 3$, the magnetization takes on half-odd-integer values and changes by one integer at the moments of transition in the ferromagnetic states.

The ground-state energy E_0 increases analytically as a function of λ before the first transition, while E_0 becomes singular at the critical interaction strength. The derivative of energy with respect to interaction strength $dE_0/d\lambda$ is shown in Fig. 5.4, which indicate E_0 increases linearly as a function of interaction strength λ in the orbital ferromagnetic state.

In the following chapter, a number of effective models are considered in order to explain the low-energy physics of the system to some extent. In the following, we interpret the observations with the aid of the characteristic of interaction matrix elements (IMEs) $V^{(m)}_{J_1 J_2}$, see chapter 4. First, we give a short review. IMEs have a number of properties which are due to the time reversal symmetry of the eigenbasis and topological restrictions of scattering processes on the (translational) momentum-space ring generated by Rashba coupling. Thereby, the matrix elements are boosted along BCS-like $J_1 = -J_2$ and exchange-type interactions $J_2 = J_1 + m$. The former correlates Kramers pairs and the latter provides exchange energy responsible for magnetization. Furthermore, there is hierarchy for IMEs that $|V^{(m)}_{J_1 J_2}|$ decays quickly by increasing exchanged momentum m.

Interaction with $m = 0$ along BCS-like channel $V^{(0)}_{-J,J} > 0$ makes the presence of Kramers pairs energetically expensive. On the other hand, if interacting electrons are nearest neighbor $J_2 = J_1 \pm 1$, then they benefit from the largest exchange energy $-V^{(\pm 1)}_{J\pm 1,J} < 0$ (the negative sign is due to fermion antisymmetry while $V^{(\pm 1)}_{J\pm 1,J} > 0$). From a mean-field point of view, $m = 0$ channel breaks the pairs and $m = \pm 1$ along the exchange-type interactions cause electrons to occupy the nearest neighbor sites. This fact indicates the magnetization of a two-electron system in ferromagnetic state must be an even number $M = (2J + 1)\hbar$. The expectation values of distribution function $n_J = c^\dagger_J c_J$ before and after transition to the orbital ferromagnetism are shown in Fig. 5.5. It is clear that before transition two electrons are Kramers pair, while they occupy the adjacent sites after transition. For $N = 3$, two electrons occupy the nearest neighbor sites and one electron is free of nearest neighbor. Therefore, the ground-state magnetization $M = (2J + 1 + J')\hbar$ can take on any half-odd-integer value.

Comparing the results for $\alpha = 10$ and $\alpha = 15$, it is evident that the transition to the orbital ferromagnetism takes place for a weaker interaction strength by increasing the Rashba coupling. For $\alpha = 10$ and $N = 2$, the first critical interaction strength occurs at $\lambda_c \approx 0.25$ at which the magnetization jumps from zero to $|M| = 6\hbar$. While for $\alpha = 15$ and $N = 2$, the first transition happens from zero magnetization to $|M| = 8\hbar$ at $\lambda_c \approx 0.17$. Similarly, for $N = 3$ the first critical interaction strength decreases from $\lambda_c \approx 0.31$ to $\lambda_c \approx 0.22$ for $\alpha = 10$ and $\alpha = 15$, respectively. The total angular momentum for $N = 3$ is and half-odd-integer. In this case, the magnetization abruptly changes from $|M| = 0.5\hbar$ to $|M| = 11.5\hbar$

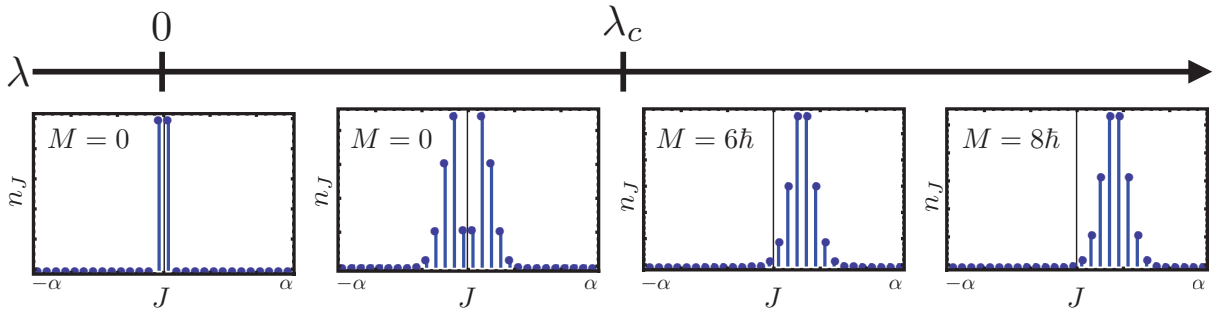

Figure 5.5: Distribution function n_J versus angular momentum J, for two-electron system in different regime of interaction strength λ. J, in the range of $-\alpha \lesssim J \lesssim \alpha$ due to the single-band approximation. The interaction strength is shown schematically by an arrow on top of the panels. The panels for $\lambda < \lambda_c$ show n_J before the transition to the orbital ferromagnetism. In this regime, the sites are occupied symmetrically with respect to the origin due to the time-reversal symmetry. For $\lambda > \lambda_c$, the panels depict n_J after the transition to the orbital ferromagnetism. In ferromagnet phase, electrons occupy nearest neighbor sites as though they constitute a composite particle which a unified peak is visible rather than two peaks. This composite-like particle moves coherently further in J-space toward the end of the band with Increase in interaction strength λ.

for $\alpha = 10$ and from $|M| = 0.5\hbar$ to $|M| = 14.5\hbar$ for $\alpha = 15$ at first critical interaction strengths.

In section 4.2.3, we studied two-particle system in the presence of the ultrastrong Rashba coupling $\alpha \to \infty$. It was shown there that the effect of zero-exchanged-momentum interaction is crucial in the realization of the orbital ferromagnetism. This fact is consistent with the exact-diagonalization results as discussed here. It reveals the pair-breaker role of interactions with zero-exchanged momentum. Besides, for $\alpha \to \infty$, the critical interaction strength vanishes in $\alpha \to \infty$ i.e. an infinitesimally weak interaction leads to the orbital ferromagnetism. This is also consistent with the results given here as the critical interaction strength decreases with increase in α, see Fig. 5.4. Another common feature in these two limits is that the magnetization for $N = 2$ takes on even values. As is discussed for the case of finite α, this fact is due to the large exchange interactions by exchanging $m = \pm 1$ momentum which is in contrast to the ultrastrong Rashba coupling. The odd-even-parity effect for $\alpha \to \infty$ indicates the absence of interactions with an odd exchanged momentum.

Since the total orbital angular momentum is conserved $[H, \hat{M}] = 0$, the eigenstates can be chosen to be the simultaneous eigenstates of H and $\hat{M}$. States with fixed M have an spectrum determined by internal degree of freedoms i.e. relative angular momentums of electrons which are not conserved quantity in the presence of interaction. Anyway, it is possible to find the state with lowest energy E_M in each sector defined by fixed M at a given interaction strength λ. In Fig. 5.6, E_M is shown versus M for $N = 2$ and $N = 3$

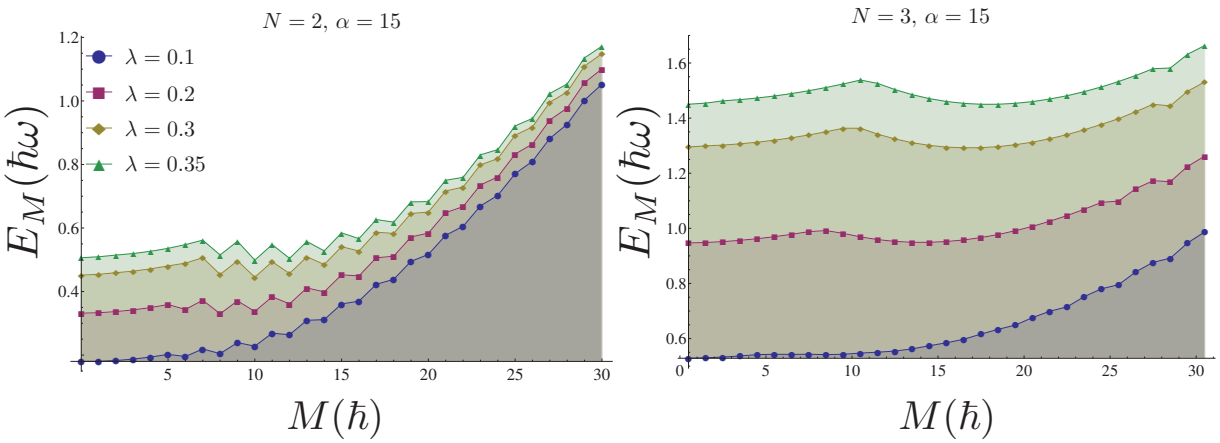

Figure 5.6: The lowest energy of states with fixed magnetization M, and Rashba coupling $\alpha = 15$, and several interaction strength λ. Increasing λ, gradually a second well appears in E_M at magnetization larger than the first dip $|M| \approx 0$, for $N = 2$ and $N = 3$ in the left and right panel, respectively. This well stabilizes itself as the ground state by further increase in λ which is called the orbital ferromagnetic state.

and several interaction strengths[1]. For larger values of λ, two dips appear in the energy of states with a given λ gradually, one corresponding to the unmagnetized state and the other to the orbital ferromagnet. Two dips are separated with a shallow energy barrier which is in order of $0.1\hbar\omega$. It should be noted that at a given λ, the lowest energies is the energy of the ground states and the other energies correspond to the excited states. The energy of two dips, unmagnetized and magnetized one, are quite degenerate. This fact indicates that even for Coulomb interacting system, the phase with strong correlation of Kramers pairs, and hence lowest magnetization, is competing with the orbital ferromagnetism, see also the following chapter. Such a competition indeed is expected from the characteristics of the interaction in the system, discussed in chapter 4. Taking into account the Kramers degeneracy, a third dip exists at the negative branch of magnetization in Fig. 5.6. The oscillations in the excited states for $N = 2$ will be discussed in the section of Hartree-Fock approximation 5.4.

5.3 Density Matrix Renormalization Group

In this section, we present the DMRG results for $N = 4$ and $\alpha = 15$. DMRG calculations reproduced the exact-diagonalization findings discussed in the preceding section with a very high accuracy, not shown here. In fact, it turned out that the study of the sys-

[1]We thank Dr. Peter Schmitteckert for pointing out the representation of data in a way shown in Fig. 5.6.

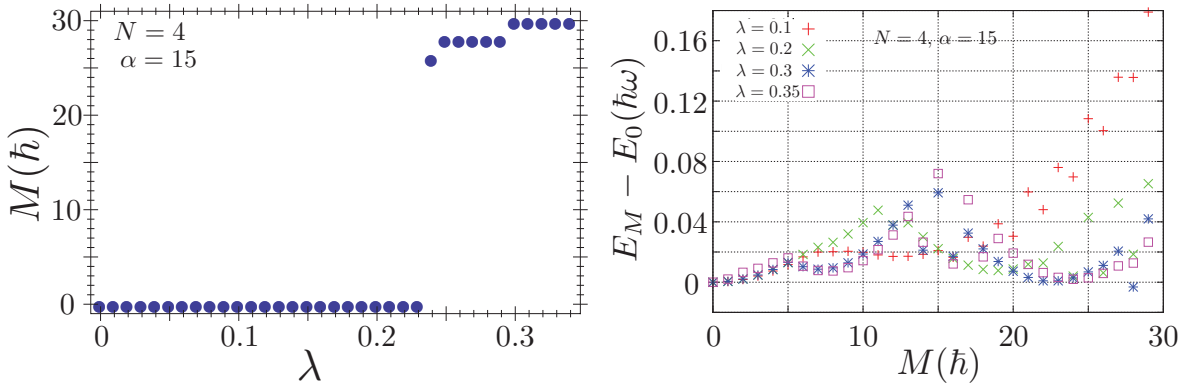

Figure 5.7: DMRG results for $N = 4$ and $\alpha = 15$. The left panel shows the ground-state magnetization M versus interaction strength λ. The right panel illustrates the lowest energy E_M of the states with a given magnetization versus magnetization of the state M for several values of interaction strength.

tem containing large number of particles with DMRG technique is computationally more efficient in comparison with the exact diagonalization. In Fig. 5.7, the magnetization is depicted versus λ for $N = 4$ and $\alpha = 15$. The transition from an unmagnetized state to the orbital ferromagnetism with $M = 26\hbar$ takes place at $\lambda_c \approx 0.24$ which is slightly larger than the value for $N = 3$ and $\alpha = 15$, see Fig. 5.4. Similar to $N = 2$, the magnetization takes on even values. That is by increase in λ, transitions take place form $M = 26\hbar$ to $M = 28\hbar$, and so on. The underlying reason for the parity of the magnetization is explained in the preceding section. Moreover, the lowest energy of states with a given magnetization M is shown in Fig. 5.7. It can be seen that the oscillatory behaviors appear for the energy of the states close to the orbital ferromagnet ground state, similar oscillations are observed for $N = 2$, see Fig. 5.6. We discuss the effect in the following section.

5.4 Hartree-Fock Approximation

The exact diagonalization becomes computationally expensive for $N > 3$. Instead, we carry out unrestricted Hartree-Fock (HF) approximation [44] in order to find the ground-state results for system of $N \leqslant 10$ particles. The HF Hamiltonian has the form

$$H_{\rm HF} = \sum_J \left(E_J + 2 \sum_{J'} \left[V^{(0)}_{JJ'} - V^{(J'-J)}_{JJ'} \right] n_{J'} \right) c^\dagger_J c_J, \tag{5.27}$$

where the occupation number $n_J = \langle c^\dagger_J c_J \rangle$ is taken as the variational parameter[2]. The self-consistentecy is found numerically by iteration, starting from randomly chosen initial

[2]An alternative way to compute the ground-state energy is as follows. The occupation number n_J is a conserved quantity in the HF theory with eigenvalues 0 or 1. And also note that $[\hat{M}, n_J] = 0$. The

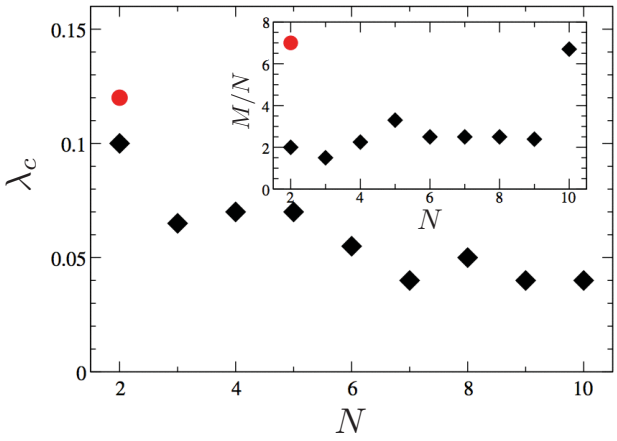

Figure 5.8: Hartree-Fock results (black diamonds) for the critical interaction strength λ_c versus particle number N for $\alpha = 30$ (main panel). The red circle shows the corresponding exact-diagonalization result for $N = 2$. Inset: Magnetization M per particle number in units of $\hbar$ found for $\lambda \gtrsim \lambda_c$ versus particle number N.

distribution. The converged set of distribution functions $\{n_J\}$ gives the ground-state energy and magnetization. The results of HF is shown in Fig. 5.8. When λ approaches the first critical value of interaction strength λ_c, the ground-state energies shows non-analytical features. For $N = 2$, the corresponding exact diagonalization results is given. The HF prediction is only slightly smaller than the exact one. This can be understood as the BCS-like interaction with $m \neq 0$, particularly $m =$ odd, are absent in $H_{\rm HF}$, see the discussion below. The inset of Fig. 5.8 the HF value of magnetization scales as $M \propto N$ is significantly smaller than the exact one. With increasing N, HF predictions show the transition can be reached at even weaker interaction.

Although HF qualitatively describes transition to the orbital ferromagnetic states with increase in λ, it becomes poor in rendering systematic results for larger N. Particularly, the critical interaction strength λ_c for $N \gtrsim 4$ does not take on a sharp value in HF analysis and is chosen as the value where the largest jump in the magnetization takes place.

This deficiency can be attributed, first, to the shallow minima of free energy, see Fig. 5.6, which is a difficult quantity to be predicted with rough approximation of HF method. The states with all the possible magnetizations are almost degenerate. The second reason is concerning dismissing the BCS-like interaction in $H_{\rm HF}$, through approximating the interaction term, which has the same importance as the exchange-type interactions $V_{JJ'}^{(J'-J)}$ relying

eigenstates can be chosen to be simultaneous eigenstate of magnetization $\hat{M}$ and set of n_J for allowed J in the single-band approximation $|J| \lesssim \alpha$. Number of eigenstates for a given particle numbers N is finite due to the discreteness of J and single-band approximation $|J| \lesssim \alpha$. The energy of the states can be evaluated readily by means of HF hamiltonian. The method for finding the ground-state energy then reduces to a sorting problem.

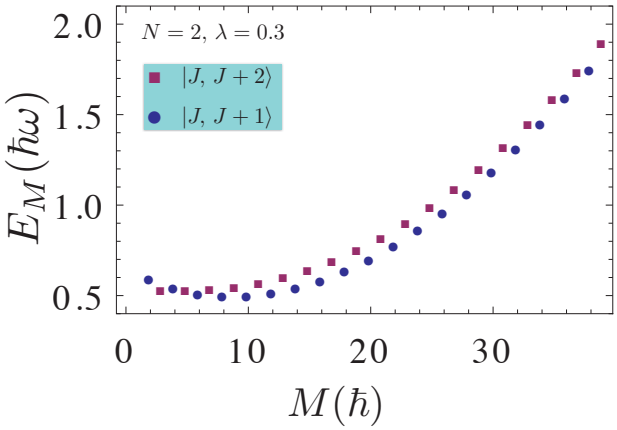

Figure 5.9: Energy of the Hartree-Fock eigenstates for $N = 2$ with even $|J, J+1\rangle$ and odd $|J, J+2\rangle$ magnetization, shown versus magnetization M of the sates. As an illustration, we set the interaction strength $\lambda = 0.3$ which indicates the interacting model is in the orbital ferromagnetic phase as $\lambda > \lambda_c$, see Fig. 5.4. The oscillation in E_M appears as the magnetization of states alternates between odd and even values. The state with $M = 8\hbar$ and $M = 10\hbar$ have the lowest energies.

on the symmetry relations of IMEs. In fact, BCS-like interaction with odd m, in coalition with the kinetic term, favors the presence of Kramers pairs although BCS-like interaction with even m, particularly $m = 0$ channel, and all the exchange-type interactions work in favor of magnetism. In the absence of BCS-like interaction with $m \neq 0$, Kramers pairs become unstable quickly after switching on the interaction.

Equivalently, one can say $H_{\rm HF}$ conserves the relative angular momentum of particles through conserving the momentum of each particles, since $H_{\rm HF}$ is a free theory. Although, the interacting model H does not bear this symmetry. In chapter 6.3, an effective model is constructed which incorporate both Hartree-Fock term and BCS-like interaction together. The latter actually breaks the extra symmetry of $H_{\rm HF}$.

Finally, we address the oscillatory behaviors observed in the lowest energies of the states with fixed magnetization M for two-particle system $N = 2$, see Fig. 5.6. According to the analysis given in the preceding section, in the orbital ferromagnetic phase, electrons of broken Kramers pairs prefer to occupy consecutive sites to reduce the energy by largest exchange interactions. And also note that the oscillations give rise while λ approaches its first critical value. Then, it is not difficult to attribute the oscillations to the constraint provided by odd-even parity of magnetization M in a mean-field argument. Indeed, for even M two particles can occupy consecutive site $J_2 = J_1 - 1 = J$ which gives an even-number magnetization $M = 2J + 1$. Otherwise, if M is an odd number, the electrons should occupy the next nearest neighbor to lower the energy by a weaker exchange energy than the nearest neighbor interaction. We study the following ansatz by $H_{\rm HF}$ to quantify

the argument

$$|M\rangle = \begin{cases} |J,\, J+1\rangle = c_J^\dagger c_{J+1}^\dagger |0\rangle & \text{For even } M = 2J+1\ , \\ \\ |J,\, J+2\rangle = c_J^\dagger c_{J+2}^\dagger |0\rangle & \text{For odd } M = 2J+2\ . \end{cases}$$

Operating with $H_{\rm HF}$ on these states, we find

$$\langle M|H_{\rm HF}|M\rangle = \begin{cases} \frac{J^2}{2\alpha^2} + \frac{(J+1)^2}{2\alpha^2} + 2\lambda \left(V^0_{J,J+1} - V^1_{J,J+1}\right) & \text{if } M = \text{even}, \\ \\ \frac{J^2}{2\alpha^2} + \frac{(J+2)^2}{2\alpha^2} + 2\lambda \left(V^0_{J,J+2} - V^2_{J,J+2}\right) & \text{if } M = \text{odd}. \end{cases}$$

A plot of the energies is shown in Fig. 5.9 which resembles the same type of oscillation observed in exact diagonalization results in Fig. 5.6. For $N = 3$, it is not necessary to break the nearest neighbor pairs as a response to the change of the total magnetization by one integer. In the orbital ferromagnetic state, there is a pair of electrons which occupy the nearest neighbor sites. The sum of angular momentum of these two electrons is even. The third electron can change its angular momentum by one integer to compensate the change of the total magnetization. The same scenario is expected to happen for larger odd or even number of particles.

5.5 Summary

We have studied Coulomb-interacting few-electron quantum dots with strong Rashba SOC. In the regime of ultrastrong Rashba coupling, we have observed that even very weak interactions give rise to a large magnetization in the system for $N = 2$. Engaging standard exact diagonalization technique and Hartree-Fock approximation, the ground-state energy and magnetization of few-electron systems are evaluated as a function of interaction strength λ. The ground state shows a transition from unmagnetized states to an orbital ferromagnetism if strength of interaction exceeds a critical value $\lambda > \lambda_c$. The results of exact diagonalization for $N = 2$ and $N = 3$ indicate clearly that transition to the magnetized state takes place for a weaker critical value of interaction strength λ_c by increasing the dimensionless Rashba coupling α. The HF calculations predicts the same transitions to orbital ferromagnetism for $N \leqslant 10$ qualitatively. Moreover, DMRG results for $N = 4$ and $\alpha = 15$ admits the physics observed by exact-diagonalization technique. That is a sharp transition to orbital ferromagnetism occurs at a critical interaction strength.

Chapter 6

Many-Body System

In this chapter, we study a 2D system of N interacting electrons in the presence of a strong Rashba spin-orbit coupling (SOC) $\alpha \gg 1$ and parabolic trap. N is taken to be an arbitrary integral number. The Fermi momentum J_F, which is taken in the noninteracting regime, and the dimensionless Rashba coupling must satisfy $N/2 \approx J_F \lesssim \alpha$ in order to maintain the single-band approximation, see section 3.3. In fact, even in the limit $\alpha \to \infty$, see section 5.1, we deal with a discrete model due to the discreteness of the total angular momentum. Remarkably, the odd-even parity is crucial in the characteristics of the interactions which emphasize the maintenance of the discreteness. Therefore in this chapter, the approach in the study of the system is to approximate the many-body Hamiltonian in different regimes of interaction and write it formally in forms similar to the well-studied discrete models which allow a prospect of analytical or numerical treatments. Note that, the exact diagonalization becomes computationally too expensive even for $N = 4$.

We start with the study of the model in the regime of very weak interactions. In this regime, the interaction matrix elements (IMEs) for the states close to the Fermi momentum J_F can be approximated by a uniform coupling constant, i.e. independent of the momentum of incoming and outgoing electrons, if the variations of IMEs in the relevant regions are small in comparison with the level spacing. The Hamiltonian is then amenable to bosonization. It shall be shown that Kramers pairs are correlated strongly even for a repulsive interaction. In fact, the strong correlation in grand-canonical ensembles is a sign of superconductivity although that is debatable in the canonical ensemble studied here [19, 18]. The ground state is shown to be unmagnetized which is plausible for such a weak interaction. Though, the singular correlation of Kramers pairs persists even in magnetized states, however, is suppressed significantly. Therefore, once more, an odd-even-parity effect arises with respect to the number of electrons: For an odd number, the ground state is magnetized which suppresses the correlation function.

Next, we construct and study another effective model based on the strong correlation of Kramers pairs. Truncating the interaction terms and keeping the uniformed BCS-like interactions of Kramers pairs, we obtain the well-studied pairing model which its exact

solution has been derived by Richardson around fifty years ago [89]. In order to find out the eigenenergy of the model, one must solve a set of nonlinear singular equations which is called Richardson equations. Instead of solving the equations, we analyze the model heuristically in two regimes of weak and strong interactions which indicates a transition takes place from pairing ground state to the orbital ferromagnetism. Although, the value of the critical interaction strength, in which the transition occurs, might violate the weak-interaction constraints on which the effective models are constructed. To check the critical interaction strength, one needs to solve the Richardson equations and find the ground-state energy in different range of interactions. However, the study of the effective pairing model gives this insight that transition from the pairing to the orbital ferromagnetism, two phases which are expected in the system, can be realized in the system only by engaging the BCS-like interactions, and also the exchange-type interactions based on symmetry relations.

The last effective model which we study in this chapter relies on the result of the pairing model. We approximate the original Hamiltonian by truncating the interaction term and maintain only BCS-like and exchange-type interactions. The significance of those interactions are based on two facts. First, the IMEs of BCS-like and exchange-type interactions are the strongest elements for a given exchanged momentum m. Next, the correlation function of Kramers pairs is shown to be singular. Restoring the inhomogeneity of IMEs, one can study the stronger interaction in comparison with the other effective uniform models. Besides, it allows to compare the role of different interaction potentials, e.g. Coulomb or contact, in the physics of the system. On the other side, such a truncated Hamiltonian is equivalent to an extended Hartree-Fock Hamiltonian since it includes Hartree-Fock Hamiltonian in addition to a term which solely describes BCS-like interactions. The effective Hamiltonian in fact can be interpreted as a lattice model. We show that it also can be represented as a Heisenberg XXZ spin model by constructing operators which satisfy $SU(2)$ algebra. Although the analytical solution of the model is not found, it can be tackled with the numerical technique appropriate for discrete 1D problems as DMRG method [107, 25, 93]. Indeed, the the effective model inspired us to apply the DMRG technique, see section 5.3, to the full system.

6.1 Bosonization

In this section, first, the interaction matrix elements are estimated by a uniform coupling constant in the regime of weakly interacting electrons. Afterward, it can be shown that the low-energy excitations in the system are density fluctuations. The boson representation of the effective Hamiltonian can be diagonalized which leads to the computation of the ground-state magnetization. We show that the ground state is unmagnetized. The effective 1D Hamiltonian is amenable to bosonization [73, 99, 104], and therefore, allows exact calculation of correlation functions. It will be shown that the correlation of Kramers pairs is singular for both repulsive and attractive interaction potentials. The preliminary

and complementary to the calculations presented in this section are relegated to appendix D.

6.1.1 Effective Uniform Hamiltonian

We study a many-body system of electrons described by the following Hamiltonian in second quantized representation

$$\begin{aligned} H &= H_0 + H_I \\ &= \sum_J \frac{J^2}{2\alpha^2} c_J^\dagger c_J + \lambda \sum_{\substack{J_1,J_2 \\ m}} V^{(m)}_{J_1,J_2}\, c^\dagger_{J_1+m} c^\dagger_{J_2-m} c_{J_2} c_{J_1}, \end{aligned} \tag{6.1}$$

where λ is the dimensionless strength of interaction. The energy unit $\hbar\omega$ is set to unity. The symmetry relations of $V^{(m)}_{J_1,J_2}$ are studied in section 4.3 and its numerical values are discussed for Coulomb and contact potentials. The non-interacting system $\lambda = 0$ has a well-defined Fermi momentum J_F which is the angular momentum of the highest occupied state. For weakly interacting electrons, low-lying excited states live in the vicinity of Fermi points $|J| \approx J_F$. We engage this fact and approximate the kinetic term and IMEs $|J_{1,2}| \approx J_F \lesssim \alpha$.

First we discuss the kinetic term. In the regime of weak interaction, the states close to the Fermi points $\pm J_F$ can be excited by interaction. Introducing a new variable through $J = \pm J_F + j$ for $j \in \mathbb{Z}$ yields to the energy dispersion $\varepsilon_j^\pm = (\pm J_F + j)^2/2\alpha^2 = \varepsilon_F \pm v_F j + j^2/2\alpha^2$ where $\varepsilon_F = J_F^2/2\alpha^2$ and $v_F = J_F/\alpha^2$ are the Fermi energy and Fermi velocity, respectively. We consider $|j| \ll J_F \lesssim \alpha$ and neglect the term second order in j/α. The creation and annihilation operator are labeled by j and chirality $\eta = \pm$ read as $c^\dagger_{j\eta} \equiv c^\dagger_{\eta J_F + j}$ and $c_{j\eta} \equiv c_{\eta J_F + j}$, respectively. The free Hamiltonian is approximated by

$$H_0 \approx v_F \sum_{j,\,\eta=\pm} \eta j\, c^\dagger_{j\eta} c_{j\eta}, \tag{6.2}$$

up to a c-number. It is worth pointing that $c^\dagger_{j\eta}$ transforms under time reversal (TR) as

$$\Theta c^\dagger_{j\eta} = (-1)^{\eta J_F + 1/2 + j} c^\dagger_{-j,-\eta}, \tag{6.3}$$

and note that $j \in \mathbb{Z}$. Therefore, the time-reversed partner of (j,η) is the state $(-j,-\eta)$. Next, we estimate IMEs. We are interested in the weakly interacting theory $\lambda \ll v_F$. This implies the states close to the narrow bandwidth around the Fermi momentum $||J| - J_F| \ll J_F \lesssim \alpha$ can be excited by interaction. This fact suggests the matrix elements $V^{(m)}_{J_1,J_2}$ with $|J_{1,2}| \approx J_F$ are relevant to the interacting theory, i.e. those elements depicted in Fig. 6.1 with highlighted squares in (J_2, J_1) planes schematically for $m =$ even and $m =$ odd. It was observed in section 4.3 that $V^{(m)}_{J_1,J_2}$ of both Coulomb and contact potentials decreases with increase in $|m|$, particularly, along the maximal absolute magnitude lines and far from

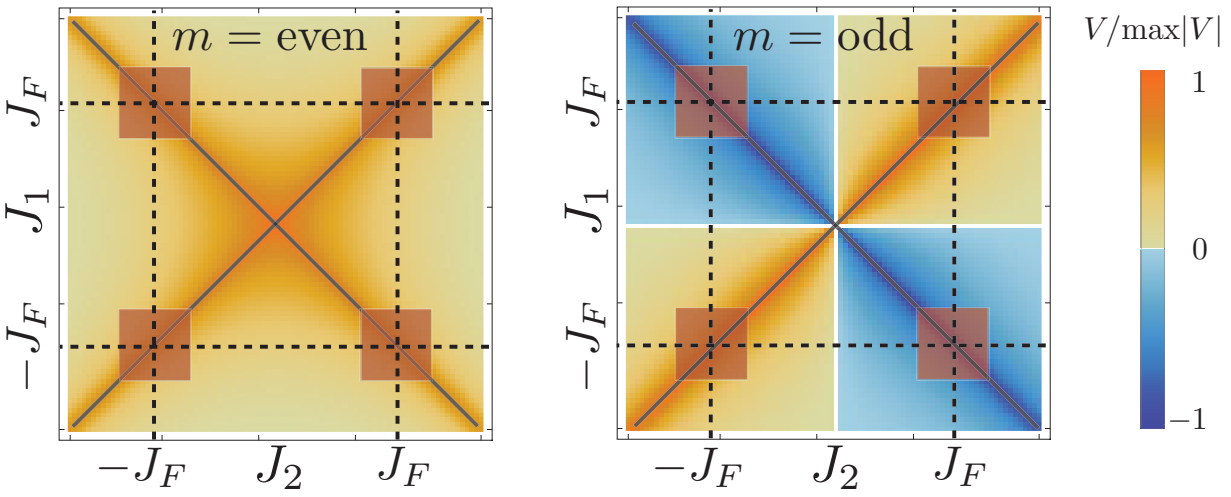

Figure 6.1: (Color online) Schematic illustration of the interaction matrix elements $V^{(m)}_{J_1,J_2}$ in the vicinity of Fermi points J_F for even/odd m. In the weak-interaction regime, the low-energy interaction-driven excitations lie close to the Fermi points. Therefore, the interaction matrix elements with $|J_{1,2}| \sim J_F$ are relevant. In the bosonization scheme, the absolute magnitude of the matrix elements incorporated in the highlighted squares, shown inside the panels, are approximated to be a c-number independent of $J_{1,2}$ and m. Although, their sign depends on m and relative chirality of interacting particles: whether $J_1 J_2 > 0$ or $J_1 J_2 < 0$.

the symmetry center $(m/2, -m/2)$. It indicates the backward scattering $m \sim 2J_F$ can be neglected by tuning $J_F \lesssim \alpha$, and hence, only the forward scatterings $|m| \ll J_F$ contribute to the low-energy physics.

In the next step, we estimate the absolute magnitude of IMEs $V^{(m)}_{J_1 J_2}$ for $|J_{1,2}| \approx J_F$ by a coupling constant and neglect the small variation of $|\lambda V^{(m)}_{J_1,J_2}|$ in comparison with the level spacing v_F

$$\lambda \left| V^{(m)}_{J_1,J_2} \right| \approx \frac{g}{4\pi}, \tag{6.4}$$

where g is independent of $J_{1,2}$ and m. The approximation can be justified if

$$||V| - |V'|| < \frac{v_F}{\lambda}, \qquad \text{for } |J_{1,2}| \approx J_F \lesssim \alpha \;\text{ and }\; |m| \ll 2J_F, \tag{6.5}$$

which is equivalent to saying that the level quantization v_F does not see the variations of IMEs in the weakly interacting theory. The constraint can be satisfied confidently in the limit $\lambda < 1$ for a short-range potential e.g. contact potential although for Coulomb potential $\lambda \ll 1$ might be required. Now, we need to determine the phase of the coupling constant g. From Fig. 6.1, it is clear that the sign of IMEs has to be assigned concerning

the chirality of the interacting particles

$$\lambda V^{(m)}_{J_1,J_2} \approx \begin{cases} g/4\pi & \text{for } J_1 J_2 > 0, \\ (-1)^m g/4\pi & \text{for } J_1 J_2 < 0. \end{cases} \tag{6.6}$$

The interaction term then has to be written separately with respect to the chirality

$$H_I = \frac{g}{4\pi} \sum_{\substack{j,j,m \\ \eta=\pm}} (-1)^m c^\dagger_{j+m\eta} c^\dagger_{j'-m,-\eta} c_{j',-\eta} c_{j\eta} + \frac{g}{4\pi} \sum_{\substack{j,j',m \\ \eta=\pm}} c^\dagger_{j+m\eta} c^\dagger_{j'-m\eta} c_{j'\eta} c_{j\eta}, \tag{6.7}$$

where the convention of this section has been employed $J = \eta J_F + j$ for $j \in \mathbb{Z}$ and chirality $\eta = \pm$. The first (second) term in H_I describes the interactions of particles with the opposite (same) chirality. Then the effective isotropic Hamiltonian can be written by assembling H_0 and H_I as

$$H = v_F \sum_{j,\,\eta=\pm} \eta j \, c^\dagger_{j\eta} c_{j\eta} + \frac{g}{4\pi} \sum_{\substack{j,\,j',\,m \\ \eta=\pm}} (-1)^m c^\dagger_{j+m\eta} c^\dagger_{j'-m-\eta} c_{j'-\eta} c_{j\eta} + \frac{g}{4\pi} \sum_{\substack{j,\,j',\,m \\ \eta=\pm}} c^\dagger_{j+m\eta} c^\dagger_{j'-m\eta} c_{j'\eta} c_{j\eta}. \tag{6.8}$$

We can represent H solely in terms of the chiral density operators which is defined by

$$n_{m\eta} = \sum_j c^\dagger_{j\eta} c_{j+m\eta}, \tag{6.9}$$

with the commutation relation

$$[n_{m\eta},\, n_{-m'\eta'}] = \delta_{\eta\eta'} \delta_{mm'} \, \eta m. \tag{6.10}$$

The Hamiltonian then up to a zero-point shift in energy takes the form

$$H = v_F \sum_{\substack{m>0 \\ \eta=\pm}} n_{-m\eta} \, n_{m\eta} + \frac{g}{4\pi} \sum_{\substack{m\neq 0 \\ \eta=\pm}} \Big\{ (-1)^m \, n_{m\eta} \, n_{-m-\eta} + n_{m\eta} \, n_{-m\eta} \Big\} + H', \tag{6.11}$$

where the kinetic term is also represented by means of the density operators [99, 104]. The zero modes are collected in

$$H' = \frac{v_F}{2} \sum_\eta \delta\hat{N}_\eta \left(\delta\hat{N}_\eta + 1 \right) + \frac{g}{4\pi} \left(\delta\hat{N}_+ + \delta\hat{N}_- \right)^2, \tag{6.12}$$

in terms of the normal ordered operator

$$\delta\hat{N}_\eta = \sum_j : c^\dagger_{j\eta} c_{j\eta} := \sum_{\eta j>0} c^\dagger_{j\eta} c_{j\eta} - \sum_{\eta j<0} c_{j\eta} c^\dagger_{j\eta}, \tag{6.13}$$

which counts the number of particles added to or removed from the corresponding branch η. The effective Hamiltonian in the current form describes the dynamics of the density

fluctuations in the system which is in fact equivalent to a boson gas. This equivalence shall be more apparent in the next subsection.

The phase factor $(-1)^m$ for the interaction of particles with the opposite chirality can be gauged out. In fact, we attach a phase factor to the density operator

$$\tilde{n}_{m\eta} = e^{i\eta m\pi/2}\, n_{m\eta}. \tag{6.14}$$

in order to remove $(-1)^m$ in the interaction term. $\tilde{n}_{m\eta}$ satisfies the same commutation relation of the density operators in Eq. 6.10. Substituting the gauged density operator in the Hamiltonian yields

$$H = v_F \sum_{\substack{m>0\\ \eta=\pm}} \tilde{n}_{-m\eta}\, \tilde{n}_{m\eta} + \frac{g}{4\pi} \sum_{\substack{m\neq 0\\ \eta=\pm}} \Big\{ \tilde{n}_{m\eta}\, \tilde{n}_{-m-\eta} + \tilde{n}_{m\eta}\, \tilde{n}_{-m\eta} \Big\} + H', \tag{6.15}$$

which leaves invariant all the other terms. Now, H takes the form of the standard Tomonaga-Luttinger model [99, 104], with length of the system $L = 2\pi$. We diagonalize this Hamiltonian in the next section. Although, we engage the bare operators to inspect the correlation functions in the interacting system, see subsection 6.1.4. It is interesting to note that the gauge $e^{i\eta m\pi/2}$ does not depend to the interaction strength λ, or g in the effective model. In this view, the gauge gives rise to non-perturbative features of the interacting model. It exists if the interaction is switched on and no matter how much the interaction is weak. The phase factor $(-1)^m$, which its effect in Eq. 6.15 is transferred to the gauge $e^{i\eta m\pi/2}$, relies on the time-reversal symmetry of the interaction potential and the eigenbsis, discussed in chapter 4. For instance, the time reversal of Coulomb potential is its fundamental feature and cannot be discarded. As will be shown later, the Kramers pairs are correlated strongly due to the presence of this robust property without any dependence to the sign of the interaction potential.

6.1.2 Diagonalizing the Full Hamiltonian

The effective Hamiltonian is quadratic and can be diagonalized readily. First, it is required to represent the Hamiltonian in terms of the boson operators. With the aid of the gauged boson operators $\tilde{b}^\dagger_m$ and $\tilde{b}_m$, defined in Eqs. D.69 and D.70, with the commutation relations

$$[\tilde{b}_m,\, \tilde{b}_{m'}] = [\tilde{b}^\dagger_m,\, \tilde{b}^\dagger_{m'}] = 0, \tag{6.16}$$

$$[\tilde{b}_m,\, \tilde{b}^\dagger_{m'}] = \delta_{mm'}, \tag{6.17}$$

the Hamiltonian takes the form

$$H = v_F \sum_m |m|\, \tilde{b}^\dagger_m \tilde{b}_m + \frac{g}{4\pi} \sum_m |m| \left(\tilde{b}^\dagger_m \tilde{b}^\dagger_{-m} + \tilde{b}_{-m} \tilde{b}_m + \tilde{b}^\dagger_m \tilde{b}_m + \tilde{b}_{-m} \tilde{b}^\dagger_{-m} \right) + H'. \tag{6.18}$$

H can be diagonalized through a canonical transformation

$$\tilde{b}_m^\dagger = \beta_m^\dagger \cosh\vartheta - \beta_{-m} \sinh\vartheta, \tag{6.19}$$

$$\tilde{b}_{-m} = \beta_{-m} \cosh\vartheta - \beta_m^\dagger \sinh\vartheta, \tag{6.20}$$

where $\beta_m^\dagger$ and β_m satisfy the boson commutation relations. The coefficients are defined by

$$\tan 2\vartheta = \frac{\widetilde{g}}{1+\widetilde{g}}, \tag{6.21}$$

$$\widetilde{g} = \frac{g}{2\pi v_F}. \tag{6.22}$$

The excitation energy in the interacting model then can be obtained as

$$H = u \sum_m |m|\, \beta_m^\dagger \beta_m + H', \tag{6.23}$$

which the renormalized Fermi velocity is

$$u = v_F \sqrt{1+2\widetilde{g}}. \tag{6.24}$$

The contribution of the zero modes to the energy is determined by H' which is defined in Eq. 6.12. The states with no particle-hole excitations are eigenstate of H. Let represent those states with $|\vec{N}\rangle$ where the number of zero modes are given by $\vec{N} = (\delta N_+, \delta N_-)$. That is δN_η electrons are added to or removed from the branch $\eta = \pm$, for $\delta N_\eta > 0$ or $\delta N_\eta < 0$, respectively[1]. Therefore, the energy of the state $|\vec{N}\rangle$ is determined solely by H'. It indicates that the ground state is the boson vacuum $\beta_m|0\rangle = 0$ with no zero mode $\delta\hat{N}_\pm|0\rangle = 0$.

6.1.3 Ground-State Magnetization

Having found the ground state of the effective Hamiltonian, it is now possible to compute the ground-state magnetization. The total angular momentum, or magnetization, operator is defined as

$$\hat{M} = \hbar \sum_j (\eta J_F + j) : c_{j\eta}^\dagger c_{j\eta} : . \tag{6.25}$$

In terms of the gauged boson operators, we find

$$\hat{M} = \hbar \sum_m m\, \tilde{b}_m^\dagger \tilde{b}_m + \hat{M}_0, \tag{6.26}$$

[1] An explicit representation of the free boson vacuum is given in appendix D.1.3.

where the contribution of the zero modes is collected in

$$\hat{M}_0 = \hbar J_F \left(\delta\hat{N}_+ - \delta\hat{N}_-\right) + \frac{\hbar}{2}\left(\delta\hat{N}_+ - \delta\hat{N}_-\right)\left(\delta\hat{N}_+ + \delta\hat{N}_- + 1\right). \tag{6.27}$$

We need to represent it in terms of the boson operators which diagonalize the Hamiltonian. The expectation value of $\hat{M}$ in the ground state of the interacting system then gives the magnetization. With the help of Eqs. 6.19 and 6.20, we obtain

$$\begin{aligned}\hat{M} &= \hbar\sum_m m\Big\{\beta_m^\dagger\beta_m\cosh^2\vartheta - \beta_m^\dagger\beta_{-m}^\dagger\cosh\vartheta\sinh\vartheta \\ &\qquad -\beta_{-m}\beta_m\cosh\vartheta\sinh\vartheta + \beta_{-m}\beta_{-m}^\dagger\sinh^2\vartheta\Big\} + \hat{M}_0.\end{aligned} \tag{6.28}$$

The vacuum expectation value of $\hat{M}$ vanishes except the contribution solely from the zero modes

$$\begin{aligned}\langle\vec{N}|\hat{M}|\vec{N}\rangle &= \hbar\sinh^2\vartheta\sum_{m=-\infty}^{\infty} m\,\langle\vec{N}|\beta_{-m}\beta_{-m}^\dagger|\vec{N}\rangle + \langle\vec{N}|\hat{M}_0|\vec{N}\rangle \\ &= \hbar\sinh^2\vartheta\sum_{m=-\infty}^{\infty} m + \langle\vec{N}|\hat{M}_0|\vec{N}\rangle \\ &= \langle\vec{N}|\hat{M}_0|\vec{N}\rangle.\end{aligned} \tag{6.29}$$

The sum does not contribute $\sum_m m = 0$ since m is an odd function. Although, the sum must be regularized, the regularization factor $\sim e^{-|m|a}$ must be an even function. The magnetized states are not energetically favored due to the contribution of zero modes: suppose $\delta N_+ = -\delta N_- = \delta N$, by means of the zero modes of the Hamiltonian (6.12), we find

$$\langle\vec{N}|H'|\vec{N}\rangle = \hbar\omega\, v_F\delta N^2, \tag{6.30}$$

which indicates that in the considered regime of weak interaction, the system is unmagnetized.

6.1.4 Correlation of Kramers Pairs

The effective uniform 1D Hamiltonian allows exact calculation of correlation functions. It is convenient to compute the correlation functions in the continuous space conjugates to the space of the good quantum number. We conjugate the total angular momentum $j = J \mp J_F$ to the azimuthal angle θ in the translational momentum space $\mathbf{k}$. In fact, it is shown in appendix D.1.1 that the density operator is only a function of the azimuthal angle θ in the momentum space representation. This is so because the localized electrons

on the Rashba ring in momentum space can be characterized by only θ.

In the bosonization technique, an equivalent representation of fermion fields can be given in terms of the boson fields. The full form of the fermion field in our system is a function of the radial degree of freedom in addition to the azimuthal one. But, in the weak interaction regime, we integrate out the radial degree of freedom and consider a field which is only a function of θ and importantly leads to the correct form of the density operator in $\mathbf{k}$ space, see section D.1.1. Indeed, the effective Hamiltonian is described by the density operators and the fermion field itself is not an observable.

As it is mentioned before, we are interested in the correlation of the bare fermions, associated with the operators $c^\dagger_{j\eta}$ and $c_{j\eta}$, in the interacting system. The corresponding fermion field is defined by

$$c^\dagger_{j\eta} = \frac{1}{\sqrt{2\pi}} \oint d\theta \, e^{ij\theta} \; \Psi^\dagger_\eta(\theta), \tag{6.31}$$

where $\theta \in [0, 2\pi)$. The boson representation of the fermion field is formulated as

$$\Psi^\dagger_+(\theta) = \frac{1}{\sqrt{2\pi a}} F^\dagger_+ \, e^{-i\sqrt{\pi}[\Phi(\theta)+\Theta(\theta)]}, \tag{6.32}$$

$$\Psi^\dagger_-(\theta) = \frac{1}{\sqrt{2\pi a}} F^\dagger_- \, e^{i\sqrt{\pi}[\Phi(\theta)-\Theta(\theta)]}. \tag{6.33}$$

where $\Phi(\theta)$ and $\Theta(\theta)$ are dual boson fields defined in Eqs. D.33 and D.34. And $F^\dagger_\pm$ is the Klein factor which insures the anticommutation relation required for the fermion field. a is a small parameter for regularization and the limit $a \to 0$ is implicit in the definition of the fields. The dual fields can be written in terms of the renormalized gauged dual fields which act in the Hilbert space of interacting model

$$\Phi(\theta) = \frac{1}{2}\left\{ \sqrt{K}\left[\overline{\Phi}(\theta - \frac{\pi}{2}) + \overline{\Phi}(\theta + \frac{\pi}{2})\right] + \frac{1}{\sqrt{K}}\left[\overline{\Theta}(\theta - \frac{\pi}{2}) - \overline{\Theta}(\theta + \frac{\pi}{2})\right] \right\}, \tag{6.34}$$

$$\Theta(\theta) = \frac{1}{2}\left\{ \sqrt{K}\left[\overline{\Phi}(\theta - \frac{\pi}{2}) - \overline{\Phi}(\theta + \frac{\pi}{2})\right] + \frac{1}{\sqrt{K}}\left[\overline{\Theta}(\theta - \frac{\pi}{2}) + \overline{\Theta}(\theta + \frac{\pi}{2})\right] \right\}, \tag{6.35}$$

where $K = v_F/u$ and $u = v_F\sqrt{1+2\widetilde{g}}$ are the Luttinger parameter and the renormalized Fermi velocity, respectively. It should be taken into account that $\partial_\theta\Phi$ and $\partial_\theta\Theta$ are proportional to the particle density and current density of the free system, respectively, in the momentum space. In the same way, $\partial_\theta\overline{\Phi}$ and $\partial_\theta\overline{\Theta}$ are proportional to the gauged particle density and current in the interacting model, respectively. It is interesting to note that the gauged density (6.14) leads to a non-local relation between the free fields and renormalized gauged dual fields. The non-locality cannot be removed by a sole rotation $\theta \to \theta + \theta_0$. Besides, the bare particle density, for instance, induces both gauged particle and current density in the interacting model. It should be remembered that all these rely

on the time-reversal symmetry of the interaction term. We shall see that this non-local features correlate strongly time-reversed pairs.

Having constructed the boson representation of the fermion fields and the relation between the bare and renormalized gauged boson fields, we are now in the position to calculate exact correlation functions in the interacting system which is the subject of the next subsections. We present result for the correlation of Kramers pairs which shows singular behavior. In fact, it is the most important result in the bosonization section. The details of the calculation is relegated to appendix D.2.4. Also, in the subsection D.2.5, we briefly discuss that correlation of density fluctuations render trivial results in the considered regime of interaction.

We investigate the correlation of pairs $c^\dagger_{j+}c^\dagger_{-j-}$ in the interacting model. Such pairs are quite similar, formally, to the s-wave Cooper pairs since the electrons seem to be time-reversed partner. Although, a subtlety should be taken into account. As we have observed in Eq. 6.3, under TR $c^\dagger_{j\eta}$ goes to $(-1)^{\eta J_F+1/2+j}c^\dagger_{-j-\eta}$. Therefore, the time-reversed pair should be multiplied by a phase factor $(-1)^{J_F+1/2+j}c^\dagger_{j+}c^\dagger_{-j-}$. We call the pairs Kramers pairs if the phase factor has the right form. We observe that

$$\oint d\theta\, \Psi^\dagger_+(\theta)\, \Psi^\dagger_-(\theta+\theta_0) = \sum_j e^{ij\theta_0}\, c^\dagger_{j+}c^\dagger_{-j-}, \tag{6.36}$$

which shows that the time-reversed partner of $\Psi^\dagger_+(\theta)$ is $\Psi^\dagger_-(\theta+\pi)$ which is expected since θ is the azimuthal angle in the momentum space. We probe the correlation function for arbitrary θ_0, although, it reveals correlation of pairs which are not constructed from time-reversed partners for $\theta_0 \neq \pi$. We calculate the static correlation function

$$\begin{aligned} \mathrm{P}(\theta_0) &= \sum_{j,j'} e^{i(j-j')\theta_0}\, \langle\vec{N}|c^\dagger_{j+}c^\dagger_{-j-}c_{-j'-}c_{j'+}|\vec{N}\rangle_{\rm int} \\ &= \oint d\theta d\theta' \langle\vec{N}|\Psi^\dagger_+(\theta)\, \Psi^\dagger_-(\theta+\theta_0)\Psi_-(\theta'+\theta_0)\Psi_+(\theta')\,|\vec{N}\rangle_{\rm int}. \end{aligned} \tag{6.37}$$

The numerical values of $\mathrm{P}(\theta_0)$ are depicted in Fig. 6.2 versus θ_0 for several K and two different boson vacuum: one with zero magnetization and the other with non-zero magnetization i.e. $\delta N_+ = -\delta N_- = \delta N \neq 0$ and hence $\langle\hat{M}\rangle \neq 0$. The latter reveals the effect of the magnetization on the correlation function. As a matter of illustration, we set $a = 0.1$. The detailed calculation of $\mathrm{P}(\theta_0)$ is given in appendix D.2.4. For interacting model $K \neq 1$, the correlation function shows spikes when pairs are constructed by time-reversed partners $\theta_0 = \pi$. The spike disappears obviously for free system $K = 1$, but shows up if the interaction is switched on, no matter the pair potential is attractive $K > 1$ or repulsive $K < 1$. It is also interesting to note that even for magnetized states $\delta N \neq 0$, the spikes persist although has been weakened relatively in comparison with unmagnetized vacuum. An analytical representation for $\mathrm{P}(\theta_0 = \pi)$ can be obtained which its singular part in the

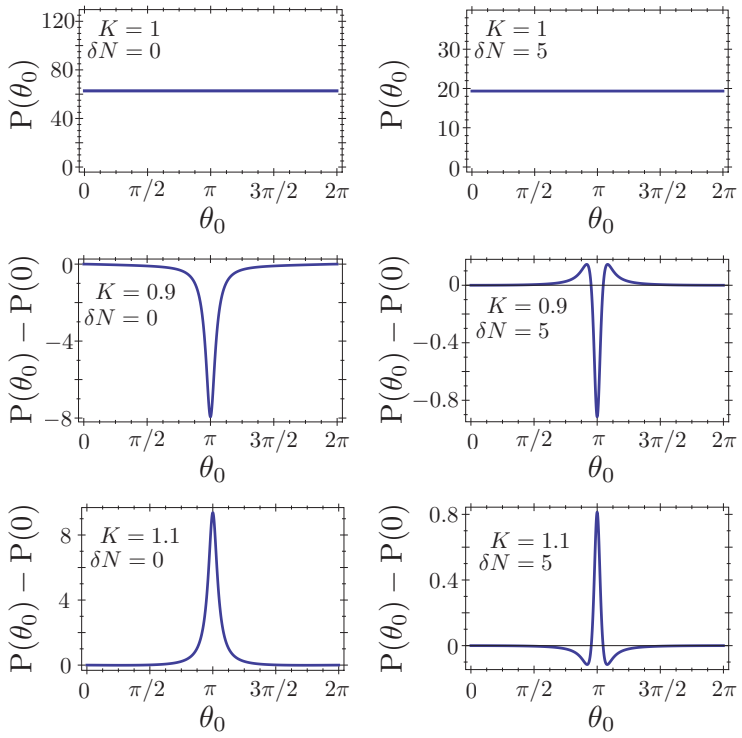

Figure 6.2: The correlation function in Eq. 6.37 versus the azimuthal angle θ_0 for non-interacting $K = 1$, repulsive $K < 1$ and attractive $K > 1$ Luttinger parameter. We set $a = 0.1$ as a matter of illustration. The numerical values of $\mathrm{P}(\theta_0)$ is shifted by $\mathrm{P}(0)$ for $K \neq 1$. The spikes appear for correlation of Kramers pairs $\theta_0 = \pi$ only in the interacting regime $K \neq 1$. The magnetized boson vacuum $\delta N = 5$ suppresses the correlation functions by almost one order of magnitude although the spikes persist for $K \neq 1$.

limit of $a \to 0$ has the form

$$\mathrm{P}(\theta_0 = \pi) \propto \lim_{a\to 0} (\cosh a - 1)^{-\frac{K^2-1}{2K}} \, {}_2F_1(\frac{1}{2}, \frac{1}{K}; 1; \frac{\mathrm{sech}^2 a}{2}), \tag{6.38}$$

where ${}_2F_1(q, b; c; z)$ is the hypergeometric function.

We discuss the observed singular behavior of the correlation function in the following. The singularity in the Cooper pairs correlation function is a sign of instability against superconductivity in a grand canonical system. The Fermi surface is destroyed in superconductivity, and hence quasiparticle excitations requires a minimum finite energy [102]. In our system, the lowest-energy particle-hole excitation is gapped by $\sim \hbar\omega u$. The zero-mode excitation is also gapped by an energy $\hbar\omega v_F$. These energy gaps rely on the quantization of angular momentum and charges, respectively, and does not have anything to do with the energy gap induced by pairing. Though, the energy gaps maintain the maximum number of Kramers pairs via adiabatically connecting the maximum number of the pairs in the free system

to the weakly interacting state. It is interesting also to note that the pair correlation is sensitive to the parity of the particle number. For an odd number of electrons, a single electron will be left without a partner, and hence, contributes to the magnetization of the ground state. As it is discussed, the magnetized states suppress the correlation function.

What is underlaying the strong correlation? The correlation of time-reversed pairs is taken into account in the original interacting model (6.1) through the boosted IMEs along BCS-like interaction. Although their significance are ruled out by neglecting variations of the IMEs in the effective model (6.8), the system is yet settled on the momentum-space ring in the way the fermion fields are exploited, (6.32) and (6.33). Consequently, the topological restriction of the scattering processes on the ring gives rise to merely the BCS-like and exchange-type interactions. The exchange-type interaction is resolved in the interaction of electrons with the same chirality in Eq. 6.15 which just renormalizes the Fermi energy. It is the BCS-like interactions which leads to the strong correlation of Kramers pairs. In other words, the time-reversed pairs are correlated by the topological restricted interactions on the ring.

Another peculiarity of the model is the phase-dependent interaction of electrons with opposite chirality, which relies on the time reversal of the representation itself. It is worth noting that this channel reflects the topologically protected BCS-like interaction on the momentum-space ring which is the interaction of Kramers pairs. The phase factor which appears in this channel can be gauged out and does not lead to any effect on the energy spectrum of the excitations (6.23). Though, it yields to a non-local relations between the free boson fields and the interacting dual fields (6.34) and (6.35). This non-locality appears when the interaction is switched on, no matter whether it is repulsive or attractive, and technically is responsible for the observed singularity of the correlation function.

As it is shown, the pairs $e^{i(J_F+1/2+j)\theta_0}c^\dagger_{j+}c^\dagger_{-j-}$ are not correlated for $K \neq 1$ unless they are constructed from time-reversed partners $\theta_0 = \pi$. The generic pairs take the from $\Psi^\dagger_+(\theta)\Psi^\dagger_-(\theta+\theta_0)$ in the momentum space. Since the momentum associated with the azimuthal angle θ on the ring is $\propto e^{i\theta}$, constructing pairs of time-reversed partners requires $\theta_0 = \pi$. In principle, there is no perturbation in the system to allow $\Psi^\dagger_+(\theta)\Psi^\dagger_-(\theta+\theta_0)\Psi_-(\theta'+\theta_0)\Psi_+(\theta')$ which violates the conservation of momentum except for $\theta_0 = \pi$, disregarding $\theta = \theta'$ which gives a regular contribution. Therefore, interplay between time reversal symmetry and conservation of momentum on the momentum-space ring leads to the strong correlation of Kramers pairs.

The Kramers pair is similar to a s-wave Cooper pair formally as the constituent electrons are time-reversed partners [102]. Although, the angular momentum of the Kramers pair is not well-defined since the angular momentum operator $\hat{L}_z = -i\hbar\partial_\theta$ does not lead to a good quantum number in our system. One should project the wavefunction of the pairs onto the basis of spin and orbital angular momentum to check the orbital symmetry of the Kramers pairs. Concerning the effective eigenstate of the free Hamiltonian, see section

3.2, we expand the fermion operator as $c_J^\dagger = a_{m\uparrow}^\dagger + a_{m+1\downarrow}^\dagger$ where J is the half-odd-integer total angular momentum, $m \in \mathbb{Z}$ is the angular momentum and $\uparrow\downarrow$ are components of spin-1/2 along the quantization axis. And therefore, $a_{m\uparrow}^\dagger$ creates an electron with angular momentum m and spin $\uparrow$. Discarding the chirality and the phase factor, the Kramers pair in terms of $a_{m\uparrow}^\dagger$ takes the form (given $J > 0$)

$$c_J^\dagger c_{-J}^\dagger = a_{m\uparrow}^\dagger a_{-m-1\uparrow}^\dagger + a_{m\uparrow}^\dagger a_{-m\downarrow}^\dagger + a_{m+1\downarrow}^\dagger a_{-m-1\uparrow}^\dagger + a_{m+1\downarrow}^\dagger a_{-m\downarrow}^\dagger, \tag{6.39}$$

which shows heuristically that the Kramers pair is a superposition of s-wave with zero angular momentum and p-wave with the angular momentum equals to ± 1. In other words, the pair is a superposition of singlet and triplet pairs.

The mechanism which leads to the strong correlation of Kramers pairs relies on the time reversal symmetry and localization of interacting electrons around a momentum-space ring and does not have anything to do with boson mediated interactions [6]. It suggests an intrinsic pairing mechanism for isotropic electronic systems even with a repulsive pair potential. However, the mechanism can be compared with Kohn-Luttinger effect [60, 69, 80]. The effect is an electronic pairing mechanism for repulsively interacting fermions, which is a many-body effect in essence and considered to be a particle-hole mediated interaction between electrons. Kohn and Luttinger have proposed the mechanism for 3D system originally. The effect in a 2D space is studied, for example, in references [26, 40, 84]. Briefly, in 2D space, the effect is weaker and requires contribution of higher orders in the bare interaction [26].

The necessary condition for Kohn-Luttinger effect is the sharpness of Fermi surface, which gives rise to the well-known singular dielectric constant at the perfect nesting [47], where particles and holes with the same energy are connected by the exchanged momentum equals to the double Fermi wavenumber $q = 2k_F$. The singularity generates an oscillatory long-range interaction in the coordinate space. Technically, in the 3D space treatment, the scattering vertex is dressed by the bubble-polarization-type diagrams up to the second order in the bare interaction which in turn leads to an effective attractive interaction. In their seminal paper, Kohn and Luttinger have shown that this effective interaction gives rise to the instability against formation of Cooper pairs in the electronic liquid.

Two essential ingredients for Kohn-Luttinger effect might be compared with the characteristic of the interacting model studied herein. The first feature is the sharpness of the Fermi surface which realizes a ring in momentum space for isotropic 2D systems. The second is that the sign of a repulsive interaction potential is switched by projecting the effective interaction onto the angular momentum basis. The sign of the interaction potential can be switched with the aids of the phase factors generated in this representation. These similarities suggest that the Kohn-Luttinger effect might root in the intrinsic pairing mechanism observed here rather than the nested Fermi surface. And therefore, it might be to put the effect on a new ground. In fact, the representation of an interacting model in the basis

compatible with the angular momentum, instead of the translational momentum, takes into account automatically the correlation of pairs. Investigating the pairing instability of an isotropic system in such a representation might shed light to the curiosity which we leave it for future study.

The system, which is studied in this chapter, hosts $N \sim \alpha$ with an estimation for Rashba coupling $\alpha \sim 10^2$. Although emergence of superconducting pairing is quite surprising in such a small system, it seems to be relevant to the recent search for superconductivity in small systems [19]. In fact, the experimental observation of superconductivity in ultrasmall metallic grains [14, 101, 85, 86, 18] containing $10^4 - 10^5$ electrons has stimulated theoretical studies for realization of superconducting pairing in metallic nanoclusters which contain $10^2 - 10^3$ delocalized electrons [63, 65, 64]. An interesting point about these ultrasmall systems is that the superconducting state also manifests the odd-even-parity effect which a similar effect is discussed above. That is the presence of an unpaired electron suppresses the superconductivity. On the other side, it is shown that Rashba SOC enhances superconductivity in 2D systems of repulsive electron gas [103, 38, 68], in spite of the weaker Kohn-Luttinger effect in 2D, which provides an encouragement for the main result of this section. These facts indicate that the observed strong correlation of pairs in our system can contribute to the path toward new superconductivity in small systems. The study presented here can be extended to include temperature-dependent correlation function and also investigation of electronic transport in the system [28]. Besides, the proposed experiments in the references [65, 62] to observe superconductivity in the metallic nanoclusters can also be relevant for our system. However, we estimate roughly that the effect should be present for temperature $k_B T \lesssim \hbar\omega v_F$.

Before leaving this section, we discuss the absence of the orbital ferromagnetism in the considered model. In the regime of weakly interacting electrons, the IMEs are estimated by a uniform coupling constant g through neglecting the variations of absolute value of matrix elements around g in comparison with the level spacing v_F. The orbital ferromagnetism requires asymmetry in chirality and therefore an stronger interaction to break the pairing and symmetric chiral population which is beyond the validity of the approximation and hence the effective model. The nonuniform IMEs need to be retained for stronger interactions. In fact, the interactions with zero-exchanged momentum in the original model contribute as a pair-breaking channel and favors the orbital ferromagnetism. In the following sections, we develop other effective models based on the results of this section which allow probing stronger interactiona in the system.

6.2 Effective Pairing Model

In this section, we proceed with our study of the system containing arbitrary number of interacting electrons but restricted by single-band approximation $N \sim \alpha$. In the preceding

section, the IMEs are replaced by a uniform coupling constant in the regime of weak interaction. Therefore, a homogeneous interaction term is realized in which the magnitude of matrix elements do not depend to the angular momentum of the incoming and outgoing particles. The effective system leads to the singular correlation of Kramers pairs. This implies that the BCS-like interactions are the most important interaction channel in the considered regime. Additionally, the maximal absolute magnitude of IMEs are along BCS-like and exchange-type interactions. And, those interactions have the same magnitude according to the symmetry relations of IMEs. Relying on these facts, we further truncate the IMEs to write down effective Hamiltonians which can capture the competition between the pairing ground state, i.e. state with strong correlation of Kramers pairs, and the orbital ferromagnetism. Those are in fact the most likely phases in the system, see chapter 4.

In the following, we solely keep the matrix elements along the maximal absolute magnitude lines, namely, the BCS-like $J_1 = -J_2$ and the exchange-type $J_2 = J_1 + m$ interactions. Based on the same argument presented in the preceding section, we neglect the variation of IMEs along those lines. Therefore, the interaction term becomes uniform which shall be shown being equivalent to the Richardson pairing model [89, 31]. The latter model bears an exact solution and is reviewed briefly in appendix E. With the aid of a heuristic analysis, we show that a transition to the orbital ferromagnetism is expectable in the model. Although, determining whether the transition takes place at a reasonable value of interaction strength, by which the constraints of weak interactions is maintained, requires solving the pairing Hamiltonian and is beyond the treatment of this section.

We begin with the effective Hamiltonian written in the preceding section in Eq. 6.8. Although, we adopt another convention to label the states. We set $J \equiv \eta J_F + \eta n$ and consider $\eta \equiv \mathrm{sgn}(J)$ as the pseudo-spin. J_F is the Fermi momentum as the highest occupied state in the non-interacting system. Therefore, we have $n \in \mathbb{Z}$. We are interested in low-energy physics where interaction-driven excitations stay in the vicinity of Fermi energy $n \ll J_F \lesssim \alpha$. We focus on $\tilde{N}$ electrons close to the Fermi points. The electron-electron interaction is required to be weak enough in order to maintain the single-band approximation $|J| \lesssim \alpha$. The fermion operators are defined in the new convention by $c^\dagger_{n\eta} \equiv c^\dagger_J$ and $c_{n\eta} \equiv c_J$. Time reversal reads

$$\Theta c^\dagger_{n\eta} = (-1)^{\eta J_F + \eta n + 1/2} c^\dagger_{n,-\eta}, \tag{6.40}$$

which indicates that (n, η) and $(n, -\eta)$ are time-reversed partners. The effective Hamiltonian takes the form

$$H = v_F \sum_{\substack{n \\ \eta=\pm}} n c^\dagger_{n\eta} c_{n\eta} + \frac{g}{4\pi} \sum_{\substack{n,\, n',\, m \\ \eta=\pm}} (-1)^m c^\dagger_{n+m\eta} c^\dagger_{n'-m,-\eta} c_{n',-\eta} c_{n\eta} + \frac{g}{4\pi} \sum_{\substack{n,\, n',\, m \\ \eta=\pm}} c^\dagger_{n+m\eta} c^\dagger_{n'-m\eta} c_{n'\eta} c_{n\eta}, \tag{6.41}$$

where the unit of energy $\hbar\omega$ is set to unity. The Fermi velocity is defined by $v_F = J_F/\alpha^2$. It is shown in the preceding section that the correlation of Kramers pairs is singular even

for a repulsive interaction $g > 0$. Therefore, the BCS-like interactions are dominant in this regime. We approximated the interaction term in H further and keep the elements along Cooper channel. That is the BCS-like interactions. According to the time-reversal symmetry of IMEs, discussed in chapter 4, the exchange-type interactions also should be kept although they give no contribution to the dynamical behavior of the system. The Hamiltonian then reads

$$\begin{aligned} H &\approx v_F \sum_{\substack{n \\ \eta=\pm}} n c^\dagger_{n\eta} c_{n\eta} + \frac{g}{4\pi} \sum_{\substack{n,m \\ \eta=\pm}} (-1)^m c^\dagger_{n+m\eta} c^\dagger_{-n-m,-\eta} c_{-n,-\eta} c_{n\eta} + \frac{g}{4\pi} \sum_{\substack{n,n' \\ \eta=\pm}} c^\dagger_{n\eta} c^\dagger_{n'\eta} c_{n\eta} c_{n'\eta} \\ &= v_F \sum_{\substack{n \\ \eta=\pm}} n c^\dagger_{n\eta} c_{n\eta} + \frac{g}{2\pi} \sum_{n,n'} (-1)^{n-n'} c^\dagger_{n+} c^\dagger_{-n-} c_{-n'-} c_{n'+} - \frac{g}{4\pi} \sum_{\substack{n,\, n' \\ \eta=\pm}} (c^\dagger_{n\eta} c_{n\eta} - \delta_{nn'}) c^\dagger_{n'\eta} c_{n'\eta}. \end{aligned} \tag{6.42}$$

The last term gives a constant proportional to the square of particle number and does not contribute to the dynamics of the system. Hence, we neglect this term to obtain

$$H = v_F \sum_{\substack{n \\ \eta=\pm}} n c^\dagger_{n\eta} c_{n\eta} + \frac{g}{2\pi} \sum_{n,n'} (-1)^{n-n'} c^\dagger_{n+} c^\dagger_{-n-} c_{-n'-} c_{n'+}. \tag{6.43}$$

The Hamiltonian then realizes a form akin to the Richardson pairing model which is solved exactly [89]. A short review of the solution is given in appendix E. In order to write the Hamiltonian in an exact form of Richardson's model, we define the boson-like operators

$$\tilde{\mathrm{b}}^\dagger_n = e^{in\pi}\, c^\dagger_{n+} c^\dagger_{n-}, \tag{6.44}$$

$$\hat{N}_n = (c^\dagger_{n+} c_{n+} + c^\dagger_{n-} c_{n-})/2, \tag{6.45}$$

which gauge out the phase factor of interaction term. The operators have the same commutation relations as those of Richardson's pairing model in Eqs. E.4 and E.5

$$[\tilde{\mathrm{b}}_n,\, \hat{N}_{n'}] = \delta_{nn'} \tilde{\mathrm{b}}_n, \tag{6.46}$$

$$[\tilde{\mathrm{b}}_n,\, \tilde{\mathrm{b}}^\dagger_{n'}] = \delta_{nn'} (1 - 2\hat{N}_{n'}). \tag{6.47}$$

The effective Hamiltonian takes the form

$$H = 2v_F \sum_n n \hat{N}_n + \frac{g}{2\pi} \sum_{n,\, n'} \tilde{\mathrm{b}}^\dagger_n\, \tilde{\mathrm{b}}_{n'}. \tag{6.48}$$

Let the system contains an even number of electrons $\tilde{N}$ = even which constructs of P pairs and ν unpaired electrons. By unpaired electrons we meant that if the state (n, η) is occupied its time-reversed $(n, -\eta)$ must be empty. Then, we have the relation $\tilde{N} = 2P + \nu$. The number of unpaired electrons ν is is called seniority and can lead to a non-zero magnetization in the system since $n = \eta J - J_F$. Suppose also (n, η) belongs to the

set S which is specified by the states near the Fermi energy. According to the Richardson, the eigenstates of the pairing model have the form

$$|\psi\rangle \;=\; \prod_{k=1}^{P}\sum_{n}\frac{1}{2v_F n - E_k}\tilde{\mathrm{b}}_n^{\dagger}|0\rangle, \tag{6.49}$$

with the eigenenergy $E=\sum_{k=1}^{P}E_k$. The sum is over those $n\in S$ which are not singly occupied. The energy of pairs E_k can be derived by solving the Richardson equation

$$1-\frac{g}{\pi}\sum_{i\neq k}^{P}\frac{1}{E_i-E_k}+\frac{g}{2\pi}\sum_{n}\frac{1}{2v_F n-E_k}=0. \tag{6.50}$$

This equations can be solved numerically in its discrete form or analytically in the continuum limit [90]. Similar to the bosonization result (6.1.2), the phase factor $(-1)^m$ in the interaction term does not have any effect on the energy spectrum of the model. Although, the pair correlation function

$$\sum_{n,\,n'}(-1)^{n-n'}\langle\psi|\tilde{\mathrm{b}}_n^{\dagger}\,\tilde{\mathrm{b}}_{n'}|\psi\rangle, \tag{6.51}$$

is expected to have a non-trivial information even for a repulsive pairing force $g>0$, see the discussion in the section 6.1. However, we are not going the solve the Richardson equation. Rather than, we exploit the effective model to show that there must be a transition from pairing ground state to the orbital ferromagnetism if g exceeds a critical value.

We analyze the model in two extreme limits. If we take the limit $\tilde{g}=g/2\pi v_F\to 0$, i.e. non-interacting model, there are maximum numbers of Kramers pair. Consequently, the seniority, which can highlight occurrence of magnetization, is zero or 1 for even or odd $\tilde{N}$, respectively. On the other hand, if $\tilde{g}\to\infty$, the ground state does not contain any doubly occupied site. That is the seniority must be maximum $\nu=\tilde{N}$ and the pairing term does not contribute to the energy. In this limit, all the possible magnetized states are degenerate which indicates the ground state is highly degenerate. Although, in this regime $\tilde{g}\to\infty$, the variation of matrix elements must be taken into account and they cannot be estimated by a uniform coupling constant g. The corrections of IMEs lift the degeneracy partly. It will be discussed in the following section that the exchange-type interactions polarize the spin η in a ferromagnetic way. This indicates that the ground state has a large magnetization. It is quite similar to the scenario discussed for the flat-band model in section 4.2.3.

To conclude, in the limit $\tilde{g}\to 0$, there is no broken Kramers pairs but in the strongly correlated regime $\tilde{g}\to\infty$ no Kramers pair exists. Switching on the interaction adiabatically, the magnetization is expected to increase gradually, that is to say, Kramers pairs are broken one by one. According to the results of the bosonization study, the Kramers pairs are correlated strongly even for a repulsive interaction $0<\tilde{g}$, and their strong correlation

persists in the orbital ferromagnetic states although it is suppressed significantly. This implies the strong correlation coexists with the orbital ferromagnetism in the moderate range of $\tilde{g}$. Absence of a sharp transition is reasonable as the system has a finite size [19].

We are actually interested at the critical value $\tilde{g}_c$ where the first Kramers pair is broken. That is the moment where the first interaction-driven magnetization occurs in the system. Determining $\tilde{g}_c$ requires solutions of the Richardson equation in the relevant regime of $\tilde{g}$. In fact, the strength of $\tilde{g}_c$ must admit the constraint to the uniform effective model and the single-band approximation i.e. the highest occupied state at $\tilde{g}_c$ must stay away from the bottom of the next band. Otherwise, one has to take into account more details of the IMEs to judge about the existence of such a transition.

The analysis of this section has shown solely BCS-like interaction can break the Kramers pairs for a repulsive interaction. In the next section, we retain more subtleties of the original interacting model. The variations of IMEs will be restored along the maximal absolute lines as a function of exchanged momentum and angular momentums of incoming/outgoing particles. Furthermore, the matrix elements by zero-exchanged momentum $m = 0$, which has a considerable role in the physics of the system, are also kept. The effective Hamiltonian resembles the Hartree-Fock theory. Although, it incorporates an extra term associated with the interaction of Kramers pairs.

6.3 Extended Hartree-Fock Hamiltonian

In two preceding sections, our study of many-body system was constrained by an extra condition for weak interactions $||V| - |V'|| < v_F/\lambda$ in addition to the single-band approximation. Interesting physics are captured even in such a weakly interacting system. With the help of the effective pairing model, we have seen that in the regime of stronger interaction, there is a transition to orbital ferromagnetism although the critical interaction strength might violate the weak interaction constraints. In the following section, we continue to work with the effective model in the preceding section while retaining variations of IMEs along the maximal absolute magnitude lines. Besides, the matrix elements of zero-exchanged momentum $m = 0$ are kept thoroughly. This allows to relax the second constraint $||V|-|V'|| < v_F/\lambda$ and consider stronger interactions in the system. The approximated Hamiltonian is equivalent to Hartree-Fock Hamiltonian plus a term which describes interaction of Kramers pairs solely. We call it extended Hartree-Fock Hamiltonian. Having retained the elements with $m = 0$, it is now possible to compare how different types of potential, for instance Coulomb and contact potential, modify the physics of the system. The effective Hamiltonian can be read as a lattice model. In this regard, discrete angular momentum J labels the sites of a 1D lattice. Similar to the preceding section, two chiral degrees of freedom can be accounted as the pseudo-spin-1/2 of the electron in site $|J|$. Although, we do not restrict the interaction of electrons to those in the vicinity of Fermi

energy and hence no linearized kinetic term. The single-band approximation $0 < |J| \lesssim \alpha$ indicates the lattice is finite. The kinetic term represents an external site-dependent potential. Therefore, the Hamiltonian describes interacting spinful electrons in a finite lattice in the presence of an external field coupled to the charge degree of freedom. The effective Hamiltonian can also be represented as a Heisenberg XXZ model [98]. The site-dependent interaction of spins and absence of translational invariance make an analytical solution of the model a formidable task. Although, such a model can be tackled with well-known numerical methods like density matrix renormalization group [107, 25, 93], which is a powerful technique for discrete 1D systems.

We begin with the full Hamiltonian

$$H = \sum_{J} E_J c_J^\dagger c_J + \lambda \sum_{\substack{J_1,J_2 \\ m}} V^{(m)}_{J_1,J_2}\, c^\dagger_{J_1} c^\dagger_{J_2} c_{J_2-m} c_{J_1+m}, \tag{6.52}$$

where $E_J = J^2/2\alpha^2$ and α is the dimensionless Rashba coupling, λ is the dimensionless strength of interaction. The unit of energy is $\hbar\omega$ which is set to unity. The IMEs $V^{(m)}_{J_1,J_2}$ are studied in chapter 4. In the many-body system, once again we assume $J_F \lesssim \alpha$ where J_F is the Fermi momentum in the absence of interactions. The number of particles N in the system is taken to be in the order of Rashba coupling $N \lesssim \alpha$. We truncate the interaction term further and keep only the matrix elements along the maximal absolute magnitude lines $J_2 = J_1 + m$ and $J_1 = -J_2$ for $m \neq 0$ but all the elements for $m = 0$, which is the strongest channel of interaction. The approximated Hamiltonian $\mathcal{H}$ has the form

$$\begin{aligned} \mathcal{H} = \sum_{J} E_J c_J^\dagger c_J \;\; &+ \;\; \lambda \sum_{J,J'} \left(V^{(0)}_{J,J'} - V^{(J'-J)}_{J,J'} \right) c^\dagger_J c_J c^\dagger_{J'} c_{J'} \\ &+ \;\; \lambda \sum_{\substack{J,J' \\ J\neq J'}} V^{(J'-J)}_{J,-J}\, c^\dagger_J c^\dagger_{-J} c_{-J'} c_{J'}. \end{aligned} \tag{6.53}$$

The first line contains the Hartree-Fock (HF) Hamiltonian. The terms in the second line correspond to the BCS-like interaction by $m \neq 0$ and in order to have contribution, presence of a Kramers pair is necessary. As shown in the preceding sections, the BCS-like interaction determines the physics of the system in the regime of weak interactions. Though, the standard HF approximation automatically excludes this term, see Sec. 5.4, which leads to instability of unmagnetized states even for a very weak interaction. In fact, the BCS-like interactions are off-diagonal and detracts the approximated Hamiltonian from HF theory. Therefore, finding a variational parameter similar to the one of the standard HF theory $\langle c_J^\dagger c_J \rangle$ is not straightforward.

6.3.1 Effective Lattice Model

The discrete angular momentum J is interpreted as if it labels sites of a 1D lattice. In order to develop the idea, we consider only the positive quantum numbers $J > 0$ and account

sign of J with an extra label $\eta = \mathrm{sgn}(J)$. The latter quantum number comprises two states of a pseudo-spin-1/2. The fermion operators in terms of the new convention are defined as $c^\dagger_{J,\eta}$ and $c_{J,\eta}$. We define the boson-like operators in the similar way of the preceding section

$$n_{J\eta} = c^\dagger_{J,\eta} c_{J,\eta}, \tag{6.54}$$

$$S^+_J = c^\dagger_{J,+} c^\dagger_{J,-} = \left(S^-_J\right)^\dagger, \tag{6.55}$$

that gives $n^2_{J_\eta} = n_{J_\eta}$, $(S^+_J)^2 = (S^-_J)^2 = 0$ and also $S^+_J S^-_J = n_{J+} n_{J-}$. The commutation relations read as

$$[n_{J\eta},\, n_{J'\eta'}] = 0, \tag{6.56}$$

$$\left[n_{J\eta},\, S^\pm_{J'}\right] = \pm\delta_{JJ'}\, S^\pm_J, \tag{6.57}$$

$$\left[S^+_J,\, S^-_{J'}\right] = \delta_{JJ'}\, (n_{J+} + n_{J-} - 1)\,. \tag{6.58}$$

With the aid of the bosonic operators and also the symmetry relations of $V^{(m)}_{J_1 J_2}$, the effective Hamiltonian $\mathcal{H}$ can be written as

$$\mathcal{H} = \sum_{\substack{J>0\\ \eta}} E_J n_{J\eta} + \lambda \sum_{\substack{J,J'>0\\ \eta,\eta'}} v^{\eta\eta'}_{JJ'}\, n_{J\eta} n_{J'\eta'} + \lambda \sum_{J>J'>0} u_{JJ'}\, \left(S^+_J S^-_{J'} + S^+_{J'} S^-_J\right), \tag{6.59}$$

where the matrix elements are defined in terms of $V^{(m)}_{J_1 J_2}$ in the following way

$$v^{++}_{JJ'} = v^{--}_{JJ'} = \left(V^{(0)}_{J,J'} - V^{(J'-J)}_{J,J'}\right), \tag{6.60}$$

$$v^{+-}_{JJ'} = v^{-+}_{JJ'} = \left(V^{(0)}_{J,J'} - V^{(J'+J)}_{-J,J'}\right), \tag{6.61}$$

$$u_{JJ'} = 2\left(V^{(J-J')}_{-J,J} - V^{(J'+J)}_{-J,J}\right). \tag{6.62}$$

The Hamiltonian then describes interacting spinful electrons in a finite 1D lattice consisting of sites in $\Lambda = \{J \in \mathbb{Z} + 1/2;\, 0 < J \lesssim \alpha\}$. The kinetic term reads as an external field coupled to the charge degree of freedom. The middle term in Eq. 6.59 is equivalent to the interaction terms in HF theory. $v^{-+}_{JJ'}$ and $v^{+-}_{JJ'}$ describe interaction of electrons at sites J and J' with opposite spin polarization and include the on-site interaction v^{-+}_{JJ}. The matrix elements $v^{++}_{JJ'}$ and $v^{--}_{JJ'}$ are the interaction strength of electrons with the same spin polarization at sites J and J'. The last term in Eq. 6.59 can be considered as it describe hopping of Kramers pairs. The lattice model resembles the features of Hubbard model [36]. Although, there is a term for hopping of electron pairs instead of a single-particle hopping. And also a long-range interaction between electrons is considered.

The symmetry relations of $V^{(m)}_{J_1J_2}$ induce constraints on the matrix elements of the lattice model. The matrix elements in HF terms are positive $v^{\eta\eta'}_{JJ'} \geqslant 0$ for arbitrary$J, J' > 0$ and $\eta, \eta' = \pm$. Obviously, self-interaction is forbidden $v^{\eta\eta}_{JJ} = 0$. For hopping term, if $J' - J$ is an odd number, we have $u_{JJ'} < 0$, and otherwise $u_{JJ'} > 0$. Hopping of Kramers pairs between the nearest neighbor sites is a processes by which the system can reduce its energy. In fact, the absence of this term in the standard HF calculation for few-electron system in section 5.4 gave rise to the instability of the unmagnetized states. Also, it can be shown that the matrix elements are invariant under interchange on the indices

$$v^{\eta\eta'}_{JJ'} = v^{\eta\eta'}_{J'J}, \tag{6.63}$$

$$u_{JJ'} = u_{J'J}. \tag{6.64}$$

The absolute magnitude of $V^{(m)}_{J_1J_2}$ has a general hierarchy, specifically, for the elements far from the symmetry center $(J_2, J_1) = (m/2, -m/2)$. This hierarchy is in fact independent of type of the potential e.g. Coulomb or contact potential. It can be engaged to characterize the strength of interaction in the lattice model. The matrix elements $V^{(J'+J)}_{-J,J'}$, in Eqs. 6.61 and 6.62, correspond to the strength of backward scattering which is negligible for $J, J' \sim J_F \lesssim \alpha$. This indicates $v^{+-}_{JJ'} > v^{++}_{JJ'}$. Consequently, the HF terms favor ferromagnetic spin polarization of the electrons. Also, they make double occupancy of sites, or in the other words, Kramers pairs unfavorable. That is due to the presence of $V^{(0)}_{-J,J}$ in $v^{-\eta\eta}_{JJ}$ which is the strongest repulsive interaction among the matrix elements. The characteristics of HF terms in the lattice model is consistent with the observed results in the few-electron systems. One significant point is that the interaction of nearest neighbors has the weakest strength among the interactions of electrons with the same spin polarization. It favors consecutive occupation of sites with the ferromagnet order which admits the observed distribution function by exact diagonalization method. The absolute magnitude of the pair-hopping amplitude $u_{JJ'}$ decreases versus increase in the hopping distance $|J' - J|$. It can be rationalized by noting that the absolute magnitude of $V^{(m)}_{-J,J}$ decreases by increase in the exchanged momentum m. Moreover, its sign depends to the parity of $|J' - J|$. $u_{JJ'}$ is negative (positive) if $|J' - J|$ is odd (even.)

The magnitudes of the matrix elements are illustrated in figure 6.3 for Coulomb and contact potential. We review their characteristics. For Coulomb potential, $v^{++}_{JJ'}$ and $v^{+-}_{JJ'}$ are in the same order of magnitude generally. In fact, both $v^{++}_{JJ'}$ and $v^{+-}_{JJ'}$ are dominated by $V^{(0)}_{J_1J_2}$ which is significantly stronger than the elements with $m \neq 0$ in the Coulomb-potential case. They decay slowly with increase in the distance of lattice sites $|J' - J|$. We note that the magnitude of the elements are not mirror symmetric with respect to $J' - J = 0$. That is because of the characteristics of interaction matrix elements which their magnitudes are larger for the elements close to the symmetry centers $(m/2, -m/2)$. On the contrary to $v^{\eta\eta'}_{JJ'}$, absolute magnitude of the pair-hopping $|u_{JJ'}|$ decays quite quickly by increase in $|J' - J|$. Finally, it can be concluded that HF interactions dominate hopping amplitude in the Coulomb interacting electrons and by increase in the interaction strength λ, a transi-

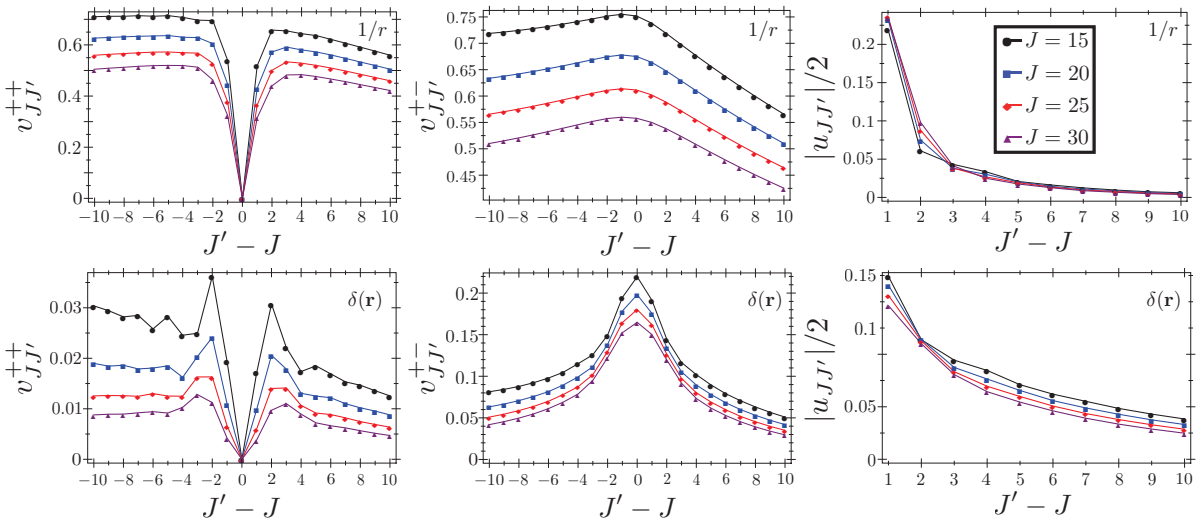

Figure 6.3: (Color online) Numerical values of the matrix elements for the lattice model in Eq. 6.59 versus $J' - J$ and several values of J, corresponding to the Coulomb $1/r$ and contact $\delta(\mathbf{r})$ potential in the upper and lower panels, respectively. As a matter of illustration, the matrix elements for $\alpha = 30$ are chosen in the evaluation of the matrix elements. $J' - J$ is equivalent to the relative distance of the lattice sites. **In the leftmost panels**, the numerical values of $v^{++}_{JJ'}$ show that the interaction of the nearest neighbors has the lowest cost energetically if the electrons have the same spin polarization. The magnitude of the Coulomb-matrix elements are larger than the ones for the contact potential by almost one order of magnitude. **The center panels** show that the on-site interaction $v^{+-}_{JJ'}$ is the strongest interaction which makes the double occupancy of a site expensive. $v^{++}_{JJ'}$ of the contact-potential decays faster than the Coulomb potential as a function of $|J' - J|$. **In the rightmost panels**, the matrix elements for hopping of the pairs $|u_{JJ'}|/2$ are given. $u_{JJ'}$ is negative if $J' - J$ is an odd number and positive otherwise. And its absolute magnitude decays faster for the Coulomb potential than the contact potential as a function of $J' - J$. Therefore, the long-range Coulomb potential emerges as a short-range interaction here. But oppositely, the short-range contact potential is a long-range interaction in the lattice model for interaction of Kramers pairs.

tion to the orbital ferromagnetism is likely.

For contact potential, $v^{++}_{JJ'}$ is weaker than $v^{+-}_{JJ'}$ by almost one order of magnitude but the absolute hopping strength $u_{JJ'}$ is comparable with the magnitude of $v^{+-}_{JJ'}$. It reflects the fact that $V^{(m)}_{J_1 J_2}$ for contact potential decays slowly by increase in $|m|$. The weak ferromagnet coupling $v^{++}_{JJ'}$ in the contact-potential interacting electrons indicates the lower chance for the orbital ferromagnetism intuitively in comparison with the Coulomb potential.

Two relevant conserved quantities are

$$\mathbf{N} = \sum_J (n_{J+} + n_{J-}), \qquad \mathbf{M} = \sum_J (n_{J+} - n_{J-}). \tag{6.65}$$

$\mathbf{N}$ and $\mathbf{M}$ count total number of particles and dimensionless magnetization, respectively. The ground state of the effective Hamiltonian $\mathcal{H}$ needs to be found among states which have the same number of particles. If a state has no doubly occupied site, it is an eigenstate of $\mathcal{H}$. In principle, the singly occupied sites are blocked and $\mathcal{H}$ is unable to move them. This fact indicates that the local operator $\mathbf{m}_J = n_{J+} - n_{J-}$, which counts magnetization of Jth site, commutes with the Hamiltonian $[\mathbf{m}_J, \mathcal{H}] = 0$. This extra conservation law is due to the neglected interactions and is absent in the original model (6.52). We define the blocked domain $\mathcal{B}$ in a state $|\Psi\rangle$ as the set of sites which are singly occupied $\mathcal{B} = \{J;\, \mathbf{m}_J|\psi\rangle \neq 0\}$ and the free domain as the remaining sites $\mathcal{F} = \Lambda \setminus \mathcal{B}$.

6.3.2 Effective Hamiltonian as Heisenberg XXZ Model

The effective Hamiltonian $\mathcal{H}$ can be written as a 1D Heisenberg XXZ spin chain in the free domain $\mathcal{F}$. The approach presented here is in a close relation with the generalized Richardson-Gaudin models [5, 79]. $SU(2)$ algebra can be completed by defining

$$S^z_J = (n_{J+} + n_{J-} - 1)/2. \tag{6.66}$$

If $J \in \mathcal{F}$, then $S^{z\,2}_J = 1/4$ as either the site is empty or doubly occupied. Using the commutation relations in Eqs. 6.57 and 6.58, we find

$$\left[S^z_{J\eta},\, S^\pm_{J'}\right] = \pm\delta_{JJ'}\, S^\pm_J, \qquad \left[S^+_J,\, S^-_{J'}\right] = \delta_{JJ'}\, 2S^z_J, \tag{6.67}$$

and hence

$$\mathbf{S}_J \cdot \mathbf{S}_J = S(S+1) = S^{z^2}_J + (S^+_J S^-_J + S^-_J S^+_J)/2 = 3/4. \tag{6.68}$$

That is the free domain is treated as a 1D chain of spin-1/2. We note that the meaning of $S^\pm_J$ is being changed from here on. S^+_J and S^-_J in Eq. 6.59 are creation and annihilation operators of Kramers pair, respectively, but in the following, we take them as the spin-1/2 raising and lowering operators, respectively.

We need to rewrite $n_{J\eta}$ in terms of spineless operators as $n_{J\eta} = S^z_J + 1/2 + \eta\mathbf{m}_J/2$. The operator $\mathbf{m}_J$ gives no contribution if $J \in \mathcal{F}$. In the following, wherever S^z_J appears, it acts on the free domain and hence its eigenvalues is $\pm 1/2$. The part of Hamiltonian acting on the free domain takes the form similar to the Heisenberg XXZ model in the presence of a magnetic field

$$\mathcal{H}^{\mathcal{F}} = \sum_{J\in\mathcal{F}} B_J S^z_J + \lambda \sum_{J>J'\in\mathcal{F}} \left\{ v_{JJ'} S^z_J S^z_{J'} + u_{JJ'} \left(S^+_J S^-_{J'} + S^+_{J'} S^-_J \right) \right\} + E^{\mathcal{F}}, \tag{6.69}$$

where the new parameters are defined as

$$v_{JJ'} = 2\sum_{\eta,\eta'} v_{JJ'}^{\eta\eta'}, \tag{6.70}$$

$$B_J = 2E_J + \lambda \sum_{\substack{J'\in\mathcal{F}\\ \eta,\eta'}} v_{JJ'}^{\eta\eta'}, \tag{6.71}$$

$$E^{\mathcal{F}} = \sum_{J\in\mathcal{F}} \left\{ E_J + \frac{\lambda}{4} \sum_{\substack{J'\in\mathcal{F}\\ \eta,\eta'}} v_{JJ'}^{\eta\eta'}(1+\delta_{-\eta\eta'}\delta_{JJ'}) \right\}. \tag{6.72}$$

Here, the kinetic term and exchange-type interactions behave as a site-dependent magnetic field B_j. The constant term $E^{\mathcal{F}}$ depends on the free domain in the state $|\Psi\rangle$ and must be kept. The part of Hamiltonian which acts on the blocked domain reads as

$$\mathcal{H}^{\mathcal{B}} = \sum_{\substack{J\in\mathcal{B}\\ \eta}} E_J n_{J\eta} + \lambda \sum_{\substack{J,J'\in\mathcal{B}\\ \eta,\eta'}} v_{JJ'}^{\eta\eta'}\, n_{J\eta} n_{J'\eta'}. \tag{6.73}$$

$\mathcal{H}^{\mathcal{B}}$ is equivalent to HF Hamiltonian. The interaction of single electrons in $\mathcal{B}$ and spin-1/2 in $\mathcal{F}$ can be captured by

$$\mathcal{H}^{\mathcal{FB}} = 2\lambda \sum_{\substack{J\in\mathcal{F},J'\in\mathcal{B}\\ \eta,\eta'}} v_{JJ'}^{\eta\eta'}\, n_{J\eta} \left(S_{J'}^z + \frac{1}{2} \right). \tag{6.74}$$

The full Hamiltonian is comprised of three terms $\mathcal{H} = \mathcal{H}^{\mathcal{F}} + \mathcal{H}^{\mathcal{B}} + \mathcal{H}^{\mathcal{FB}}$. A general eigenstate of the effective Hamiltonian has the form

$$|\Psi\rangle = \sum_{\substack{l_1<l_2<\cdots<l_M\\ (l_i\in\mathcal{F} \text{ for } i=1,\cdots,M)}} f(l_1,l_2,\cdots,l_M)\, S_{l_1}^+ S_{l_2}^+ \cdots S_{l_M}^+ |\psi\rangle, \tag{6.75}$$

$$|\psi\rangle = \prod_{p\in\mathcal{B}} c_p^\dagger |0\rangle. \tag{6.76}$$

Although the lack of translational symmetry of $\mathcal{H}$ in addition to the long-range site-dependent interactions are major obstacles to obtain an analytical solution, the model can be solved numerically. Particularly, the discreetness of the theory makes it amenable to methods suitable for 1D lattice models as density matrix renormalization group technic [107, 25, 93].

6.4 Summary

In this chapter, we have studied interacting many-electron dot with strong Rashba coupling. The number of electrons is considered to be $N \sim \alpha$. In the regime of very weak

interactions, we have approximated the interaction term by a uniform one which allows bosonizing the Hamiltonian. The significant results of this regime were strong correlation of Kramers pairs even for a repulsive interaction. And also no spontaneous magnetization occurs in this regime. We studied the static correlation functions, or zero temperature, though, the study can readily be generalized to non-zero temperature. Based on the strong correlation of Kramers pairs, a pairing model was constructed. Although the pairing model has an exact analytical solution, we engaged the model to demonstrate that solely the BCS-like interactions might realize a transition from strong correlation of Kramers pairs to orbital ferromagnetism. In the end, relying on the results derived from two effective models, we have approximated the full Hamiltonian and constructed an extended Hartree-Fock Hamiltonian. The latter includes the standard Hartree-Fock Hamiltonian and an extra term which corresponds to the BCS-like interaction. Furthermore, we analyzed the representation of Coulomb and contact potential in the model and the probable physics they can realize for the system. The extended Hartree-Fock Hamiltonian can be represented as a Heisenberg XXZ spin model. The lattice model is not solved but has a proper form to be studied with numerical techniques like DMRG.

Chapter 7

Summary and Conclusion

In this thesis, we studied interacting 2D electrons in the presence of a parabolic trap and strong Rashba spin-orbit coupling. The system models mainly quantum dots which are realized at the interfaces of semiconductors. Absence of external magnetic fields indicates the system enjoys time-reversal symmetry. The trap breaks translational symmetry. The crucial feature is that strong Rashba coupling causes the low-energy physics to take place on a ring in momentum space. This attributes a quasi-one-dimensional character to the system which the immediate consequence is the profound effect of even very weak interactions in the system. Specifically, two classes of interactions are boosted due to the settlement of the system on a momentum-space ring, namely, BCS-like and exchange-type interactions. We named the two-body scattering processes in this way since the conservation of momentum on the ring restricts the interactions solely to the interaction of Kramers pairs with zero net total momentum and the exchange interaction. Therefore, the BCS-like interaction does not mean that the interacting electrons form Cooper pairs necessarily, in the way that is concerned in the BCS theory. Although, strong correlation of Kramers pairs and exchange interactions are two types of interactions which are known to be responsible for competing phases in many-body systems, which are superconductivity and magnetism, respectively. It is interesting that the study presented herein shows that the system resembles those phases in different regime of characteristic parameters as follows.

First, we review the study of the system hosting few Coulomb interacting electrons. In the regime of ultrastrong Rashba coupling, we found that the system of two interacting electrons becomes orbital ferromagnet even for very weak interactions. The magnetization predicted here is very large which rules out any explanation based on the spin of electrons. In fact, the orbital ferromagnetism labels a transition from the helical state, in which two electrons counterpropagate, to the state which electrons circulate in the same direction. Therefore, by the magnetization we meant the net total angular momentum of electrons. We showed that an energy barrier separates the doubly degenerate ground state labeled with opposite sign of total magnetization. That is the time-reversal symmetry is broken practically, since if the system chooses one of the degenerate states, the tunneling rate between two degenerate states takes an astronomically long time. Next, we engaged

numerical techniques like exact diagonalization and standard Hartree-Fock approximation to study the ground-state properties of interacting electrons in the presence of finite but strong Rashba coupling. It is observed that if the strength of Coulomb interaction exceeds a critical value, a transition from unmagnetized ground state, or almost unmagnetized state for an odd number of electrons, to orbital ferromagnetism takes place. The investigation of the system with different strength of Rashba coupling suggests that the transition occurs at a weaker interaction strength by increasing the strength of Rashba coupling. In addition, the Hartree-Fock calculations have been carried out for particle numbers up to ten which admit the spontaneous magnetization of the system qualitatively. Moreover, a few results of DMRG are presented to illustrate the power of this technique on tackling the system studied herein. The DMRG calculations reproduce the exact-diagonalization findings with a very high accuracy and further results are expected in the near future.

The system containing arbitrary but finite number of particles is also studied in this thesis. We constructed a number of effective models to follow this purpose. In the regime of very weak interaction, it is possible to approximate the interaction terms by uniform terms if the variations of interaction matrix elements are small in comparison with the level spacing. This condition can be fulfilled more easier for the contact potential, in coordinate space, rather than the Coulomb potential. Such an effective 1D Hamiltonian is amenable to bosonozation and therefore exact calculation of correlation functions. Strong correlation of Kramers pairs even for a repulsive interaction potential is the significant result of bosonization study. Furthermore, absence of spontaneous magnetizations can be demonstrated which is expectable for the very weak interaction. Another effective model is constructed to analyze the possibility of a transition to orbital ferromagnetism. Relying on the strong correlation of Kramers pairs, we singled out the uniform interaction of Kramers pairs. The model is shown to be equivalent to Richardson pairing model though for a repulsive pairing force. Although the model bears an exact solution, we merely assessed it heuristically in two extreme regimes, non-interacting and strong interaction. It is then shown that the model predicts a transition to a magnetic state. Although, one must solve the model exactly, to check whether the critical interaction strength satisfies the low-energy constraints or not, which is beyond the treatment for the model considered here. Based on the result of the effective models, we wrote down an approximated Hamiltonian by keeping the BCS-like and exchange-type interactions for non-zero exchanged momentum. The resulting Hamiltonian is called extended Hartree-Fock Hamiltonian since it includes the Hartree-Fock terms plus an extra term which describes solely interactions of time-reversed partners. The interesting feature of the model is that it sets the scene for competition between states with zero magnetization and orbital ferromagnetism, by incorporating the minimal but crucial features of the full interacting model. It is worth noting that those states, i.e. unmagnetized with the maximum number of Kramers pairs and orbital ferromagnetism, are expected intuitively due to the characteristics of the interaction matrix elements. The Hamiltonian can be written as the Heisenberg XXZ spin model. Although we could not find an analytical solution for the model, application of numerical technique is promising since there exist powerful methods for 1D discrete models.

Although it is reported that increasing Rashba coupling enhances Wigner crystallization, where the electrostatic repulsion suppresses quantum fluctuations and interelectron distances are maximized, we did not found any clue for the Wigner molecule in our system. In fact, one should increase the interaction strength, beyond the regime we studied, in order to achieve the crystallization. Therefore, it remains an open question to address the transition from orbital ferromagnetism to Wigner molecule.

In the end, we hope that our predictions find the chance to be testified in a laboratory and also stimulate further theoretical and experimental study of Rashba spin-orbit coupled materials.

Appendix A

Strictly 1D Ring in Momentum Space

A toy model is studied which describes an electron on a ring in momentum space with Rashba spin-orbit coupling. The model assumes the same symmetry of the original model studied herein at the single-particle level, introduced in chapter 3. Consequently. the interaction matrix elements (IMEs) have the same symmetry relations of the original model, considered in chapter 4. In fact, the model was developed initially to investigate the phase constraints associated with the IMEs of the original interacting model. The maximal absolute magnitude of IMEs are BCS-like and exchange-type interactions associated with the restricted scattering processes on a ring in momentum space. Although the latter feature was touched on by the original model in the regime of ultrstrong Rashba coupling, see subsection 4.2.2, the IMEs were zero for odd-exchanged momentum and a constant otherwise. Also, we draw a connection between scattering processes on the momentum-space ring and moduli space of equilateral tetragons [71, 70]. In the end, it is shown that the interacting toy model is well approximated with the Richardson-Gaudin pairing model, see appendix E, which is exactly solvable.

A.1 Single-Particle Hamiltonian

We begin with a dimensionless one-dimensional Hamiltonian which describes a particle on a unit circle in the (translational) momentum space

$$H_0^{\mathrm{r}} \;=\; -\partial_\theta^2 - \Delta\mathcal{P}, \tag{A.1}$$

where θ is the azimuthal angle in momentum space and $\mathcal{P} = \sigma_x \sin\theta - \sigma_y \cos\theta$ is the helicity operator. Δ is the dimensionless strength of Rashba coupling. The toy model respects the same symmetries of the original model introduced in chapter 3. Namely, H_0^{r} is even under time reversal and conserves the total angular momentum $[H_0^{\mathrm{r}}, \hat{J}_z] = 0$, and clearly it is not translational invariant $[H_0^{\mathrm{r}}, \hat{\mathbf{p}}] \neq 0$, where $\hat{J}_z$ is the generator of rotation in orbital and spin angular momentum around $\hat{z}$ axis, and $\hat{\mathbf{p}}$ is the generator of translation. Although, the toy model is scale invariance as it does have dependence only on the angular degree

of freedom despite the original model in chapter 3. The orthonormal eigenfunctions and corresponding eigenenergies of the model can be found readily

$$\Phi_J^+(\theta) = \frac{1}{\sqrt{2\pi}} \begin{pmatrix} \cos\vartheta^+ e^{i(J-1/2)\theta} \\ \\ -i\sin\vartheta^+ e^{i(J+1/2)\theta} \end{pmatrix}, \tag{A.2}$$

$$\Phi_J^-(\theta) = \frac{1}{\sqrt{2\pi}} \begin{pmatrix} \cos\vartheta^- e^{i(J-1/2)\theta} \\ \\ i\sin\vartheta^- e^{i(J+1/2)\theta} \end{pmatrix}, \tag{A.3}$$

$$E_J^{\pm} = J^2 + 1/4 \mp \sqrt{(J/2)^2 + \Delta^2}, \tag{A.4}$$

where $\pm$ are the positive and negative helicity indices. The coefficients of the eigenfunctions have the form

$$\cos\vartheta^{\pm} = \frac{\Delta}{\sqrt{\Delta^2 + \left[\left(J-\frac{1}{2}\right)^2 - E_J^{\pm}\right]^2}}, \tag{A.5}$$

$$\sin\vartheta^{\pm} = \frac{\pm\left[\left(J-\frac{1}{2}\right)^2 - E_J^{\pm}\right]}{\sqrt{\Delta^2 + \left[\left(J-\frac{1}{2}\right)^2 - E_J^{\pm}\right]^2}}. \tag{A.6}$$

Dispersion of the model is shown in Fig. A.1. A band gap $\sim \Delta$ separates the positive and negative helicity bands and the positive helicity has the lower energy similar to the original model, see Sec. 3.2. We are interested in the low-lying excitations of the system where $(\Delta/J)^2 \gg 1$. In this regime, the coefficients take the form

$$\left(\frac{\Delta}{J}\right)^2 \gg 1 \quad \rightarrow \quad \cos\vartheta^{\pm} = \sin\vartheta^{\pm} \approx \frac{1}{\sqrt{2}}, \tag{A.7}$$

and, consequently, the positive helicity eigenstate reads

$$\Phi_J^+(\theta) \rightarrow \Phi_J(\theta) = \frac{1}{\sqrt{4\pi}} \begin{pmatrix} e^{i(J-1/2)\theta} \\ \\ -ie^{i(J+1/2)\theta} \end{pmatrix}. \tag{A.8}$$

From here on, we consider only the low-energy eigenstate $\Phi_J(\theta)$. The eigenstate of H_0^{r} in the regime of strong Rashba coupling is the same as the angular part of the original model in its momentum space representation, see Eq. 3.14. Therefore, it seems to be plausible expecting similarities between the features observed for IMEs of the original model, discussed in chapter 4, and the toy model. The matrix elements of a non-singular potential will be carried out in the next section. Integral of matrix elements has the form similar to the one derived for ultrastrong Rashba coupling in subsection 4.40.

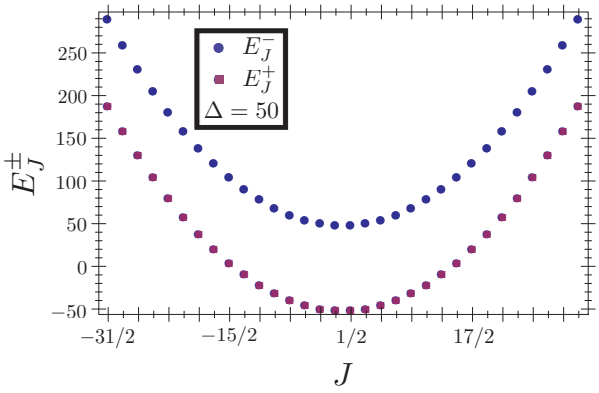

Figure A.1: Energy dispersion for a particle on a momentum-space ring with a Rashba coupling $\Delta = 50$. Two bands are associated with positive, the lower band, and negative, the upper band, helicity.

A.2 Interaction Matrix Elements

We proceed with the positive helicity eigenstate, and hence, the angular momentum is the only quantum number which labels the states. The full Hamiltonian in the second quantization can be written formally as

$$H_{\rm I}^{\rm r} = \frac{\lambda}{2} \sum_{\substack{J_1,J_2 \\ J_1',J_2'}} \langle \Phi_{J_1'}, \Phi_{J_2'} | V | \Phi_{J_2}, \Phi_{J_1} \rangle c_{J_1'}^\dagger c_{J_2'}^\dagger c_{J_2} c_{J_1}, \tag{A.9}$$

where $c_J^\dagger$ and c_J are the fermion creation and annihilation operators, respectively. λ is the dimensionless interaction strength. We assume a short-range interaction potential V which is rotational and translational invariant, and use the completeness of the angular eigenkets

$$\oint d\theta |\theta\rangle\langle\theta| = 1, \tag{A.10}$$

to evaluate the matrix elements as

$$\begin{aligned} V_{J_1',J_2'}^{J_1,J_2} &= \langle \Phi_{J_1'}, \Phi_{J_2'} | V | \Phi_{J_2}, \Phi_{J_1} \rangle \\ &= \oint \prod_{i=1}^{4} d\theta_i \Phi_{J_1'}^*(\theta_1') \Phi_{J_2'}^*(\theta_2') V\left(\theta_1', \theta_2', \theta_2, \theta_1\right) \Phi_{J_2}(\theta_2) \Phi_{J_1}(\theta_1). \end{aligned} \tag{A.11}$$

For the sake of simplicity, we assume a contact-type potential in coordinate space which takes the following form in the basis

$$\langle \theta_1', \theta_2' | V | \theta_2, \theta_1 \rangle = \delta(e^{i\theta_1} + e^{i\theta_2} - e^{i\theta_1'} - e^{i\theta_2'}). \tag{A.12}$$

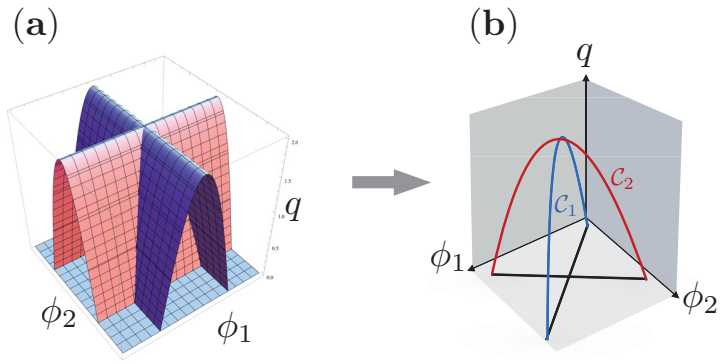

Figure A.2: (Color online) (**a**) Two surfaces $q = \mp 2\cos\phi_{1,2}$ in 3D space of (ϕ_1, ϕ_2, q). (**b**). Two curves $\mathcal{C}_{1,2}$ defined by the intersections of the surfaces characterize all the momentum conserving scattering processes on a momentum-space ring up to an in-plane rotation. The blue curve corresponds to BCS-like interactions $\phi_2 = \phi_1 + \pi$ while the red curve describes exchange-type interactions $\phi_2 = \pi - \phi_1$. A plane defined by a given q with $0 < q < 2$ crosses at four points with the curves which demonstrates that for a given $\mathbf{q}$ there exist four processes, see Fig. A.3. The processes with $q = 0$ are shown by two black solid lines schematically. The resulting set of curves can be identified with the moduli space of equilateral tetragons which is a connected 1D space with four holes, see the text.

Taking into account that θ is the azimuthal angle in momentum space, we can assign a translational momentum $\mathbf{k} = e^{i\theta}$ to the particle being on the unit circle $|\mathbf{k}| = 1$. Therefore, the delta function guarantees the conservation of translational momentum of interacting particles. We treat this constraint in an approach based on a physical reasoning rather than a strict algebraic steps. Practically, we find a curve which parametrizes all the possible scattering processes on the ring. Afterwards, taking into account the constraints, we carry out the integral over this curve to evaluate the interaction matrix elements.

We write $\mathbf{k}'_{1,2} = \mathbf{k}_{1,2} \pm \mathbf{q}$ by means of the exchanged momentum $\mathbf{q} = qe^{i\phi}$ with $0 \leqslant q \leqslant 2$ to satisfy the conservation law. The azimuthal angle of outgoing particles $\theta'_{1,2}$ can be written in terms of $\theta_{1,2}$ and ϕ as

$$e^{i\theta'_{1,2}} = e^{i\theta_{1,2}} \left(\frac{1 \pm q e^{i(\phi - \theta_{1,2})}}{1 \pm q e^{-i(\phi - \theta_{1,2})}} \right)^{1/2}. \tag{A.13}$$

We define new variables

$$\phi_{1,2} = \phi - \theta_{1,2}. \tag{A.14}$$

The outgoing particles must stay on the ring $|\mathbf{k}'_{1,2}| = 1$ which leads to the following constraints on the magnitude of the exchanged momentum

$$\left(1 \pm q e^{-i\phi_{1,2}}\right)\left(1 \pm q e^{i\phi_{1,2}}\right) = 1 \quad \Rightarrow \quad q = \mp 2\cos\phi_{1,2} \geqslant 0. \tag{A.15}$$

These two equations for q must be satisfied simultaneously. Therefore, their intersections define connected curves in the 3D space of (ϕ_1, ϕ_2, q), see Fig. A.2. Each point of these curves corresponds to a momentum conserving scattering process on a ring while the orientation of the exchanged momentum $\mathbf{q}$ is fixed by ϕ. Before parametrizing this curve, we find the conditions on $\phi_{1,2}$ to satisfy Eq. A.15.

In section 4.2.2, it is shown that momentum conserving scattering processes on a ring are classified into two groups, namely, BCS-like and exchange-type interactions, see Fig. A.3. This fact introduces two constraints, the first $\phi_2 = \phi_1 + \pi$ for BCS-like interactions and the second $\phi_2 = \pi - \phi_1$ for exchange-type interactions. Therefore, the intersection of two surfaces in the (ϕ_1, ϕ_2, q) space can be parametrized by two curves

$$\mathcal{C}_1 = (\vartheta, \vartheta + \pi, -2\cos\vartheta), \tag{A.16}$$

for BCS-like interactions and

$$\mathcal{C}_2 = (\vartheta, \pi - \vartheta, -2\cos\vartheta), \tag{A.17}$$

for exchange-type interactions. One should note that the interactions with $q = 0$ is singular since ϕ is not defined. In this case, $\theta_1' = \theta_1$ and $\theta_2' = \theta_2$ can take on values independently. These processes can be considered as the two lines which connect $\mathcal{C}_{1,2}$, see Fig. A.2. The processes with $q = 0$ contributes as a constant term to the Hamiltonian and can be neglected.

Now, firstly, the integral in Eq. A.11 can be written in terms of $\phi_{1,2}$ and q. Thereafter, the integral can be evaluated along two curves $\mathcal{C}_{1,2}$ parametrized by a single variable ϑ. The magnitude of the exchanged momentum needs to be positive definite $q \geqslant 0 \Rightarrow -2\cos\vartheta \geqslant 0$ which gives $\pi/2 \leqslant \vartheta \leqslant -\pi/2$. The measures of the line integrals are

$$d\mathcal{C}_{1,2} = \sqrt{d\phi_1^2 + d\phi_2^2 + dq^2}\Big|_{\mathcal{C}_{1,2}} = d\vartheta\sqrt{2}\sqrt{1 + 2\sin^2\vartheta}. \tag{A.18}$$

The matrix elements in Eq. A.11 after some algebras take the form

$$V^{(m)}_{J_1J_2} = (-1)^{J_1+J_2+m}\frac{\sqrt{2}\lambda}{8\pi}\int_{-\pi/2}^{\pi/2} d\vartheta \sin^2\vartheta\sqrt{1+2\sin^2\vartheta}\Big\{\cos\left[2(J_1+J_2)\vartheta\right] - \cos\left[2(J_1-J_2+m)\vartheta\right]\Big\}, \tag{A.19}$$

where $V^{J_1J_2}_{J_1'J_2'} = V^{(m)}_{J_1J_2}\delta_{J_1+J_2,J_1'+J_2'}$ and the exchanged angular momentum is defined through $J_{1,2}' = J_{1,2} \pm m$. The first cosine in the brackets is associated with BCS-like scattering processes on the ring parametrized by the curve $\mathcal{C}_1$. The contribution of this term is maximum if the interacting particles have zero net total angular momentum $J_1 = -J_2$. The second cosine in the brackets originates from exchange-type interactions parametrized by $\mathcal{C}_2$. This term is maximum if $J_2 = J_1 + m$. The numerical values of IMEs are shown in

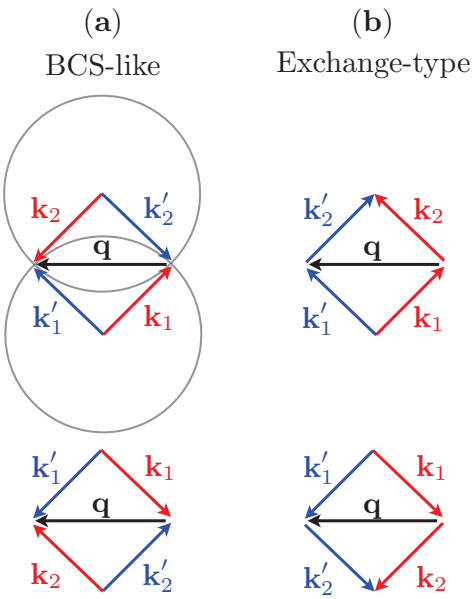

Figure A.3: Scattering processes $\mathbf{k}_{1,2} \to \mathbf{k}'_{1,2} = \mathbf{k}_{1,2} \pm \mathbf{q}$ for a given exchanged momentum $\mathbf{q}$, on a momentum-space ring $|\mathbf{k}_{1,2}| = |\mathbf{k}'_{1,2}| = 1$. For a non-zero exchanged momentum $|\mathbf{q}| \neq 0$, there exist four processes which can be classified into (**a**) BCS-like interactions where $\mathbf{k}_1 = -\mathbf{k}_2$ are scattered to $\mathbf{k}'_1 = -\mathbf{k}'_2$, and (**b**) exchange-type interactions by which $\mathbf{k}_2 = \mathbf{k}_1 + \mathbf{q}$, or equivalently $\mathbf{k}_1 = \mathbf{k}'_2$ and $\mathbf{k}_2 = \mathbf{k}'_1$. Consequently, the same types of interactions are boosted in the angular momentum space, see Fig. A.4.

Fig. A.4 which demonstrate the maximal absolute magnitudes of $V^{(m)}_{J_1 J_2}$ lie along two lines $J_1 = -J_2$ and $J_2 = J_1 + m$. Therefore, the IMEs along $J_1 = -J_2$ and $J_2 = J_1 + m$ are boosted due to the topological restriction of scattering processes on a momentum-space ring to the same kinds of interactions, namely, BCS-like and exchange-type ones, see Fig. A.3. The features of the IMEs are summarized in subsection 4.2.1.

The absolute magnitude of $V^{(m)}_{J_1 J_2}$ along $J_1 = -J_2$ and $J_2 = J_1 + m$ is almost independent of $J_{1,2}$ and m, but decays quickly otherwise. It can be rationalized, for instance, if we consider the IMEs along $J = J_2 = J_1 + m$ that yields

$$V^{(m)}_{J+m,J} = \frac{\sqrt{2}\lambda}{8\pi} \int_{-\pi/2}^{\pi/2} d\vartheta \sin^2\vartheta \sqrt{1 + 2\sin^2\vartheta} \Big\{ 1 - \cos\left[2(2J+m)\vartheta\right] \Big\}. \tag{A.20}$$

The integral of the oscillatory term $\cos\left[2(2J+m)\vartheta\right]$ almost vanishes and can be neglected

$$V^{(m)}_{J+m,J} \approx \frac{\sqrt{2}\lambda}{8\pi} \int_{-\pi/2}^{\pi/2} d\vartheta \sin^2\vartheta \sqrt{1 + 2\sin^2\vartheta}, \tag{A.21}$$

which is independent of $J_{1,2}$ and m. The exception is if $2J = m$ by which the matrix element vanishes identically, that is, the direct scattering into the time-reversed partner is

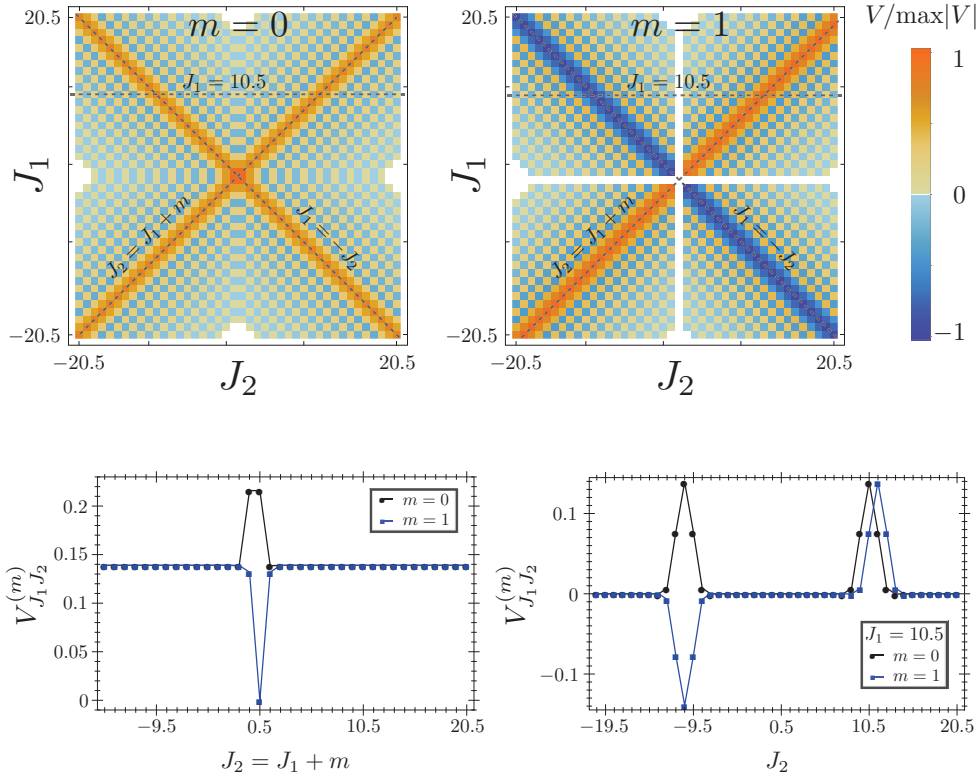

Figure A.4: Interaction matrix elements $V^{(m)}_{J_1,J_2}$ of the toy model in (J_2, J_1) plane, normalized to their maximum value in the shown region. The top row shows matrix elements for $m = 0$ and $m = 1$. The values along the exchange-type interactions $J_2 = J_1+m$ and the horizontal line $J_1 = 10.5$ are shown in the lower plots.

forbidden due to the time reversal symmetry. With the help of the symmetry relations of IMEs, we write

$$V^{(m)}_{J+m,J} = (-1)^m V^{(m)}_{J,-J} \approx \text{cons.}, \tag{A.22}$$

where the c-number is independent of J and m.

Before leaving this section, we mention a connection between the set of all the momentum conserving scattering processes on the momentum-space ring and the moduli space of equilateral tetragons [71, 70]. Given a string $L = (l_1, \cdots, l_n)$ with $l_i > 0$, the moduli space of closed planar polygons is defined by

$$M_L = \Big\{(u_1, \cdots, u_n) \in S^n; \sum_{i=1}^{n} l_i u_i = 0\Big\}/\mathrm{SO}(2),$$

where l_i and u_i denote the length and direction of the ith side of the polygon, respectively.

Consider now momentum-conserving interaction of N particles on a momentum-space ring

$$\sum_{i=1}^{N} \mathbf{k}_i = \sum_{i=1}^{N} \mathbf{k}'_i, \tag{A.23}$$

where $\mathbf{k}_i$ and $\mathbf{k}'_i$ are the momentum of ith particle before and after interaction, respectively, while $|\mathbf{k}_i| = |\mathbf{k}'_i| = 1$. In fact, the constraint for momentum conservation of N interacting particles defines an equilateral $2N$-gon. In the case of $N = 2$, the scattering processes construct equilateral tetragons, see Fig. A.3. Identifying the scattering processes which are equivalent under $SO(2)$, that is fixing the orientation of exchanged momentum $\mathbf{q}$ for instance, we arrive at the moduli space of equilateral tetragons, let call it $\mathcal{Q}_{\rm r}$. This space is comprised of the curves $\mathcal{C}_{1,2}$ in the 3D space (ϕ_1, ϕ_2, q), plus lines in the plane of $q = 0$ which contribute as a constant term into the Hamiltonian. It is known [70] that $\mathcal{Q}_{\rm r}$ is a compact 1D manifold (hyperplane) with finitely many singular points. The rank of zeroth Homology group [75] of $\mathcal{Q}_{\rm r}$ is $\dim H_0(\mathcal{Q}_{\rm r}; \mathbb{Z}) = 1$ that shows it is a connected manifold, and the rank of its first Homology group is $\dim H_1(\mathcal{Q}_{\rm r}; \mathbb{Z}) = 4$ which gives the number of holes in $\mathcal{Q}_{\rm r}$, see Fig. A.2. The singularities of this space are those points where $\mathcal{C}_1$ and $\mathcal{C}_2$ intersect and also the points which connects $\mathcal{C}_{1,2}$ to the lines corresponding to the processes with $q = 0$.

A.3 Effective Pairing Model

As it is shown in the preceding section, the interaction matrix elements have a constant value for given m along maximal absolute magnitude lines and decay rapidly otherwise. If we neglect the interactions for $J_1 \neq -J_2$ and $J_2 \neq J_1 + m$ and the anomalies of $V^{(m)}_{J_1,J_2}$ around the symmetry centers $(J_2, J_1) = (m/2, -m/2)$, the resulting Hamiltonian takes the form

$$H^{\rm r} \approx \sum_{J} J^2 c^\dagger_J c_J + \frac{g}{2} \sum_{J,J'} (-1)^{J-J'} c^\dagger_J c^\dagger_{-J} c_{-J'} c_{J'} - \frac{g}{2} \sum_{J,J'} c^\dagger_J c_J c^\dagger_{J'} c_{J'}, \tag{A.24}$$

where the absolute values of interaction matrix elements along the lines are replaced by a coupling constant g. The last term gives a constant contribution $\sim N^2$ and can be neglected. Only the pairing term determines the interaction-driven dynamics of the system. The interacting model can be written as the Richardson-Gaudin pairing model which bears an exact solution, see section 6.2 and appendix E.

A.4 Summary

A toy model is proposed and studied which describe an electron on a ring in momentum space in the presence of Rashba spin-orbit coupling. The eigenstates of the model can be

derived analytically on contrast to the original model which an effective eigenfunction can be constructed. The main aim for studying the toy model was to investigate the sign of the interaction matrix elements of the original model. In the regime of the strong Rashba coupling, the matrix elements can be represented by an integral equation. The compact form of the integral equation pave the way to dig out the symmetry relations of IMEs and also the reason of the boosted IMEs, i.e. the maximal absolute magnitude elements. As is discussed in chapter 4, the time reversal of the eigenbasis and the pair potential imposes phase constraints on IMEs. Furthermore, the topological restriction of scattering processes on momentum-space ring gives rise to boosted IMEs of the same type, namely, BCS-like and exchange-type interactions. The interacting model is equivalent to Richardson pairing model effectively which bears an exact solution.

Appendix B

Interaction Matrix Elements in 2D and 3D Systems

In this appendix, we briefly mention that the symmetry relations and the boosted classes of interaction, observed in chapter 4, are present also in the isotropic 2D and 3D Fermi liquid. In fact, the phase constraints are the consequence of the representation in the angular momentum basis. And the boosted matrix elements rely on the restricted scattering processes for the states close to the Fermi surface. The interests of such a generalization is that the representation takes into account the intrinsic correlation of interacting particles, particularly in 2D. For sure, the representation does not change the physics of systems, however, it can be constructive if the system is going to be treated effectively, in contrast to the exact solutions.

Consider a 2D isotropic system $[H, L_z] = 0$ where H is the Hamiltonian of the system and L_z is the angular momentum operator. In such cases, it is possible to choose a simultaneous eigenket of H and L_z that is $|k, j\rangle$ where k is a discrete or continues wavenumber. Coordinate-space representation of the eigenket up to a normalization constant can be $\langle \mathbf{r}|k, j\rangle = J_j(kr)e^{j\theta}$ for $j \in \mathbb{Z}$. We abbreviate the quantum numbers by $|\xi\rangle \equiv |k, j\rangle$. The eigenket under time reversal (TR) gives [91]

$$\Theta|k, j\rangle = (-1)^j|k, -j\rangle, \tag{B.1}$$

or in the shortened notation $\Theta|\xi\rangle = (-1)^j|\bar{\xi}\rangle$. The same relations as in Eq. 4.4 can be written for a two-body potential represented in the basis

$$\begin{aligned}\langle \xi_1', \xi_2'|V|\xi_2, \xi_1\rangle &= \langle \bar{\xi}, \xi_2'|V|\xi_2, \bar{\xi}_1'\rangle(-1)^{j_1+j_1'} \\ &= \langle \xi_1', \bar{\xi}_2|V|\bar{\xi}_2', \xi_1\rangle(-1)^{j_2+j_2'} \\ &= \langle \bar{\xi}_1, \bar{\xi}_2|V|\bar{\xi}_2', \bar{\xi}_1'\rangle(-1)^{j_1+j_1'+j_2+j_2'}.\end{aligned} \tag{B.2}$$

Rotational invariance of the interaction potential gives $j_1 + j_2 = j_1' + j_2'$ and reduces the phase factors to $(-1)^{j_1+j_1'} = (-1)^{j_2+j_2'} = (-1)^m$ and $(-1)^{j_1+j_2+j_1'+j_2'} = 1$ with m being the exchanged momentum $j_{1,2}' = j_{1,2} \pm m$. For 2D isotropic fermion systems, the Fermi surface

is a ring in momentum space. Low-lying excitations live in the vicinity of Fermi surface $k \approx k_F$ and once again due to the restriction of scattering processes on a momentum-ring, here Fermi surface, the BCS-like and exchange-type interactions are boosted in j-space.

The characteristics summarized in the ending part of Sec. 4.2.1 also apply to the general representation in Eq. B.2, although, since $j \in \mathbb{Z}$, the corresponding modifications should be taken into account. For instance, the symmetry center $(m/2, -m/2)$ refers to a matrix elements in (j_2, j_1) plane for even m. And also there is no forbidden interaction due to TR symmetry as the the eigenbasis is spin-independent, or in other words, because j is not half-odd-integer. It is straightforward to generalize the scheme and incorporate spin.

In 3D isotropic systems, the eigenbasis can be constructed by $|n, l, j\rangle$ where n is the radial quantum number, l and j are angular momentum and its projection along the quantization axis, respectively. The coordinate representation of the eigenket reads $\langle \mathbf{r}|n, l, j\rangle = R_{nl}(r)Y_l^m(\theta, \phi)$ where $R_{nl}(r)$ is the real-value radial wave-function and $Y_l^m(\theta, \phi)$ is the spherical harmonics [91]. Once again we introduce the abbreviation $|\Xi\rangle = |n, l, j\rangle$. TR symmetry yields

$$\Theta|n, l, j\rangle = (-1)^j|n, l, -j\rangle, \tag{B.3}$$

and in the abbreviated notation $\Theta|\Xi\rangle = (-1)^j|\bar{\Xi}\rangle$. We arrive at The same symmetry relations like Eq. B.2. The Fermi surface in 3D isotropic fermion system is defines by a sphere in momentum space. The low-energy excitations take place around the Fermi surface. The phase space of scattering processes in 3D is not restricted as 2D space. In fact, fixing the momentum transfer $\mathbf{q}$ in Fig. 4.5, the either joint point of $\mathbf{k}_1$ and $\mathbf{k}'_1$ or $\mathbf{k}_2$ and $\mathbf{k}'_2$ in Fig.4.5 can be rotated toward the third dimension around the momentum transfer $\mathbf{q}$ which gives neither BCS-like nor exchange-type interaction. One then expects that those boosted channels of interaction in 2D, namely BCS-like and exchange type, should be less significant for 3D in the angular momentum representation. Incidentally, a study of electronic systems involved in the reduced scattering processes on 2D and 3D Fermi surface can be found, for instance, in the reference [96].

Appendix C

Representation in N Fermion Basis

In this appendix, we represent the full Hamiltonian in the basis of N fermions. The representation is used in the exact-diagonalization calculations. Consider the following generic state of N fermions

$$|a_1, a_2, \cdots, a_N\rangle = c^\dagger_{a_1} c^\dagger_{a_2} \cdots c^\dagger_{a_N} |0\rangle, \tag{C.1}$$

where $c^\dagger_{a_i}$ is the fermion creation operator with $a_i \in \mathbb{Z} + 1/2$ for $i = 1, 2, \cdots, N$. The state $|0\rangle$ is the vacuum with zero number of particle. We consider the states with $a_1 < a_2 < \cdots < a_N$ which indicate that the kets are orthonormal

$$\langle b_1, b_2, \cdots, b_N | a_1, a_2, \cdots, a_N\rangle = \prod_{i=1}^{N} \delta_{a_i b_i}. \tag{C.2}$$

Now, we can construct an orthonormal basis

$$\sum_{a_1<\cdots<a_N} |a_1, a_2, \cdots, a_N\rangle\langle a_1, a_2, \cdots, a_N| = 1. \tag{C.3}$$

The eigenvalue problem $H|\Phi_n\rangle = E^n|\Phi_n\rangle$ can be expanded in this basis

$$\sum_{b_1<\cdots<b_N} \langle a_1, a_2, \cdots, a_N|H|b_1, b_2, \cdots, b_N\rangle\, \varphi^n_{b_1,b_2,\cdots,b_N} = E^n\, \varphi^n_{a_1,a_2,\cdots,a_N}, \tag{C.4}$$

where

$$\varphi^n_{a_1,a_2,\cdots,a_N} = \langle a_1, a_2, \cdots, a_N|\Phi_n\rangle, \tag{C.5}$$

is the projection of nth eigenstate along $|a_1, a_2, \cdots, a_N\rangle$. For convenience in the representation of the matrix elements, we define

$$\bar{\varphi}^n_{a_1,a_2,\cdots,a_N} = \begin{cases} \varphi^n_{a_1,a_2,\cdots,a_N} & \text{if } a_1 < a_2 < \cdots < a_N, \\ \\ 0 & \text{otherwise,} \end{cases} \tag{C.6}$$

and also the interaction matrix elements

$$V^{J_1J_2}_{J'_1J'_2} = 2V^{(m)}_{J_1J_2}\,\delta_{J_1+J_2,J'_1+J'_2}, \tag{C.7}$$

with $J'_{1,2} = J_{1,2} \pm m$. Furthermore, we assume the convention of summation over repeated indices, unless the indices are presented in parenthesis. The matrix elements of the Hamiltonian take the form

$$\langle a_N \cdots a_1|H_0|b_1 \cdots b_N\rangle\, \bar{\varphi}^n_{b_1,\cdots,b_N} = \hbar\omega\left(E_{(a_1)} + E_{(a_2)} + \cdots + E_{(a_N)}\right)\bar{\varphi}^n_{(a_1),\cdots,(a_N)}, \tag{C.8}$$

$$\langle a_N \cdots a_1|H_I|b_1 \cdots b_N\rangle\, \bar{\varphi}^n_{b_1,\cdots,b_N} = \frac{\lambda\hbar\omega}{N!}\,V^{J_1J_2}_{J'_1J'_2}\binom{N}{2}\bar{\varphi}^n_{b_1,b_2,\cdots,b_N}(\epsilon_{a_ia_j}\epsilon_{J'_1J'_2})(\epsilon_{J_1J_2a_k\cdots a_l}\epsilon_{b_1b_2b_3\cdots b_N})\epsilon_{ij\cdots l}. \tag{C.9}$$

The Levi-Civita symbols represent determinant of Kronecker delta functions

$$\epsilon_{a_1a_2\cdots a_N}\epsilon_{b_1b_2\cdots b_N} = \begin{vmatrix} \delta_{a_1b_1} & \delta_{a_1b_2} & \cdots & \delta_{a_1b_N} \\ \delta_{a_2b_1} & \delta_{a_2b_2} & \cdots & \delta_{a_2b_N} \\ \vdots & \vdots & & \vdots \\ \delta_{a_Nb_1} & \delta_{a_Nb_2} & \cdots & \delta_{a_Nb_N} \end{vmatrix}. \tag{C.10}$$

which is used to make the formula concise. The explicit representation of H in two-particle basis has the following form

$$\begin{aligned} E^n\,\varphi^n_{a_1a_2} &= \hbar\omega\left(\varepsilon_{(a_1)} + \varepsilon_{(a_2)}\right)\,\varphi^n_{(a_1)(a_2)} + \frac{\lambda\hbar\omega}{4}\,V^{J_1J_2}_{J'_1J'_2}\varphi^n_{b_1b_2}(\epsilon_{a_ia_j}\epsilon_{J'_1J'_2})(\epsilon_{J_1J_2}\epsilon_{b_1b_2})\epsilon_{ij} \\ &= \hbar\omega\left(\varepsilon_{(a_1)} + \varepsilon_{(a_2)}\right)\,\varphi^n_{(a_1)(a_2)} + \lambda\hbar\omega\left(V^{J_1J_2}_{a_2a_1} - V^{J_1J_2}_{a_1a_2}\right)\varphi^n_{J_1J_2}. \end{aligned} \tag{C.11}$$

Similarly, for $N = 3$, we find

$$\begin{aligned} E^n\,\varphi^n_{a_1a_2a_3} &= \hbar\omega\left(\varepsilon_{(a_1)} + \varepsilon_{(a_2)} + \varepsilon_{(a_3)}\right)\,\varphi^n_{(a_1)(a_2)(a_3)} \\ &+ \lambda\hbar\omega\,\left(V^{J_1J_2}_{a_3a_2} - V^{J_1J_2}_{a_2a_3}\right)\left(\varphi^n_{a_1J_1J_2} - \varphi^n_{J_1a_1J_2} + \varphi^n_{J_1J_1a_1}\right) \\ &+ \lambda\hbar\omega\,\left(V^{J_1J_2}_{a_1a_3} - V^{J_1J_2}_{a_3a_1}\right)\left(\varphi^n_{a_2J_1J_2} - \varphi^n_{J_1a_2J_2} + \varphi^n_{J_1J_1a_2}\right) \\ &+ \lambda\hbar\omega\,\left(V^{J_1J_2}_{a_2a_1} - V^{J_1J_2}_{a_1a_2}\right)\left(\varphi^n_{a_3J_1J_2} - \varphi^n_{J_1a_3J_2} + \varphi^n_{J_1J_1a_3}\right). \end{aligned} \tag{C.12}$$

Single-band approximation, discussed in section 3.3, truncates the matrix elements by $|J| \lesssim \alpha$. Therefore, the effective matrix-representation of H with finite dimensions can be diagonalized numerically, although, for few electrons.

Appendix D

Preliminary and Complementary to Bosonization

In this appendix, we present preliminary and complementary calculations to the bosonization machinery applied to the system in chapter 6. Also parts of the results which are missed there shall be given here. Our approach is mainly based on the bosonization technique reviewed in Ref. [99].

D.1 System of Non-Interacting Electrons

In the following section, we deal with the non-interacting Hamiltonian. The ingredients for bosonizing the Hamiltonian are discussed. Fermion and boson field operators are introduced. In the next section, we compute the correlation of interacting boson.

D.1.1 Operator Identities for Free System

We propose the following fermion field operator

$$\Xi_\eta^\dagger(\theta) \;=\; \frac{1}{\sqrt{4\pi}}\sum_j \left(e^{-i\{(\eta J_F+j)-1/2\}\theta} \quad ie^{-i\{(\eta J_F+j)+1/2\}\theta}\right) c_{j\eta}^\dagger, \tag{D.1}$$

where the angular part of the wave-function in momentum representation (3.14) has been used by substitution $J = \eta J_F + j$ where $j \in \mathbb{Z}$. The creation operator can be written in term of $\Xi_\eta^\dagger(\theta)$ through an inverse Fourier transform

$$c_{j\eta}^\dagger \;=\; \frac{1}{\sqrt{4\pi}}\oint d\theta\, \Xi_\eta^\dagger(\theta) \begin{pmatrix} e^{i\{(\eta J_F+j)-1/2\}\theta} \\ \\ -ie^{i\{(\eta J_F+j)+1/2\}\theta} \end{pmatrix}. \tag{D.2}$$

In order to work only with the dynamical part of the field operator i.e. j-dependent part, we rewrite the spinor field $\Xi^\dagger_\eta(\theta)$ in terms of a scaler field as

$$\Xi^\dagger_\eta(\theta) = \frac{\Psi^\dagger_\eta(\theta)}{\sqrt{2}}\left(e^{-i(\eta J_F-1/2)\theta} \quad ie^{-i(\eta J_F+1/2)\theta}\right). \tag{D.3}$$

$$\Psi^\dagger_\eta(\theta) = \frac{1}{\sqrt{2\pi}}\sum_j e^{-ij\theta}\, c^\dagger_{j\eta}. \tag{D.4}$$

The inverse Fourier transform gives

$$c^\dagger_{j\eta} = \frac{1}{\sqrt{2\pi}}\oint d\theta\, e^{ij\theta}\ \Psi^\dagger_\eta(\theta). \tag{D.5}$$

The anticommutation relations of the field operators can be derived by $\{c^\dagger_{j\eta}, c^\dagger_{j'\eta'}\} = 0$ and $\{c^\dagger_{j\eta}, c_{j'\eta'}\} = \delta_{jj'}\delta_{\eta\eta'}$ which leads to [104]

$$\left\{\Psi^\dagger_\eta(\theta),\ \Psi^\dagger_{\eta'}(\theta')\right\} = \left\{\Psi_\eta(\theta),\ \Psi_{\eta'}(\theta')\right\} = 0, \tag{D.6}$$

$$\begin{aligned}\left\{\Psi^\dagger_\eta(\theta),\ \Psi_{\eta'}(\theta')\right\} &= \frac{\delta_{\eta\eta'}}{2\pi}\sum_j e^{-ij(\theta-\theta')} \\ &= \delta_{\eta\eta'}\sum_{n\in\mathbb{Z}}\delta\left(\theta-\theta'-2\pi n\right).\end{aligned} \tag{D.7}$$

Since $\theta, \theta' \in [0, 2\pi)$, the anticommutation relation reduces to

$$\left\{\Psi^\dagger_\eta(\theta),\ \Psi_{\eta'}(\theta')\right\} = \delta_{\eta\eta'}\delta\left(\theta-\theta'\right). \tag{D.8}$$

A comment is here in order. The fermion field operator $\Xi^\dagger_\eta(\theta)$ (D.1) is independent of the radial degree of freedom i.e. it is merely a function of azimuthal angle θ although the system is 2D. In principle, the field operator representation of $c^\dagger_J$ (the half-odd-integer angular momentum is retained and the chirality is relaxed for the moment) in momentum space has the form

$$a^\dagger(\mathbf{k}) = \sum_J \frac{u_k}{\sqrt{4\pi}}\left(e^{-i(J-1/2)\theta} \quad ie^{-i(J+1/2)\theta}\right) c^\dagger_J, \tag{D.9}$$

where u_k is the normalized radial part of the eigenfunction which is missed in Eq. D.1 and Eq. D.2. We have taken into account the single-band approximation i.e. no summation

on the band index although the treatment can be readily generalized to incorporate band indices. We are going to show that both $a^\dagger(\mathbf{k})$ and $\Xi^\dagger_\eta(\theta)$ generate the same density of particles. This relies on the fact that the radial and angular degrees of freedom are decoupled. Therefore, we can adopt the 1D field operator $\Xi^\dagger_\eta(\theta)$ as is needed in the bosonization scheme. To do so, we write down the total occupation number operator per volume in terms of $a^\dagger(\mathbf{k})$ and $a(\mathbf{k})$ as

$$\hat{N} \;=\; \int d\mathbf{k}\, a^\dagger(\mathbf{k}) a(\mathbf{k}). \tag{D.10}$$

Substituting the field operator (D.9), we obtain

$$\hat{N} \;=\; \int k\, dk\, u_k^2 \oint d\theta \sum_J \frac{1}{\sqrt{4\pi}} \left(e^{-i(J-1/2)\theta} \;\; ie^{-i(J+1/2)\theta}\right) c_J^\dagger \sum_{J'} \frac{1}{\sqrt{4\pi}} \begin{pmatrix} e^{i(J'-1/2)\theta} \\ -ie^{i(J'+1/2)\theta} \end{pmatrix} c_{J'}. \tag{D.11}$$

The radial part of the eigenfunction is normalized $\int k\, dk\, u_k^2 = 1$ which leads to

$$\hat{N} = \oint d\theta\, \Xi^\dagger(\theta)\, \Xi(\theta), \tag{D.12}$$

by means of

$$\Xi^\dagger(\theta) \;=\; \frac{1}{\sqrt{4\pi}} \sum_J \left(e^{-i(J-1/2)\theta} \;\; ie^{-i(J+1/2)\theta}\right) c_J^\dagger. \tag{D.13}$$

Introducing the chirality through $J = \eta J_F + j$, the chiral field operator $\Xi^\dagger_\eta(\theta)$ (D.1) can be achieved. This shows that solely the azimuthal degree of freedom in momentum space determines the density of particles i.e. $\delta\hat{N} = d\theta\, \Xi^\dagger(\theta)\Xi(\theta) = d\theta\, n(\theta)$, independent of the radial degree of freedom.

In fact, a quasi-one-dimensional system emerges in the low-energy physics of the strong Rashba coupling. The decoupling of the radial degree of freedom from angular one in the momentum space (3.14) manifests this dimension reduction. The radial part of the eigenfunction constrains the electrons on a ring in momentum space and the only dynamical degree of freedom is the azimuthal one. The fermion fields can be taken as a function of the azimuthal angle merely. Therefore, we are going to bosonize the fermion field operators which are defined in the translational momentum space $\mathbf{k}$. Although it is inconvenient conceptually, practically it allows us to derive the correlation functions which are defined in terms of the discrete angular momentum.

In the following, we introduce the quantities which are needed to reformulate the theory in terms of boson fields. The angular momentum representation of the density operator results from Eq. D.12

$$\hat{N} = \oint d\theta\, n(\theta) = \oint d\theta \sum_m \frac{e^{im\theta}}{2\pi} n_m, \tag{D.14}$$

where

$$n(\theta) = \Xi^\dagger(\theta)\Xi(\theta), \tag{D.15}$$

$$n_m = \sum_J c_J^\dagger c_{J+m}. \tag{D.16}$$

The normal-ordered Fourier transform of the chiral density operator reads

$$\begin{aligned} n_\eta(\theta) &= :\Psi_\eta^\dagger(\theta)\Psi_\eta(\theta): \\ &= \frac{1}{2\pi}\sum_{m\neq 0} e^{im\theta - a|m|/2}\, n_{m\eta} + \frac{1}{2\pi}\delta\hat{N}_\eta, \end{aligned} \tag{D.17}$$

where a is a positive infinitesimal number to regularize the infinite sum. Note that the scaler field operator (D.3) leads to $\Xi_\eta^\dagger(\theta)\Xi_\eta(\theta) = \Psi_\eta^\dagger(\theta)\Psi_\eta(\theta)$. The chiral density $n_{m\eta}$ is introduced in Eq. 6.9. The bosonic phase fields are defined by means of $n_{m\eta}$ like

$$\varphi_\eta(\theta) = -i\sum_{m>0}\frac{1}{m}\, e^{im\theta - am/2}\, n_{m\eta} + \frac{\theta}{2}\,\delta\hat{N}_\eta, \tag{D.18}$$

$$\varphi_\eta^\dagger(\theta) = i\sum_{m>0}\frac{1}{m}\, e^{-im\theta - am/2}\, n_{-m\eta} + \frac{\theta}{2}\,\delta\hat{N}_\eta, \tag{D.19}$$

and the Hermitian chiral bosonic phase fields $\phi_\eta = \varphi_\eta^\dagger + \varphi_\eta$ is

$$\phi_\eta(\theta) = -i\sum_{m\neq 0}\frac{1}{m} e^{im\theta - a|m|/2}\, n_{m\eta} + \theta\,\delta\hat{N}_\eta. \tag{D.20}$$

The bosonic creation and annihilation operators are defined in terms of the chiral density operators

$$b_m = \begin{cases} \frac{1}{\sqrt{m}}\, n_{m+} & m > 0, \\ \\ \frac{1}{\sqrt{|m|}}\, n_{m-} & m < 0, \end{cases} \tag{D.21}$$

$$b_m^\dagger = \begin{cases} \frac{1}{\sqrt{m}}\, n_{-m+} & m > 0, \\ \\ \frac{1}{\sqrt{|m|}}\, n_{-m-} & m < 0. \end{cases} \tag{D.22}$$

The commutation relations of the bosonic operators are written in the following way

$$[b_m,\, b_{m'}] = [b_m^\dagger,\, b_{m'}^\dagger] = 0, \tag{D.23}$$

$$[b_m,\, b_{m'}^\dagger] = \delta_{mm'}. \tag{D.24}$$

The chiral density operators $n_\pm(\theta)$ in terms of $b_m^\dagger$ and b_m take the form

$$n_+(\theta) = \frac{1}{2\pi} \sum_{m>0} \sqrt{m}\, \left(e^{im\theta} b_m + e^{-im\theta} b_m^\dagger \right) e^{-am/2} + \frac{1}{2\pi}\, \delta\hat{N}_+, \tag{D.25}$$

$$n_-(\theta) = \frac{1}{2\pi} \sum_{m>0} \sqrt{m}\, \left(e^{im\theta} b_{-m}^\dagger + e^{-im\theta} b_{-m} \right) e^{-am/2} + \frac{1}{2\pi}\, \delta\hat{N}_-. \tag{D.26}$$

And also the chiral bosonic phase fields can be written in terms of the boson creation and annihilation operators

$$\varphi_+(\theta) = -i \sum_{m>0} \frac{1}{\sqrt{m}}\, e^{im\theta - am/2}\, b_m + \frac{\theta}{2}\, \delta\hat{N}_+, \tag{D.27}$$

$$\varphi_-(\theta) = i \sum_{m>0} \frac{1}{\sqrt{m}}\, e^{im\theta - am/2}\, b_{-m} + \frac{\theta}{2}\, \delta\hat{N}_-. \tag{D.28}$$

The Hermitian chiral bosonic phase fields $\phi_\eta = \varphi_\eta^\dagger + \varphi_\eta$ reads

$$\phi_+(\theta) = -i \sum_{m>0} \frac{1}{\sqrt{m}}\, \left(e^{im\theta}\, b_m - e^{-im\theta}\, b_m^\dagger \right)\, e^{-am/2} + \theta\, \delta\hat{N}_+, \tag{D.29}$$

$$\phi_-(\theta) = -i \sum_{m>0} \frac{1}{\sqrt{m}}\, \left(e^{im\theta}\, b_{-m}^\dagger - e^{-im\theta}\, b_{-m} \right)\, e^{-am/2} + \theta\, \delta\hat{N}_-. \tag{D.30}$$

Commutation relation of the phase fields can be derived which has the following form

$$\begin{aligned}[\phi_+(\theta),\,\phi_+(\theta')] &= \sum_{m>0}\frac{1}{m}\Big\{e^{im(\theta-\theta')}-e^{-im(\theta-\theta')}\Big\}e^{-am} \\ &= \ln\left(\frac{1-e^{-i(\theta-\theta')-a}}{1-e^{i(\theta-\theta')-a}}\right), \end{aligned} \tag{D.31}$$

where $\ln(1-x) = -\sum_{n=1}^{\infty} x^n/n$ is used in the evaluation of the sum. Similarly

$$[\phi_-(\theta),\,\phi_-(\theta')] = \ln\left(\frac{1-e^{i(\theta-\theta')-a}}{1-e^{-i(\theta-\theta')-a}}\right). \tag{D.32}$$

The dual fields are defined by the following linear combinations

$$\Phi(\theta) = \frac{1}{\sqrt{4\pi}}\big\{\phi_+(\theta)+\phi_-(\theta)\big\}, \tag{D.33}$$

$$\Theta(\theta) = \frac{1}{\sqrt{4\pi}}\big\{\phi_+(\theta)-\phi_-(\theta)\big\}. \tag{D.34}$$

D.1.2 Boson Form of Free Hamiltonian

We write down the free Hamiltonian in terms of the chiral field operators

$$H_0 = v_F\sum_{\substack{j\\ \eta=\pm}}\eta j\, c^\dagger_{j\eta}c_{j\eta} \tag{D.35}$$

$$= v_F\sum_{\eta=\pm}\oint d\theta\,\Xi^\dagger_\eta(\theta)\left(-i\partial_\theta+\frac{\sigma_z}{2}-\eta J_F\right)\Xi_\eta(\theta), \tag{D.36}$$

where the translation by ηJ_F in the second line is due to the definition of the new parameter $J = \eta J_F + j$. Substituting the spinor representation of the field operators yields

$$H_0 = v_F\oint d\theta\,\Big\{:\Psi^\dagger_-(\theta)\,i\partial_\theta\,\Psi_-(\theta):-:\Psi^\dagger_+(\theta)\,i\partial_\theta\,\Psi_+(\theta):\Big\}, \tag{D.37}$$

where the normal ordering is introduced. The free Hamiltonian can also be represented in terms of the boson operators

$$H_0 = v_F\sum_{m\neq 0}|m|b^\dagger_m b_m + \frac{v_F}{2}\sum_\eta \delta\hat{N}_\eta\left(\delta\hat{N}_\eta+1\right), \tag{D.38}$$

where the contribution of $m = 0$, i.e. zero modes, is represented separately. The boson form of H_0 can be readily justified by computing the commutation relations of fermonic Hamiltonian (D.35) with boson operators

$$[H_0,\, b_m] = -v_F|m|b_m, \tag{D.39}$$

$$[H_0,\, b_m^\dagger] = v_F|m|b_m^\dagger, \tag{D.40}$$

which have the sane algebra if H_0 is replaced by its boson representation (D.38). The H_0 can readily be presented by an equivalent form

$$H_0 = \pi v_F \oint d\theta \, \left[n_+^2(\theta) + n_-^2(\theta)\right]. \tag{D.41}$$

It is more convenient to have H_0 represented by $\Phi(\theta)$ and its dual fields

$$H_0 = \frac{v_F}{2} \oint d\theta \left\{ \left[\partial_\theta \Theta(\theta)\right]^2 + \left[\partial_\theta \Phi(\theta)\right]^2 \right\}. \tag{D.42}$$

The interacting Hamiltonian has a representation identical to the latter form of H_0 but with renormalized Fermi velocity and dual fields. This equivalency allows to compute quantities of the interacting model using the non-interacting one.

D.1.3 Eigenstates of Free Hamiltonian

In the following, we construct the ground states of H_0. Consider $|\vec{N}\rangle$ defined by

$$|\vec{N}\rangle = |\delta N_+,\, \delta N_-\rangle = C_+^{\delta N_+} C_-^{\delta N_-} |0\rangle, \tag{D.43}$$

and

$$C_\eta^{\delta N_\eta} = \begin{cases} c_{\delta N_\eta \eta}^\dagger \, c_{\delta N_\eta - 1\eta}^\dagger \cdots c_{1\eta}^\dagger & \text{if } \delta N_\eta > 0, \\ 1 & \text{if } \delta N_\eta = 0, \\ c_{\delta N_\eta + 1\eta} \, c_{\delta N_\eta + 2\eta} \cdots c_{0\eta} & \text{if } \delta N_\eta < 0, \end{cases} \tag{D.44}$$

where we have adopted the convention of Ref. [104]. The null state $|0\rangle$ is the Fermi sea where all the states are occupied up to Fermi points $\pm J_F$ which is set by $j = 0$, note that $J = \eta J_F + j$. If $\delta N_\eta > 0$, then δN_η electrons are added to the branch η. Otherwise, if $\delta N_\eta < 0$, then $|\delta N_\eta|$ electrons are reduced from the corresponding branch. Since $|\vec{N}\rangle$ has no particle-hole excitation, it is a vacuum for the boson operator $b_m|\vec{N}\rangle = 0$. In principle, the states with non-zero δN_η are excited states due to the contribution of zero modes

$$H_0|\vec{N}\rangle = \frac{v_F}{2} \sum_\eta \delta N_\eta \left(\delta N_\eta + 1\right) |\vec{N}\rangle. \tag{D.45}$$

D.1.4 Klein Factors

The boson operators maintain the number of particles in each branch. Formally, an extra operator is needed to connect the sections of Hilbert space with different number of particles. Consider a state with extra δN_η particles on branch η without any particle-hole excitation $b_m|\delta N_\eta\rangle = 0$. The Klein factors $F_\eta^\dagger$ and F_η add one particle to the lowest energy state or remove one particle from the highest occupied state

$$F_\eta^\dagger|\delta N_\eta\rangle = |\delta N_\eta + 1\rangle, \tag{D.46}$$
$$F_\eta|\delta N_\eta\rangle = |\delta N_\eta - 1\rangle. \tag{D.47}$$

They are unitary operators

$$F_\eta^\dagger F_\eta = F_\eta F_\eta^\dagger = 1, \tag{D.48}$$

and commute with the boson operators

$$[F_\eta^\dagger,\, b_m] = [F_\eta^\dagger,\, b_m^\dagger] = [F_\eta,\, b_m] = [F_\eta,\, b_m^\dagger] = 0. \tag{D.49}$$

The Klein factors satisfy the following anticommutation relations

$$\{F_\eta^\dagger,\, F_{\eta'}^\dagger\} = \{F_\eta,\, F_{\eta'}\} = 0, \qquad \text{for } \eta \neq \eta', \tag{D.50}$$

$$\{F_\eta^\dagger,\, F_{\eta'}\} = 2\delta\eta\eta'. \tag{D.51}$$

We do not explore the subtleties of Klein factors in details as they will not be of significance in our treatment for bosonizing the interacting theory. The Klein factors appear in the definition of the bosonized fermion fields which are exploited in the calculation of correlation functions. In the absence of backward scattering and any other impurities in our theory, the particle number in each branch is conserved and the Klein factors can be discarded safely.

D.1.5 Bosonized Fermion Fields

The fermion field operators are defined in terms of boson fields as

$$\Psi_+(\theta) = \frac{1}{\sqrt{2\pi a}} F_+\, e^{i\phi_+}$$
$$= \frac{1}{\sqrt{2\pi a}} F_+\, e^{i\sqrt{\pi}[\Phi(\theta)+\Theta(\theta)]}, \tag{D.52}$$

and

$$\Psi_-(\theta) = \frac{1}{\sqrt{2\pi a}} F_-\, e^{-i\phi_-}$$
$$= \frac{1}{\sqrt{2\pi a}} F_-\, e^{-i\sqrt{\pi}[\Phi(\theta)-\Theta(\theta)]}. \tag{D.53}$$

The adjoint operators take the form

$$\begin{aligned}\Psi_+^\dagger(\theta) &= \frac{1}{\sqrt{2\pi a}} F_+^\dagger \, e^{-i\phi_+} \\ &= \frac{1}{\sqrt{2\pi a}} F_+^\dagger \, e^{-i\sqrt{\pi}[\Phi(\theta)+\Theta(\theta)]},\end{aligned} \tag{D.54}$$

and

$$\begin{aligned}\Psi_-^\dagger(\theta) &= \frac{1}{\sqrt{2\pi a}} F_-^\dagger \, e^{i\phi_-} \\ &= \frac{1}{\sqrt{2\pi a}} F_-^\dagger \, e^{i\sqrt{\pi}[\Phi(\theta)-\Theta(\theta)]}.\end{aligned} \tag{D.55}$$

The Klein factors $F_\pm$ are necessary to ensure the anticommutation relations of the fermion fields. The limit $a \to 0$ is implicit in the definition of the field operators.

D.1.6 Correlation Functions in Free System

In this subsection, we compute a generic correlation function of free boson fields which later will be used in the calculation of the correlation functions in the interacting theory. Consider the following expectation value in the bosonic vacuum

$$C_{AB\eta\nu}(x,x',y,y') = \langle \vec{N}|\hat{O}_{AB,\eta\nu}(x,y)\,\hat{O}^\dagger_{AB,\eta\nu}(x',y')|\vec{N}\rangle, \tag{D.56}$$

where $\hat{O}_{AB,\eta\nu}$ is defined explicitly in terms of the dual fields (D.33) and (D.34)

$$\hat{O}_{AB,\eta\nu} = \exp\Big\{ -i\sqrt{\pi}\,A\,[\eta\Phi(x)+\nu\Phi(y)] - i\sqrt{\pi}\,B\,[\Theta(x)+\Theta(y)] \Big\} = e^{-\mathbf{arg}(x,y)}. \tag{D.57}$$

A and B are arbitrary real constants and $\eta,\nu = \pm$ are introduced for the later convenience. $\mathbf{arg}(x,y)$ has been introduced as an abbreviation of the argument. The Klein factors are dropped from very beginning as in the absence of the backward scattering, the sector of Hilbert space with different number of particles cannot be connected via boson fields. We construct the correlation function with dual fields Φ and Θ since the correlation functions of the interacting fields can be mapped to the dual free fields. We rewrite the field operators in terms of the chiral fields as working with them are more convenient. We find then

$$A\,[\eta\Phi(x)+\nu\Phi(y)] - B\,[\Theta(x)+\Theta(y)] = \frac{1}{\sqrt{\pi}}\Big\{ \sum_{k=\pm} \Lambda_{\eta k}\,\phi_k(x) + \sum_{k=\pm} \Lambda_{\nu k}\,\phi_k(y) \Big\}, \tag{D.58}$$

where we have defined

$$\Lambda_{\eta\nu} = \frac{\eta A + \nu B}{2}. \tag{D.59}$$

The following identities for two arbitrary operators P and Q

$$e^P\, e^Q = e^{P+Q}\, e^{(1/2)[P,\,Q]}, \tag{D.60}$$

$$\langle e^{-iP} \rangle = e^{-(1/2)\langle P^2 \rangle}, \tag{D.61}$$

is helpful in the calculation of the correlation function. The commutation relations of the chiral boson fields are demonstrated in Eqs. D.31 and D.32. We pursue to calculate the expectation values of the fields. We need to know the expectation value of the following combination in the boson vacuums

$$[\mathbf{arg}(x,y) - \mathbf{arg}(x',y')]^2 \;=\; -\Big\{ \sum_{k=\pm} \Lambda_{\eta k}\, [\phi_k(x) - \phi_k(x')] + \sum_{k=\pm} \Lambda_{\nu k}\, [\phi_k(y) - \phi_k(y')] \Big\}^2. \tag{D.62}$$

Among many terms, we present the ultimate form of some typical terms using the definition of free bosonic fields in Eqs. D.29 and D.30.

$$\begin{aligned}
\langle \vec{N}|\phi_+^2(x)|\vec{N}\rangle &= -\sum_{\substack{m>0\\ m'>0}} \frac{e^{-a(m+m')/2}}{\sqrt{mm'}} \langle \vec{N}| \left(e^{imx} b_m - e^{-imx} b_m^\dagger\right) \left(e^{im'x} b_{m'} - e^{-im'x} b_{m'}^\dagger\right) |\vec{N}\rangle + x^2 \delta N_+^2 \\
&= \sum_m \frac{e^{-am}}{m} + x^2 \delta N_+^2 \\
&= -\ln\left(1 - e^{-a}\right) + x^2 \delta N_+^2,
\end{aligned} \tag{D.63}$$

where the boson vacuum $|\vec{N}\rangle$ has been defined in Eq. D.43. The next example is

$$\begin{aligned}
\langle \vec{N}|\phi_+(x)\phi_+(x')|\vec{N}\rangle &= \sum_m \frac{1}{m} e^{im(x-x')-am} + x\, x' \delta N_+^2 \\
&= -\ln\left(1 - e^{i(x-x')-a}\right) + x\, x' \delta N_+^2,
\end{aligned} \tag{D.64}$$

and similarly

$$\langle \vec{N}|\phi_-^2(x)|\vec{N}\rangle = -\ln\left(1 - e^{-a}\right) + x^2 \delta N_-^2, \tag{D.65}$$

$$\langle \vec{N}|\phi_-(x)\phi_-(x')|\vec{N}\rangle = -\ln\left(1 - e^{i(x'-x)-a}\right) + x\, x' \delta N_-^2. \tag{D.66}$$

Collecting together all the terms, we obtain

$$\exp\left(\frac{1}{2}\langle[\mathbf{arg}(x,y)-\mathbf{arg}(x',y')]^2\rangle\right)=\left(1-e^{-a}\right)^{2\left(\Lambda_{\eta+}^2+\Lambda_{\eta-}^2\right)}$$
$$\times\exp\left\{(\sum_{k=\pm}\Lambda_{\eta k}^2\delta N_k^2)(x-x')^2+(\sum_{k=\pm}\Lambda_{\nu k}^2\delta N_k^2)(y-y')^2+2(\sum_{k=\pm}\Lambda_{\eta k}\Lambda_{\nu k}\delta N_k^2)(x-x')(y-y')\right\}$$
$$\times\left\{\left(1-e^{i(x-x')-a}\right)\left(1-e^{-i(x-x')-a}\right)\left(1-e^{i(y-y')-a}\right)\left(1-e^{-i(y-y')-a}\right)\right\}^{-\left(\Lambda_{\eta+}^2+\Lambda_{\eta-}^2\right)/2}$$
$$\times\left\{\frac{\left(1-e^{i(x-y')-a}\right)\left(1-e^{i(y'-x)-a}\right)\left(1-e^{i(x'-y)-a}\right)\left(1-e^{i(y-x')-a}\right)}{\left(1-e^{i(x-y)-a}\right)\left(1-e^{i(y-x)-a}\right)\left(1-e^{i(x'-y')-a}\right)\left(1-e^{i(y'-x')-a}\right)}\right\}^{-(\Lambda_{\eta+}\Lambda_{\nu+}+\Lambda_{\eta-}\Lambda_{\nu-})/2}. \quad \text{(D.67)}$$

D.2 System of Interacting Electrons

In this section, we proceed to consider the boson form of the interacting model. First, we construct the operator identities required here. Next, we compute response functions of the system and correlation of interacting fermion fields.

D.2.1 Operators Identities of Interacting Model

The Full Hamiltonian is defined in terms of the gauged density operators (6.15). Therefore, we require to construct the boson operators by means of the gauged density operators. The Fourier transform of the gauged density operator can be readily obtained

$$\begin{aligned}\tilde{n}_\eta(\theta) &= \frac{1}{2\pi}\sum_{m\neq 0}e^{im\theta-a|m|/2}\,\tilde{n}_{m\eta}+\frac{1}{\pi}\delta\hat{N}_\eta,\\ &= \frac{1}{2\pi}\sum_{m\neq 0}e^{im(\theta+\eta\pi/2)-a|m|/2}\,n_{m\eta}+\frac{1}{\pi}\delta\hat{N}_\eta,\\ &= n_\eta(\theta+\eta\pi/2), \quad \text{(D.68)}\end{aligned}$$

which is equal to the bare density (D.17) up to a transformation of the argument $\theta\rightarrow\theta+\eta\pi/2$. In fact, that is a rotation in momentum space. The boson operators in terms of

$\tilde{n}_{m\eta}$ take the form

$$\tilde{b}_m = \begin{cases} \frac{1}{\sqrt{m}}\,\tilde{n}_{m+} & m>0, \\ \\ \frac{1}{\sqrt{|m|}}\,\tilde{n}_{m-} & m<0, \end{cases} \tag{D.69}$$

$$\tilde{b}^\dagger_m = \begin{cases} \frac{1}{\sqrt{m}}\,\tilde{n}_{-m+} & m>0, \\ \\ \frac{1}{\sqrt{|m|}}\,\tilde{n}_{-m-} & m<0. \end{cases} \tag{D.70}$$

The commutation relations of the gauged bosonic operators reads

$$[\tilde{b}_m,\,\tilde{b}_{m'}] = [\tilde{b}^\dagger_m,\,\tilde{b}^\dagger_{m'}] = 0, \tag{D.71}$$

$$[\tilde{b}_m,\,\tilde{b}^\dagger_{m'}] = \delta_{mm'}, \tag{D.72}$$

where is the same as the bare boson operators. $\tilde{n}_\eta(\theta)$ in terms of $\tilde{b}^\dagger_m$ and $\tilde{b}_m$ takes the form

$$\tilde{n}_+(\theta) = \frac{1}{2\pi}\sum_{m>0}\sqrt{m}\,\left(e^{im\theta}\tilde{b}_m + e^{-im\theta}\tilde{b}^\dagger_m\right)e^{-am/2} + \frac{1}{2\pi}\,\delta\hat{N}_+, \tag{D.73}$$

$$\tilde{n}_-(\theta) = \frac{1}{2\pi}\sum_{m>0}\sqrt{m}\,\left(e^{im\theta}\tilde{b}^\dagger_{-m} + e^{-im\theta}\tilde{b}_{-m}\right)e^{-am/2} + \frac{1}{2\pi}\,\delta\hat{N}_-. \tag{D.74}$$

The gauged bosonic operator lead to the transformed bosonic phase fields

$$\tilde{\varphi}_\eta(\theta) = \varphi_\eta(\theta+\eta\pi/2), \tag{D.75}$$

$$\tilde{\varphi}^\dagger_\eta(\theta) = \varphi^\dagger_\eta(\theta+\eta\pi/2), \tag{D.76}$$

$$\tilde{\phi}_\eta(\theta) = \tilde{\varphi}^\dagger_\eta(\theta) + \tilde{\varphi}_\eta(\theta) = \phi_\eta(\theta+\eta\pi/2). \tag{D.77}$$

The relations between the gauged and the bare dual fields are not similar to the phase fields a sole rotation

$$\tilde{\Phi}(\theta) = \frac{1}{2}\Big\{\Phi(\theta+\pi/2) + \Phi(\theta-\pi/2) + \Theta(\theta+\pi/2) - \Theta(\theta-\pi/2)\Big\}, \tag{D.78}$$

$$\tilde{\Theta}(\theta) = \frac{1}{2}\Big\{\Phi(\theta+\pi/2) - \Phi(\theta-\pi/2) + \Theta(\theta+\pi/2) + \Theta(\theta-\pi/2)\Big\}. \tag{D.79}$$

D.2.2 Density-Density Response Function

The density-density response function of Luttinger-Tomonaga model can be computed exactly through solving the equation of motion for density operators. The chiral density-density response function is defined by ($\hbar = 1$)

$$\begin{aligned}\Pi_{\eta\eta'}(m,\omega) &= \frac{1}{2\pi i}\int_0^\infty dt\, e^{i\omega t}\,\langle[n_\eta(m,\,t),\,n_{\eta'}(-m,\,0)]\rangle \\ &= \int_{-\infty}^{\infty} dt\, e^{i\omega t}\,\Pi_{\eta\eta'}(m,t),\end{aligned} \tag{D.80}$$

where $\hat{\theta}(t)$ is the heavy-side theta function, and

$$\begin{aligned}\Pi_{\eta\eta'}(m,t) &= \frac{\hat{\theta}(t)}{2\pi i}\,\langle[n_\eta(m,\,t),\,n_{\eta'}(-m,\,0)]\rangle\,. \\ &= e^{i(\eta'-\eta)m\pi/2}\,\frac{\hat{\theta}(t)}{2\pi i}\,\langle[\tilde{n}_\eta(m,\,t),\,\tilde{n}_{\eta'}(-m,\,0)]\rangle\,,\end{aligned} \tag{D.81}$$

where in the second line, the gauged density operators are substituted. By writing down an equation for $\partial_t\Pi_{\eta\eta'}(m,t)$ through $\partial_t\,\tilde{n}_\eta(m,t) = i\,[H,\,\tilde{n}_\eta(m,t)]$ and taking the inverse Fourier transform to frequency space, the response function can be solved exactly [99]. The final results have the form

$$\Pi_{++}(m,\omega) = \frac{1}{2\pi}\frac{m\big\{\omega + (v_F + g/2\pi)\,m\big\}}{\omega^2 - m^2u^2}, \tag{D.82}$$

$$\Pi_{-+}(m,\omega) = -\frac{(-1)^m}{2\pi}\frac{m^2 g/2\pi}{\omega^2 - m^2u^2},$$

$$\Pi_{+-}(m,\omega) = -\frac{(-1)^m}{2\pi}\frac{m^2 g/2\pi}{\omega^2 - m^2u^2}, \tag{D.83}$$

$$\Pi_{--}(m,\omega) = -\frac{1}{2\pi}\frac{m\big\{\omega - (v_F + g/2\pi)\,m\big\}}{\omega^2 - m^2u^2}, \tag{D.84}$$

where $u = v_F\sqrt{1+2\widetilde{g}}$ is the renormalized Fermi velocity. Due to the phase-dependent interaction matrix elements of particles with opposite chirality, the corresponding density-density response function also acquires a phase factor. The total density-density response read

$$\Pi(m,\omega) = \frac{1}{\pi}\,\frac{m^2\big\{v_F + (g/2\pi)\,[1-(-1)^m]\,\big\}}{\omega^2 - m^2u^2}, \tag{D.85}$$

which shows a parity effect. The parity effect appears if $g \neq 0$ although for $|g| \ll v_F$, it would be negligible in the total response function.

D.2.3 Correlation Functions in Interacting Model

The full Hamiltonian (6.15) has the same form as the free system in terms of the dual fields (D.42) up to the renormalization of fields and parameters. Therefore, it is straightforward to exploit the correlation functions of the free model to carry out the correlation functions of the interacting model. Representing the full Hamiltonian by the gauged dual fields, in Eqs. D.78 and D.79, yields

$$H = \frac{u}{2}\oint d\theta \left\{ \frac{1}{K}\left[\partial_\theta \tilde{\Phi}(\theta)\right]^2 + K\left[\partial_\theta \tilde{\Theta}(\theta)\right]^2 \right\}, \tag{D.86}$$

where $u = v_F\sqrt{1+2\widetilde{g}}$ and $K = v_F/u$ are renormalized Fermi velocity and the Luttinger parameter, respectively. The renormalized dual fields

$$\overline{\Phi} = \frac{\tilde{\Phi}}{\sqrt{K}}, \tag{D.87}$$

$$\overline{\Theta} = \sqrt{K}\,\tilde{\Theta}, \tag{D.88}$$

transform H to the same analytical form as H_0

$$H = \frac{u}{2}\oint d\theta \left\{ \left[\partial_\theta \overline{\Phi}(\theta)\right]^2 + \left[\partial_\theta \overline{\Theta}(\theta)\right]^2 \right\}. \tag{D.89}$$

In order to inspect the correlation of electrons in the interacting system, it is required to represent the bare operators by means of the fields of the interacting model. The boson fields of the noninteracting system in term of $\overline{\Phi}$ and $\overline{\Theta}$ have the following forms

$$\Phi(x) = \frac{1}{2}\left\{ \sqrt{K}\left[\overline{\Phi}(x-\frac{\pi}{2}) + \overline{\Phi}(x+\frac{\pi}{2})\right] + \frac{1}{\sqrt{K}}\left[\overline{\Theta}(x-\frac{\pi}{2}) - \overline{\Theta}(x+\frac{\pi}{2})\right] \right\}, \tag{D.90}$$

$$\Theta(x) = \frac{1}{2}\left\{ \sqrt{K}\left[\overline{\Phi}(x-\frac{\pi}{2}) - \overline{\Phi}(x+\frac{\pi}{2})\right] + \frac{1}{\sqrt{K}}\left[\overline{\Theta}(x-\frac{\pi}{2}) + \overline{\Theta}(x+\frac{\pi}{2})\right] \right\}. \tag{D.91}$$

Here, we summarize the procedure by which the correlation functions will be calculated:

I) In the noninteracting system, the correlation functions of an arbitrary linear combination of boson fields $\langle \hat{O}^\dagger \hat{O} \rangle$, where

$$\hat{O}^\dagger = \sum_{i=1}^{n} \left(A_i \Phi(x_i) + B_i \Theta(y_i) \right), \tag{D.92}$$

can be calculated straightforwardly.

II) Correlation functions of the interacting system in terms of $\overline{\Phi}$ and $\overline{\Theta}$ have the same form as the corresponding correlation functions of the noninteracting system while u is replaced by v_F.

III) We are interested in the correlation functions of the bare boson fields in the ground state of the interacting system. Hence, we use the relations in Eqs. D.90 and D.91 to rewrite the correlation functions since $\overline{O}$ acts on the ground state of the interacting system.

As an example, we calculate $\Big\langle \Psi_{+}(\theta,\, t)\Psi_{+}^{\dagger}(0,\, 0)\Big\rangle$ in the boson representation for both ground states of noninteracting $\langle\cdots\rangle_0$ and interacting $\langle\cdots\rangle_{\rm int}$ system. The boson forms of the fermion field operators in Eqs. D.52 and D.53 yield

$$\Psi_{+}(\theta,\, t)\,\Psi_{+}^{\dagger}(0,\, 0) = \frac{1}{2\pi a} e^{i\sqrt{\pi}[\Phi(\theta,\, t)+\Theta(\theta,\, t)]}\, e^{-i\sqrt{\pi}[\Phi(0,\, 0)+\Theta(0,\, 0)]}. \tag{D.93}$$

The Klein factors are dismissed since the number of particles in each branch is conserved. We have $\phi_{\pm}(\theta,\, t) = \phi_{\pm}(\theta \mp v_F t)$ due to the linear dispersion. Using identities $e^{A}\, e^{B} = e^{A+B}\, e^{\frac{1}{2}[A,\, B]}$ and $\big\langle e^{A}\big\rangle = e^{\frac{1}{2}\langle A^2\rangle}$, we find

$$\Big\langle \Psi_{+}(\theta,\, t)\,\Psi_{+}^{\dagger}(0,\, 0)\Big\rangle_0 = \big(1 - e^{i(\theta - v_F t) - a}\big)^{-1}, \tag{D.94}$$

where in the calculation, we have engaged $e^{-a} \simeq 1 - a$ that cancels the regularization factor in the denominator. For interacting ground state, we use the relations given in Eq. D.91 and Eq. D.90 in Eq. D.93 which provide

$$\Big\langle \Psi_{+}(\theta,\, t)\,\Psi_{+}^{\dagger}(0,\, 0)\Big\rangle_{int} \propto \big(1 - e^{i(\theta - ut) - a}\big)^{-(\sqrt{K}+1/\sqrt{K})^2/4}\, \big(1 - e^{-i(\theta - ut) - a}\big)^{-(\sqrt{K}-1/\sqrt{K})^2/4}. \tag{D.95}$$

In the noninteracting limit $K = 1$, the results coincide obviously.

D.2.4 Correlation of Kramers Pairs

We calculate the static correlation function

$$\begin{aligned} \mathrm{P}(\theta_0) &= \sum_{j,\, j'} e^{i(j - j')\theta_0}\, \langle c_{j+}^{\dagger} c_{-j-}^{\dagger} c_{-j'-} c_{j'+}\rangle_{\rm int} \\ &= \oint d\theta d\theta' \langle \Psi_{+}^{\dagger}(\theta)\, \Psi_{-}^{\dagger}(\theta + \theta_0) \Psi_{-}(\theta' + \theta_0) \Psi_{+}(\theta')\,\rangle_{\rm int}, \end{aligned} \tag{D.96}$$

which reveals the correlation of Kramers pairs if $\theta_0 = \pi$, see the discussion in section 6.1.4. In the boson form, first, we calculate the following generic correlation function

$$\Big\langle \Psi_{+}^{\dagger}(x)\, \Psi_{-}^{\dagger}(y)\, \Psi_{-}(y')\, \Psi_{+}(x')\Big\rangle_{\rm int} \;\propto\; \mathrm{P}(X,\, Y) = \Big\langle e^{-i\phi_{+}(x)}\, e^{i\phi_{-}(y)}\, e^{-i\phi_{-}(y')}\, e^{i\phi_{+}(x')}\Big\rangle_{\rm int}, \tag{D.97}$$

where $X = (x,\, x')$ and $Y = (y,\, y')$ and $x,\, y \in [0, 2\pi)$. With the aid of $e^{A}\, e^{B} = e^{A+B}\, e^{\frac{1}{2}[A,\, B]}$, we obtain

$$\begin{aligned} \mathrm{P}(X,\, Y) &= \langle \vec{N}|\exp\Big\{ - i\phi_{+}(x) + i\phi_{-}(y) - i\phi_{-}(y') + i\phi_{+}(x')\Big\}|\vec{N}\rangle_{\rm int} \\ &\quad \times \exp\Big\{\frac{1}{2}\,[\phi_{+}(x),\, \phi_{+}(x')] + \frac{1}{2}\,[\phi_{-}(y),\, \phi_{-}(y')]\,\Big\}, \end{aligned} \tag{D.98}$$

where the bosonic vacuum defined in Eq. D.43 is used. The linear combination of the fields in the first line should be written in terms of the interacting bosonic fields by means of the relations in Eqs. D.33, D.34, D.90 and D.91, which yield

$$\frac{1}{\sqrt{\pi}}\big\{\phi_+(x)-\phi_+(y)\big\}=\sqrt{K}\left\{\overline{\Phi}(x-\frac{\pi}{2})-\overline{\Phi}(y+\frac{\pi}{2})\right\}+\frac{1}{\sqrt{K}}\left\{\overline{\Theta}(x-\frac{\pi}{2})+\overline{\Theta}(y+\frac{\pi}{2})\right\}. \quad \text{(D.99)}$$

Transforming two other fields in the exponent in the same way, we arrive at the form which makes it possible to exploit the correlation function of the free model derived in sec. D.1.6 according to the recipe given in the preceding section. Adjusting the coefficients and chirality of the fields in Eq. D.67, we find the result. Before writing down the final form of $\mathrm{P}(X,\,Y)$, we calculate the term associated with the commutation relations of the field (D.98). The commutation relations in Eqs. D.31 and D.32 give

$$\exp\left\{\frac{1}{2}\left[\phi_+(x),\,\phi_+(x')\right]+\frac{1}{2}\left[\phi_-(y),\,\phi_-(y')\right]\right\}=\left[\frac{(1-e^{-i(x-x')-a})(1-e^{i(y-y')-a})}{(1-e^{i(x-x')-a})(1-e^{-i(y-y')-a})}\right]^{\frac{1}{2}}. \quad \text{(D.100)}$$

Collecting all the terms and setting $\delta N_+=-\delta N_-=\delta N\geqslant 0$ in the boson vacuum defined in Eq. D.43, we obtain

$$\begin{aligned}\mathrm{P}(X,\,Y) &= a^{K+1/K}\,\exp\left\{-\frac{\delta N^2}{4}\Big\{K\left[(x-x')+(y-y')\right]^2+\frac{1}{K}\left[(x-x')-(y-y')\right]^2\Big\}\right\}\\ &\times\ \Big[(1-e^{i(x-x')-a})(1-e^{-i(y-y')-a})\Big]^{-\frac{(K+1)^2}{4K}}\\ &\times\ \Big[(1-e^{-i(x-x')-a})(1-e^{i(y-y')-a})\Big]^{-\frac{(K-1)^2}{4K}}\\ &\times\ \left[\frac{(1+e^{i(x-y')-a})(1+e^{-i(x-y')-a})(1+e^{i(x'-y)-a})(1+e^{-i(x'-y)-a})}{(1+e^{i(x-y)-a})(1+e^{-i(x-y)-a})(1+e^{i(x'-y')-a})(1+e^{-i(x'-y')-a})}\right]^{\frac{K^2-1}{4K}}. \quad \text{(D.101)}\end{aligned}$$

Note that in the fourth line, due to the gauged boson fields, cf. Eqs. D.90 and D.91, the sign of the exponential terms are switched. We set $y=x+\theta_0$ and $y'=x'+\theta_0$ in order to obtain the correlation function in Eq. D.96, which yield

$$\begin{aligned}\mathrm{P}(x,\,x';\,\theta_0) &\propto e^{-K[\delta N(x-x')]^2}\left[\cosh a-\cos\left(x-x'\right)\right]^{-\frac{K^2+1}{2K}}\\ &\times\ \left\{\frac{\left[\cosh a+\cos\left(x-x'-\theta_0\right)\right]\left[\cosh a+\cos\left(x-x'+\theta_0\right)\right]}{\left(\cosh a+\cos\theta_0\right)^2}\right\}^{\frac{K^2-1}{4K}}. \quad \text{(D.102)}\end{aligned}$$

The correlation function is rotational invariant $\mathrm{P}(x,\,x';\,\theta_0)\equiv\mathrm{P}(x-x';\,\theta_0)$. For correlation of Kramers pairs $\theta_0=\pi$, we find

$$\mathrm{P}(x-\,x';\,\pi)\propto e^{-K[\delta N(x-x')]^2}\left[\cosh a-\cos\left(x-x'\right)\right]^{-\frac{1}{K}}\left[\cosh a-1\right]^{-\frac{K^2-1}{2K}}. \quad \text{(D.103)}$$

The magnetized bosonic vacuum $|\vec{N}\rangle_{\rm int}$, such as $\delta N_+ = -\delta N_- = \delta N \neq 0$ and hence $\langle \hat{M} \rangle \neq 0$, suppresses the pair correlation function by a Gaussian factor. $\mathrm{P}(\theta_0)$ in Eq. D.96 can be obtained through

$$\mathrm{P}(\theta_0) \propto \oint d\theta \, \mathrm{P}(\theta;\, \theta_0). \tag{D.104}$$

$\mathrm{P}(\theta_0)$ is illustrated in Fig. 6.2 for several K and in different boson vacuums.

D.2.5 Density-Density Correlations

In this subsection, we compute the correlation of density fluctuations in different branches. In principle, density-density correlation functions can reveal information about the spontaneous magnetization in the system. In fact, we are interested to know how the fluctuations of magnetization density are correlated. The magnetization density $\hat{M} = \oint d\theta \, \mathcal{M}(\theta)$ has the form

$$\begin{aligned} \mathcal{M}(\theta) &= \frac{1}{2\pi} \sum_{J,\, m} (J - m)\, e^{im\theta}\, c_J^\dagger c_{J-m} \\ &= \frac{1}{2\pi} \sum_{m} e^{im\theta}\, \mathcal{J}_m, \end{aligned} \tag{D.105}$$

where the chirality has been discarded in the representation and $J + 1/2,\, m \in \mathbb{Z}$. Information tied with $\langle \mathcal{M}(\theta,\, t)\, \mathcal{M}^\dagger(\theta,\, 0) \rangle$ would be interesting. But in the following, we follow another path. The magnetization emerges if an asymmetry in the population of the left and right moving particles occurs. Therefore, we define $\delta n_m = n_{m+} - n_{m-}$, which is a measure of the asymmetry, and investigate

$$\langle \delta n_m\, \delta n_m^\dagger \rangle = \oint d\theta\, d\theta' \, \left\langle \delta n(\theta)\, \delta n^\dagger(\theta') \right\rangle \, e^{-im(\theta - \theta')}, \tag{D.106}$$

where $n_\eta(\theta) = \Psi_\eta^\dagger(\theta) \Psi_\eta(\theta)$, see Eq. D.17. We need to calculate

$$\left\langle \Psi_+^\dagger(x)\, \Psi_+(x)\, \Psi_+^\dagger(y)\, \Psi_+(y) \right\rangle_{\rm int} \propto \mathrm{D}^{++}(x,\, y), \tag{D.107}$$

$$\left\langle \Psi_+^\dagger(x)\, \Psi_+(x)\, \Psi_-^\dagger(y)\, \Psi_-(y) \right\rangle_{\rm int} \propto \mathrm{D}^{+-}(x,\, y). \tag{D.108}$$

Calculating the correlation functions in the same way as presented in the preceding subsection, it turns out that they are c-number. The same is true for the following correlation function

$$\left\langle \Psi_+^\dagger(x)\, \Psi_-(x)\, \Psi_-^\dagger(y)\, \Psi_+(y) \right\rangle_{\rm int} \propto \text{const.}, \tag{D.109}$$

which reveals information about the correlation of particle-hole excitations across the Fermi sea

$$\oint d\theta\, \Psi_+^\dagger(\theta)\, \Psi_-(\theta) = \sum_j c_{j+}^\dagger c_{j-} \equiv \sum_{J>0} c_J^\dagger c_{J-2J_F}. \tag{D.110}$$

The system is unable to correlate the population in different branches due to the absence of the backward scattering which expectable in the regime of weak interactions.

Appendix E

Richardson Pairing Model

In this appendix, we review briefly the Richardson pairing model [89, 31] and write down its exact eigenstates. Consider the following Hamiltonian

$$\begin{aligned} H^R &= H_0^R + H_p^R \\ &= \sum_f 2\epsilon_f \hat{N}_f - g \sum_{f,\,f'} \mathrm{b}_f^\dagger \mathrm{b}_{f'}, \end{aligned} \tag{E.1}$$

where ϵ_f is an arbitrary function of the discrete quantum number f and

$$\hat{N}_f = \frac{1}{2}(a_{f+}^\dagger a_{f+} + a_{f-}^\dagger a_{f-}), \tag{E.2}$$

$$\mathrm{b}_f = a_{f-} a_{f+}. \tag{E.3}$$

$a_{f+}^\dagger$ and a_{f+} are fermion creation and annihilation operators, respectively, which indicate $\mathrm{b}_f^2 = 0$. The quantum numbers $(f,\,\sigma)$ and $(f,\,-\sigma)$ label time-reversed partners for $\sigma = \pm 1$. $(f,\,\sigma) \in S$ that S is a finite set of states, say, in the vicinity of Fermi surface. The commutation relations of the operators read

$$[\mathrm{b}_f,\,\hat{N}_{f'}] = \delta_{ff'}\mathrm{b}_f, \tag{E.4}$$

$$[\mathrm{b}_f,\,\mathrm{b}_{f'}^\dagger] = \delta_{ff'}(1 - 2\hat{N}_{f'}). \tag{E.5}$$

b_f annihilates any state $|\psi\rangle$ if the levels $f\pm$ are empty or singly occupied. Therefore, the singly occupied levels contributes to the energy solely through H_0^R, and are blocked for the pairing term H_p^R. The number of singly occupied levels ν is called seniority. The total number of particles N and number of pairs P make the relation $N = 2P + \nu$. The pair degeneracy Ω is defined as the number of different values of f in S. Here, we represent the solutions have been derived by Richardson [89] for two specific models which are relevant to our system: **I)** The flat-band pairing model $\epsilon_f = \epsilon =$ constant and **II)** a model with $\epsilon_f \neq$ constant. The number of particles N in the both models is taken to be an even number.

I) For P pairs in a flat-band pairing model, the eigenstate with $\nu = 0$ is

$$|\psi^{FB}\rangle = \frac{\psi^{FB}}{\sqrt{P!}} \sum_{f_1, f_2, \cdots, f_P} \mathrm{b}^\dagger_{f_1} \mathrm{b}^\dagger_{f_2} \cdots \mathrm{b}^\dagger_{f_P} |0\rangle, \tag{E.6}$$

where the sum is over distinct f_i. The ground state energy is $E_0^{FB} = 2P\epsilon - gP(\Omega - P + 1)$ and corresponding coefficient $\psi_0^{FB} =$ constant. The excited states are constructed by breaking pairs and increasing ν. The energy of nth excited states, $\nu = 2n$ for $n = 0, \cdots, P$, and the corresponding coefficient are

$$E_n^{FB} = 2P\epsilon - g(P-n)(\Omega - P - n + 1), \tag{E.7}$$

$$\psi_n^{FB} = \sqrt{\frac{(\Omega - P - n)!}{(\Omega - 2n)!}}. \tag{E.8}$$

II) For pairing model with arbitrary ϵ_f, the exact eigenstates for P pairs and $\nu = 0$ has the form

$$|\psi^R\rangle = \prod_{k=1}^{P} B_k^\dagger |0\rangle, \tag{E.9}$$

$$B_k^\dagger = \sum_{f=1}^{\Omega} \frac{1}{2\epsilon_f - E_k} \mathrm{b}^\dagger_f, \tag{E.10}$$

where the pair energies E_k are the solutions of P non-linear equations which are called Richardson equations

$$1 + 2g \sum_{j \neq k}^{P} \frac{1}{E_j - E_k} - g \sum_{f=1}^{\Omega} \frac{1}{2\epsilon_f - E_k} = 0. \tag{E.11}$$

The eigenenergies $H^R|\psi^R\rangle = E^R|\psi^R\rangle$ is simply $E^R = \sum_{k=1}^{P} E_k$ [27].

Bibliography

[1] A. A. Abrikosov, L. P. Gorkov, and I. E. Dzyaloshinski. *Methods of quantum field theory in statistical physics*. Prentice-Hall Inc., 1963.

[2] Jason Alicea. New directions in the pursuit of majorana fermions in solid state systems. *Rep. Prog. Phys.*, 75:076501, 2012.

[3] A. Altland and B. Simons. *Condensed Matter Field Theory*. Cambridge University Press, second edition, 2010.

[4] A. Ambrosetti, F. Pederiva, and E. Lipparini. Quantum monte carlo study of circular quantum dots in presence of Rashba interaction. *Phys. Rev. B*, 83:155301, 2011.

[5] Luigi Amico, Antonio Di Lorenzo, and Andreas Osterloh. Integrable models for confined fermions: applications to metallic grains. *Nucl. Phys. B*, 614:449–466, 2001.

[6] Philip W. Anderson. Is there glue in cuprate superconductors? *Science*, 316:1705, 2007.

[7] R. Egger andW. Häusler, C. H. Mak, and H. Grabert. Crossover from fermi liquid to Wigner molecule behavior in quantum dots. *Phys. Rev. Lett.*, 82:3320, 1999.

[8] C. R. Ast, J. Henk, A. Ernst, L. Moreschini, M. C. Falub, D. Pacilé, P. Bruno, K. Kern, and M. Grioni. Giant spin splitting through surface alloying. *Phys. Rev. Lett.*, 98:186807, 2007.

[9] C. R. Ast, D. Pacilé, L. Moreschini, M. C. Falub, M. Papagno, K. Kern, M. Grioni, J. Henk, A. Ernst, S. Ostanin, and P. Bruno. Spin-orbit split two-dimensional electron gas with tunable Rashba and fermi energy. *Phys. Rev. B*, 77:081407(R), 2008.

[10] Assa Auerbach. *Interacting Electrons and Quantum Magnetism*. Springer, 1994.

[11] Siranush Avetisyan, Tapash Chakraborty, and Pekka Pietilainen. Magnetization of quantum dots: A measure of anisotropy and the Rashba interaction. *arXiv:1501.01025v1 [cond-mat.mes-hall]*, 2015.

[12] V. M. Bedanov and F. M. Peeters. Ordering and phase transitions of charged particles in a classical finite two-dimensional system. *Phys. Rev. B*, 49:2667, 1994.

[13] E. Berg, M. S. Rudner, and S. A. Kivelson. Electronic liquid crystalline phases in a spin-orbit coupled two-dimensional electron gas. *Phys. Rev. B*, 85:035116, 2012.

[14] C. T. Black, D. C. Ralph, and M. Tinkham. Spectroscopy of the superconducting gap in individual nanometer-scale aluminum particles. *Phys. Rev. Lett.*, 76:688–691, Jan 1996.

[15] A. C. Bleszynski-Jayich, W. E. Shanks, B. Peaudecerf, E. Ginossar, F. von Oppen, L. Glazman, and J. G. E. Harris. Persistent currents in normal metal rings. *Science*, 326:272, 2009.

[16] F. Bolton and U. Rössler. Classical model of a Wigner crystal in a quantum dot. *Superlattices Microstruct.*, 13:139, 1993.

[17] Max Born and J. Robert Oppenheimer. Zur Quantentheorie der Molekeln. *Annalen der Physik*, 389:457–484, 1927.

[18] Sangita Bose, Antonio M. García-García, Miguel M. Ugeda, Juan D. Urbina, Christian H. Michaelis, Ivan Brihuega, and Klaus Kern. Observation of shell effects in superconducting nanoparticles of Sn. *Nature Materials*, 9:550, 2010.

[19] Fabian Braun and Jan Von Delft. Superconductivity in ultrasmall metallic grains. *Phys. Rev. B*, 59(14):9527, 1999.

[20] M. Büttiker, Y. Imry, and M. Ya. Azbel. Quantum oscillations in one-dimensional normal-metal rings. *Phys. Rev. A*, 30:1982, 1984.

[21] Y. A. Bychkov and E. I. Rashba. Properties of a 2d electron gas with lifted spectral degeneracy. *J. Exp. Theor. Phys. Lett.*, 39:78–81, 1984.

[22] A. Cavalli, F. Malet, J. C. Cremon, , and S. M. Reimann. Spin-orbit-enhanced Wigner localization in quantum dots. *Phys. Rev. B*, 84:235117, 2011.

[23] T. Chakraborty and P. Pietiläinen. Electron-electron interaction and the persistent current in a quantum ring. *Phys. Rev. B*, 50:8460, 1994.

[24] T. Chakraborty and P. Pietiläinen. Electron correlations in a quantum dot with Bychkov-Rashba coupling. *Phys. Rev. B*, 71:113305, 2005.

[25] Garnet Kin-Lic Chan, Jonathan J. Dorando, Debashree Ghosh, Johannes Hachmann, Eric Neuscamman, Haitao Wang, and Takeshi Yanai. An introduction to the density matrix renormalization group ansatz in quantum chemistry. *Progress in Theoretical Chemistry and Physics*, 18:49–65, 2008.

[26] Andrey V. Chubukov. Kohn-Luttinger effect and the instability of a two-dimensional repulsive fermi liquid at $T = 0$. *Phys. Rev. B*, 48:1097–1104, Jul 1993.

[27] Michel Crouzeix and Monique Combescot. Energy of N Cooper pairs by analytically solving the Richardson-Gaudin equations for conventional superconductors. *Phys. Rev. Lett.*, 107:267001, 2011.

[28] Supriyo Datta. *Electronic Transport in Mesoscopic Systems*. Cambridge University Press, 1997.

[29] C. F. Destefani, S. E. Ulloa, and G. E. Marques. Spin-orbit and electronic interactions in narrow-gap quantum dots. *Phys. Rev. B*, 70:205315, 2004.

[30] C. F. Destefani, S. E. Ulloa, and G. E. Marques. Spin-orbit coupling and intrinsic spin mixing in quantum dots. *Phys. Rev. B*, 69:125302, 2004.

[31] J. Dukelsky, S. Pittel, and G. Sierra. Colloquium: Exactly solvable Richardson-Gaudin models for many-body quatum systems. *Rev. Mod. Phys.*, 76, 2004.

[32] C. Echeverría-Arrondo and E. Ya. Sherman. Position and spin control by dynamical ultrastrong spin-orbit coupling. *Phys. Rev. B*, 88:155328, 2013.

[33] R. Egger, A. De Martino, E. Stockmeyer, and H. Siedentop. Multiparticle equations for interacting dirac fermions in magnetically confined graphene quantum dots. *J. Phys. A*, 43:215202, 2010.

[34] Steven R. Elliott and Marcel Franz. *Colloquium* : Majorana fermions in nuclear, particle, and solid-state physics. *Rev. Mod. Phys.*, 87:137–163, Feb 2015.

[35] A. Emperador, E. Lipparini, and F. Pederiva. Role of spin-orbit interaction in the chemical potential of quantum dots in a magnetic field. *Phys. Rev. B*, 70:125302, 2004.

[36] F. H. L. Essler, H. Frahm, F. Göhmann, A. Klm̈per, and V. E. Korepin. *The One-Dimensional Hubbard Model*. Cambridge University Press, 2005.

[37] Zyun Francis Ezawa. *Quantum Hall Effects Recent Theoretical and Experimental Developments*. World Scientific Publishing, third edition, 2013.

[38] Aaron Farrell and T. Pereg-Barnea. Zeeman-field-induced nontrivial topology in a spin-orbit-coupled superconductor. *Phys. Rev. B*, 90:144518, Oct 2014.

[39] Alexander L. Fetter and John Dirk Walecka. *Quantum theory of many-particle systems*. McGraw-Hill Inc., 1971.

[40] V. M. Galitski and S. Das Sarma. Kohn-Luttinger pseudopairing in a two-dimensional fermi liquid. *Phys. Rev. B*, 67:144520, Apr 2003.

[41] Victor Galitski and Ian B. Spielman. Spin-orbit coupling in quantum gases. *Nature*, 494:49, 2013.

[42] S. K. Ghosh, J. P. Vyasanakere, and V. B. Shenoy. Trapped fermions in a synthetic non-abelian gauge field. *Phys. Rev. A*, 84:053629, 2011.

[43] I. Gierz, T. Suzuki, E. Frantzeskakis, S. Pons, S. Ostanin, A. Ernst, J. Henk, M. Grioni, K. Kern, and C. R. Ast. Silicon surface with giant spin splitting. *Phys. Rev. Lett.*, 103:046803, 2009.

[44] G. F. Giuliani and Vignale. *Quantum theory of the electron liquid*. Cambridge University Press, 2005.

[45] A. O. Gogolin and N. V. Prokof'ev. Simple formula for the persistent current in disordered one-dimensional rings: Parity and interaction effects. *Phys. Rev. B*, 50:4921, 1994.

[46] M. Governale. Quantum dots with Rashba spin-orbit coupling. *Phys. Rev. Lett.*, 89:206802, 2002.

[47] George Grüner. *Density Waves In Solids*. Frontiers In Physics, first edition, 1994.

[48] M. Z. Hasan and C. L. Kane. Colloquium: Topological insulators. *Rev. Mod. Phys.*, 82:3045, 2010.

[49] W. Häusler. Influence of spin on the persistent current of strongly interacting electrons. *Physica (Amsterdam) 222B*, page 43, 1996.

[50] Gervasi Herranz, Gyanendra Singh, Nicolas Bergeal, Alexis Jouan, Jérôme Lesueur, Jaume Gázquez, María Varela, Mateusz Scigaj, Nico Dix, Florencio Sánchez, and Josep Fontcuberta. Engineering two-dimensional superconductivity and Rashba spin-orbit coupling in $LaAlO_3/SrTiO_3$ quantum wells by selective orbital occupancy. *Nat. Commun.*, 6(6028), 2015.

[51] H. Hu, B. Ramachandhran, H. Pu, and X. J. Liu. Spin-orbit coupled weakly interacting Bose-Einstein condensates in harmonic traps. *Phys. Rev. Lett.*, 108:010402, 2012.

[52] H. Y. Hwang, Y. Iwasa, M. Kawasaki, N. Nagaosa, and Y. Tokura. Emergent phenomena at oxide interfaces. *Nature Materials*, 11:103, 2012.

[53] Jainendra K. Jain. *Composite Fermions*. Cambridge University Press, 2007.

[54] K. Jauregui, W. Häusler, and B. Kramer. Wigner molecules in nanostructures. *Europhys. Lett.*, 24:581, 1993.

[55] Arjun Joshua, S. Pecker, J. Ruhman, E. Altman, and S. IIani. A universal critical density underlying the physics of electrons at $LaAlO_3/SrTiO_3$ interface. *Nature communication*, 3:1129, 2012.

[56] Y. Kanai, R. S. Deacon, S. Takahashi, A. Oiwa, K. Yoshida, K. Shibata, K. Hirakawa, Y. Tokura, and S. Tarucha. Electrically tuned spin-orbit interaction in an $InAs$ self-assembled quantum dot. *Nat. Nanotechnol.*, 6:511, 2011.

[57] A.Yu. Kitaev. Fault-tolerant quantum computation by anyons. *Annals of Physics*, 303:2–30, 2003.

[58] K. v. Klitzing, G. Dorda, and M. Pepper. New method for high-accuracy determination of the fine-structure constant based on quantized Hall resistance. *Phys. Rev. Lett.*, 45:494–497, Aug 1980.

[59] M. Kohda, T. Bergsten, and J. Nitta. Manipulating spin-orbit interaction in semiconductors. *J. Phys. Soc. Jpn.*, 77:031008, 2008.

[60] W. Kohn and J. M. Luttinger. New mechanism for superconductivity. *Phys. Rev. Lett.*, 15:524–526, Sep 1965.

[61] L. P. Kouwenhoven, D. G. Austing, and S. Tarucha. Few-electron quantum dots. *Rep. Prog. Phys.*, 64:701, 2001.

[62] V. Kresin and Yu. Ovchinnikov. Superconducting state of metallic nanoclusters and Josephson tunneling networks. *Physica C*, 506:201–206, 2014.

[63] V. Z. Kresin and Yu. N. Ovchinnikov. "giant" strengthening of superconducting pairing in metallic nanoclusters: large enhancement of T_c and potential for room-temperature superconductivity. *Physics-Uspekhi*, 51(5):427–435, 2008.

[64] Vladimir Z. Kresin, Hans Morawitz, and Stuart A. Wolf. *Superconducting State: Mechanisms and Properties*. Oxford University Press, 2014.

[65] Vladimir Z. Kresin and Yurii N. Ovchinnikov. Superconducting state of metallic clusters: Potential for room temperature superconductivity, novel nano-based tunneling networks. *Journal of Superconductivity and Novel Magnetism*, 26:745–748, 2013.

[66] Y. Li, S.C. Zhang, and C. Wu. Topological insulators with $SU(2)$ Landau levels. *Phys. Rev. Lett.*, 111:186803, 2013.

[67] Y. Li, X. Zhou, and C. Wu. Two- and three-dimensional topological insulators with isotropic and parity-breaking Landau levels. *Phys. Rev. B*, 85:125122, 2012.

[68] Florian Loder, Arno P Kampf, and Thilo Kopp. Superconductivity with Rashba spin-orbit coupling and magnetic field. *J. Phys.: Condens. Matter*, 25(362201), 2013.

[69] J. M. Luttinger. New mechanism for superconductivity. *Phys. Rev.*, 150:202–214, Oct 1966.

[70] D. Schuetz M. Farber. Homology of planar polygon spaces. *Geom. Dedicata*, 125(75), 2007.

[71] J. Millson M. Kapovich. On the moduli space of polygons in the Euclidean plane. *J. Differential Geom.*, 42(1):133–164, 1995.

[72] L. Meier, G. Salis, I. Shorubalko, E. Gini, S. Schön, and K. Ensslin. Measurement of Rashba and Dresselhaus spin-orbit magnetic fields. *Nat. Phys.*, 3:650, 2007.

[73] G. Morandi, P. Sodano, A. Tagliacozzo, and V. Tognetti, editors. *Field Theories for Low-Dimensional Condensed Matter Systems*. Springer Series in Solid-State Sciences. Springer, 2000.

[74] H. Murakawa, M. S. Bahramy, M. Tokunaga, Y. Kohama, C. Bell, Y. Kaneko, N. Nagaosa, H. Y. Hwang, and Y. Tokura. Detection of Berry's phase in a bulk Rashba semiconductor. *Science*, 342:1490, 2013.

[75] Mikio Nakahara. *Geometry, Topology and Phsyics*. Institute of Physics Publishing, second edition, 2003.

[76] Amin Naseri, Alex Zazunov, and Reinhold Egger. Orbital ferromagnetism in interacting few-electron dots with strong spin-orbit coupling. *Phys. Rev. X*, 4:031033, Aug 2014.

[77] Yu. V. Nazarov and Ya. M. Blanter. *Quantum Transport: Introduction to Nanoscience*. Cambridge University Press, 2009.

[78] A. Ohtomo and H. Y. Hwang. A high-mobility electron gas at the $LaAlO_3/SrTiO_3$ heterointerface. *Nature*, 427:423, 2004.

[79] G. Ortiz, R. Somma, J. Dukelsky, and S. Rombouts. Exactly-solvable models derived from a generalized Gaudin algebra. *Nucl. Phys. B*, 707:421–457, 2005.

[80] D. Pines P. Monthoux and G. G. Lonzarich. Superconductivity without phonons. *Nature*, 450:1177–1183, 2007.

[81] Dmytro Pesin and Allan H. MacDonald. Spintronics and pseudospintronics in graphene and topological insulators. *Nature Materials*, 11:409–416, 2012.

[82] P. Pietiläinen and T. Chakraborty. Energy levels and magneto-optical transitions in parabolic quantum dots with spin-orbit coupling. *Phys. Rev. B*, 73:155315, 2006.

[83] X. L. Qi and S. C. Zhang. Topological insulators and superconductors. *Rev. Mod. Phys.*, 83:1057, 2011.

[84] S. Raghu and S. A. Kivelson. Superconductivity from repulsive interactions in the two-dimensional electron gas. *Phys. Rev. B*, 83:094518, 2011.

[85] D. C. Ralph, C. T. Black, and M. Tinkham. Spectroscopic measurements of discrete electronic states in single metal particles. *Phys. Rev. Lett.*, 74:3241–3244, Apr 1995.

[86] D. C. Ralph, C. T. Black, and M. Tinkham. Gate-voltage studies of discrete electronic states in aluminum nanoparticles. *Phys. Rev. Lett.*, 78:4087–4090, May 1997.

[87] E. Rashba. Quantum nanostructures in strongly spin-orbit coupled two-dimensional systems. *Phys. Rev. B*, 86:125319, 2012.

[88] S. M. Reimann and M. Manninen. Electronic structure of quantum dots. *Rev. Mod. Phys.*, 74:1283, 2002.

[89] R. W. Richardson and N. Sherman. Exact eigenstates of the pairing-force hamiltonian. *Nucl. Phys.*, 52:221, 1964.

[90] J. M. Roman, G. Sierra, and J. Dukelsky. Large-N limit of the exactly solvable BCS model: analytics versus numerics. *Nucl. Phys. B*, 634:483, 2002.

[91] J. J. Sakurai. *Modern Quantum Mechanics*. Addison-Wesley Publishing Company, revised edition edition, 1994.

[92] Mathias S. Scheurer and Jörg Schmalian. Topological superconductivity and unconventional pairing in oxide interfaces. *Nat. Commun.*, 6(6005), 2015.

[93] Ulrich Schollwöck. The density-matrix renormalization group in the age of matrix product states. *Annals of Physics*, 326:96–192, 2011.

[94] Franz Schwabl. *Advanced Quantum Mechanics*. Springer-Verlag, third edition, 2005.

[95] T. A. Sedrakyan, A. Kamenev, and L. I. Glazman. Composite fermion state of spin-orbit-coupled bosons,. *Phys. Rev. A*, 86:063639, 2012.

[96] R. Shankar. Renormalization-group approach to interacting fermions. *Rev. Mod. Phys.*, 66:129, 1994.

[97] P. G. Silvestrov and O. Entin-Wohlmann. Wigner crystal of a two-dimensional electron gas with a strong spin-orbit interaction. *Phys. Rev. B*, 89:155103, 2014.

[98] Jenő Sólyom. *Fundamentals of the Physics of Solids*, volume 1. Springer, 2007.

[99] Jenő Sólyom. *Fundamentals of the Physics of Solids*, volume 3. Springer, 2010.

[100] W. C. Tan and J. C. Inkson. Magnetization, persistent currents, and their relation in quantum rings and dots. *Phys. Rev. B*, 60:5626, 1999.

[101] M. Tinkham, J. M. Hergenrother, and J. G. Lu. Temperature dependence of even-odd electron-number effects in the single-electron transistor with a superconducting island. *Phys. Rev. B*, 51:12649–12652, May 1995.

[102] Michael Tinkham. *Introduction To Superconductivity*. Dover Publication, INC., second edition, 1996.

[103] Oskar Vafek and Luyang Wang. Spin-orbit coupling induced enhancement of superconductivity in a two-dimensional repulsive gas of fermions. *Phys. Rev. B*, 84:172501, Nov 2011.

[104] Jan von Delft and Herbert Schoeller. Bosonization for beginners – refermionization for experts. *arXiv:cond-mat/9805275*, 1998.

[105] O. Voskoboynikov, C. P. Lee, and O. Tretyak. Spin-orbit splitting in semiconductor quantum dots with a parabolic confinement potential. *Phys. Rev. B*, 63:165306, 2001.

[106] S. Weiss and R. Egger. Path-integral Monte Carlo simulations for interacting few-electron quantum dots with spin-orbit coupling. *Phys. Rev. B*, 72:245301, 2005.

[107] S. R. White and D. A. Huse. Numerical renormalization-group study of low-lying eigenstates of the antiferromagnetic $s = 1$ heisenberg chain. *Phys. Rev. B*, 48, 1993.

[108] Roland Winkler. *Spin-Orbit Coupling Effects in Two-Dimensional Electron and Hole Systems*. Springer-Verlag, 2003.

[109] W. Witczak-Krempa, G. Chen, Y. B. Kim, and L. Balents. Correlated quantum phenomena in the strong spin-orbit regime. *Annu. Rev. Condens. Matter Phys.*, 5:57, 2014.

[110] C. Wu, B. A. Bernevig, and S. C. Zhang. Helical liquid and the edge of quantum spin Hall systems. *Phys. Rev. Lett.*, 96:106401, 2006.

[111] C. Wu, I. Mondragon Shem, and X.-F. Zhou. Unconventional Bose-Einstein condensations from spin-orbit coupling. *Chin. Phys. Lett.*, 28:097102, 2011.

[112] Di Xiao, Ming-Che Chang, and Qian Niu. Berry phase effects on electronic properties. *Rev. Mod. Phys.*, 82:1959, 2010.

[113] C. Xu and J. E. Moore. Stability of the quantum spin Hall effect: Effects of interactions, disorder, and z2 topology. *Phys. Rev. B*, 73:045322, 2006.

[114] X. Q. Xu and J. H. Han. Emergence of chiral magnetism in spinor Bose-Einstein condensates with Rashba coupling. *Phys. Rev. Lett.*, 108:185301, 2012.

[115] K. Yaji, Y. Ohtsubo, S. Hatta, H. Okuyama, K. Miyamoto, T. Okuda, A. Kimura, H. Namatame, M. Taniguchi, and T. Aruga. Large Rashba spin splitting of a metallic surface-state band on a semiconductor surface. *Nat. Commun.*, 1:17, 2010.

[116] C. Yannouleas and U. Landman. Symmetry breaking and quantum correlations in finite systems: Studies of quantum dots and ultracold bose gases and related nuclear and chemical methods. *Rep. Prog. Phys.*, 70:2067, 2007.

[117] Hui Zhai. Degenerate quantum gases with spin-orbit coupling: a review. *Rep. Prog. Phys.*, 78:026001, 2015.

[118] S. C. Zhang. The Chern-Simons-Landau-Ginzburg theory of the fractional quantum Hall effect. *Int. J. Mod. Phys. B*, 6:25, 1992.

[119] Shou-Cheng Zhang and Jiang-Ping Hu. A four dimensional generalization of the quantum Hall effect. *Science*, 294:823, 2001.

[120] Zhicheng Zhong, Anna Tóth, and Karsten Held. Theory of spin-orbit coupling at $LaAlO_3/SrTiO_3$ interfaces and $SrTiO_3$ surfaces. *Phys. Rev. B*, 87:161102(R), 2013.

[121] X. Zhou, Y. Li, Z. Cai, and C. Wu. Unconventional states of bosons with synthetic spin-orbit coupling. *J. Phys. B*, 46:134001, 2013.

Erklärung

Die hier vorgelegte Dissertation habe ich eingeständig und ohne unerlaubte Hilfe angefertigt. Die Dissertation wurde in der vorgelegten oder ähnlichen Form noch bei keiner anderen Institution eingereicht. Ich habe bisher keine erfolglosen Promotionsversuche unternommen.

Düsseldorf, den . .2015

(Amin Naseri Jorshari)